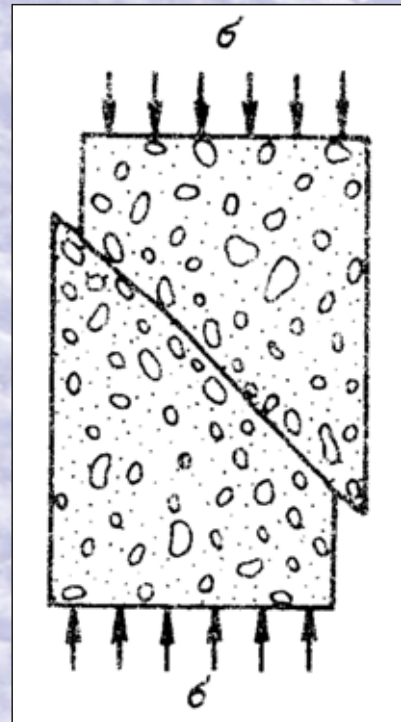
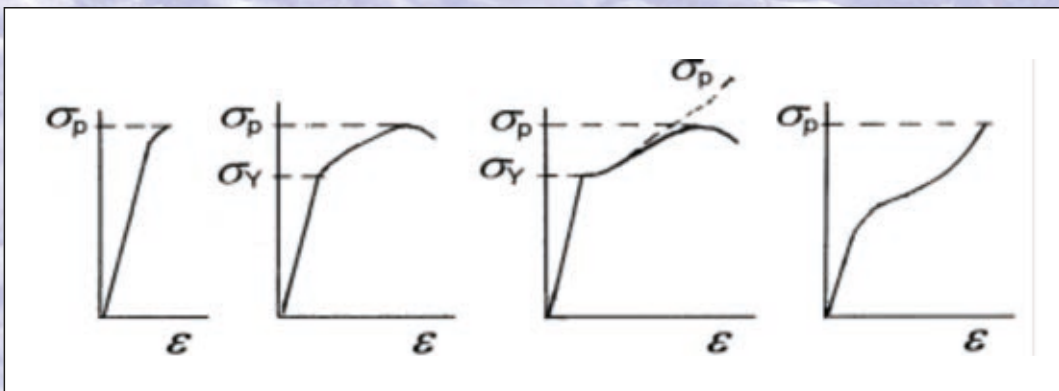


Jaroslav Menčík



# Applied Mechanics of Materials



**Jaroslav Menčík**

# **Applied Mechanics of Materials**

**University of Pardubice, 2019**

Reviewers:

Prof. Dr. Ing. Libor Beneš

Doc. Ing. Iva Petříková, PhD.

© prof. Ing. Jaroslav Menčík, CSc., 2019

ISBN 978-80-7560-228-2 (print)

ISBN 978-80-7560-229-9 (pdf)

Book is accessible freely via <https://hdl.handle.net/10195/72948> or after writing its title into Google.

## **Applied mechanics of materials**

Components and structures in mechanical and civil engineering are made of various materials, and design engineers must have a good knowledge of their mechanical properties. This book deals with this area. The first chapter summarises the principal terms: stress, strain, and strain energy. The second chapter compares the finite element method and analytical methods for the determination of stresses and deformations. Chapter 3 presents the principal criteria for fracture and for the onset of permanent deformations. The following chapter is devoted to plastic deforming. Attention is also paid to thermal stresses. Chapter 6 deals with stress concentration at sudden changes of shape. Chapters on fatigue, fracture mechanics and analysis of fractures follow. Chapter 10 explains the mechanics of viscoelastic materials, whose deformations depend on the duration and time course of loading. The following chapters are devoted to components with treated or coated surfaces, to the properties of composite materials and of elastomeric materials. The methods of shape optimisation for improvement of strength and material economy are the topic of Chapter 14. The last chapter is devoted to the theory of similarity and dimensional analysis and their use for increasing the design effectiveness.

The book contains numerous figures and examples, which illustrate the use of the described methods.

The book is accessible freely via <https://hdl.handle.net/10195/72948> or after writing its title into Google.

### **Acknowledgment**

The author expresses thanks to his teacher at the VŠST in Liberec, Professor Ing. Cyril Höschl, who aroused his interest in mechanics of materials.

For the care devoted to the manuscript reading and for valuable comments, the author also thanks to both reviewers:

Associate Professor Ing. Iva Petriková, PhD., of the Technical University in Liberec, and Professor Dr. Ing. Libor Beneš of the Czech Technical University in Prague.



## **Aplikovaná mechanika materiálů**

Konstruktor či projektant musí mít dobré znalosti o chování různých materiálů při zatížení. K tomu přispívá v patnácti kapitolách i tato kniha. První kapitola shrnuje základní pojmy: napětí, přetvoření a deformační energie. Druhá kapitola stručně porovnává metodu konečných prvků a metody analytické pro stanovení napětí a deformací v konstrukcích. Třetí kapitola uvádí kritéria pro posuzování porušení nebo vzniku trvalých deformací. Následuje kapitola o plastickém deformování. Pozornost je dále věnována napětím, která vznikají při změnách teploty. Kapitola šestá pojednává o koncentraci napětí v místech náhlých změn tvaru, kapitola sedmá je o únavě materiálů. Následují kapitoly o lomové mechanice, analýze lomů a o mechanice viskoelastických látek, kde deformace závisí na časovém průběhu zatížení. Další kapitola je věnována součástem se speciálními povrchovými vrstvami pro dosažení vyšší životnosti nebo specifických vlastností. Další kapitoly podávají základy mechaniky kompozitních materiálů, elastomerních materiálů a velmi poddajných těles, včetně textilních. Následují metody optimalizace tvaru těles. Poslední kapitola je věnována použití teorie podobnosti a rozměrové analýzy pro zvýšení efektivity vývoje a konstruování.

Kniha obsahuje četné obrázky i příklady, které ilustrují použití popisovaných metod.

Kniha je volně přístupná na <http://hdl.handle.net/10195/947> nebo po zadání jejího názvu do vyhledávače Google.

# CONTENTS

<b>1</b>	<b>Stress – strain – strain energy</b>	<b>9</b>
1.1	Stress	9
1.2	Plane stress, Mohr’s circle	10
1.3	Triaxial state of stress	16
1.4	Strain	17
1.5	Work of loading forces and strain energy	20
<b>2</b>	<b>Finite element method, analytical and numerical methods</b>	<b>23</b>
2.1	Finite element method	23
2.2	Use of numerical and analytical methods for problems in mechanics	26
<b>3</b>	<b>Failure hypotheses and criteria</b>	<b>31</b>
3.1	Brittle fracture	31
3.2	Onset of plastic deformations	32
<b>4</b>	<b>Basics of plasticity</b>	<b>35</b>
4.1	Material properties	36
4.2	System of rods loaded by tension	39
4.3	Deformations in elastic-plastic state	41
4.4	Situation after unloading	42
4.5	Elastic-plastic bending	44
4.6	Elastic-plastic condition of thick-walled cylindrical pressure vessel	48
4.7	Criterion of plastic flow under multiaxial stress state	51
4.8	Increasing of fatigue resistance of metallic components	52
<b>5</b>	<b>Thermal stresses</b>	<b>54</b>
5.1	Principal equations	54
5.2	Procedures for strength increasing by thermal treatment	58
<b>6</b>	<b>Stress concentration</b>	<b>64</b>
6.1	Introduction	64
6.2	Stresses around holes	67
6.3	Stress state at concentrated contact	70
<b>7</b>	<b>Response under alternating load; fatigue</b>	<b>74</b>
7.1	Change of mechanical properties	74
7.2	Initiation and growth of fatigue cracks	75
7.3	Time to fatigue failure	76

7.4	Factors influencing the fatigue endurance	78
7.5	Damage accumulation	79
<b>8</b>	<b>Principles of fracture mechanics</b>	<b>81</b>
8.1	Situation in bodies with cracks, principles of fracture mechanics	81
8.2	Growth of fatigue cracks	88
8.3	Increasing the resistance to crack propagation	90
<b>9</b>	<b>Fracture analysis</b>	<b>93</b>
<b>10</b>	<b>Mechanics of viscoelastic materials</b>	<b>98</b>
10.1	Ideally elastic material	98
10.2	Ideally viscous material	99
10.3	Maxwell model	100
10.4	Kelvin-Voigt model	103
10.5	Standard linear solid	105
10.6	Burgers model	106
10.7	Determination of deformations under varying load	108
10.8	Response of viscoelastic materials to alternating load	109
<b>11</b>	<b>Mechanics of components with treated surface</b>	<b>112</b>
10.1	Introduction	112
10.2	Stresses due to the difference of thermal expansions	113
10.3	Stresses caused by membrane forces	116
10.4	Stresses in coatings on curved surfaces	118
10.5	Situation at coating edges	119
10.6	Elastic-plastic deforming	120
10.7	Fracture mechanics of interfaces	124
10.8	Determination of mechanical properties of coatings	132
<b>12</b>	<b>Mechanics of composite materials</b>	<b>136</b>
12.1	Introduction	136
12.2	Composites with long fibres	137
12.3	Composites with short fibres	143
12.4	Dispersion of fiber properties	146
12.5	Failure of composites	147
12.6	Elastic response of orthotropic materials	149
12.7	Multilayer composites (laminates)	150

<b>13</b>	<b>Mechanics of elastomers and very compliant bodies</b>	<b>153</b>
13.1	Mechanics of elastomeric (hyperelastic) materials	153
13.2	Models for response of elastomeric materials	155
13.3	Textile fibers and structures	157
13.4	Membrane structures	158
<b>14</b>	<b>Optimisation of shape and dimensions of constructions</b>	<b>161</b>
14.1	Components and structures of constant stress	161
14.2	Optimisation of large structures	167
14.3	Optimisation for complicated shapes and loads	168
14.4.	Determination of the necessary tolerances	172
<b>15</b>	<b>Dimensional analysis and theory of similarity</b>	<b>182</b>
14.1	Dimensional analysis	182
14.2	Similarity	184
14.3	Further recommendations	185
14.4	Limitations of similarity principle	187
14.5	Examples of non-dimensional quantities	191
	<b>Index</b>	<b>192</b>

## **Foreword**

The components and constructions for mechanical, civil, chemical and transport engineering are made of various materials. The design engineer thus must have a good knowledge of their behaviour under load. This book wants to help in the selection of material and finding the optimum shape and dimensions. It wants to remind what should not be forgotten in design, if mistakes should be prevented. The calculations alone are not sufficient. The designer should understand all in context. The author assumes that the reader has absolved or is attending the basic course of the mechanics of materials. This book reminds the basic terms, shows the interesting features of the Mohr's circle, including its use in the analysis of fractures, reminds thermal stresses and how they can be influenced. It explains briefly the fatigue processes. It shows the importance of stress concentrators, and their unexpected consequences. It also brings the reader brief introduction into newer branches of mechanics of materials, such as plasticity, fracture mechanics, mechanics of viscoelastic materials, polymeric and composite materials, and of components with coated or treated surface.

The book also explains briefly the principle of the finite element method, which today represents the major tool for the analysis of complex components and structures. Also it presents general approach to their optimisation, including the robust design, with emphasis on setting the appropriate tolerances during the design stage. The advantages of similarity theory and dimensional analysis in design are also shown.

All principal relationships are explained by means of simple formulae; the knowledge of college mathematics is sufficient. The text is accompanied by numerous figures, simple solved examples, and references.

The author wishes that the reading of this book brings the readers similar pleasure, as its writing made to the author.

# 1. Stress - strain - strain energy

## 1.1 Stress

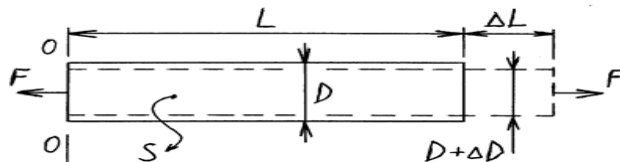
Loads generate in components internal forces and stresses. Stress is defined as force per unit of area. In general case, the internal forces are obtained by the **method of fictitious cut**: the component is cut in the investigated place by an artificial cut, into which normal and shearing forces are placed, as well as bending and twisting moments. Their magnitudes are then determined from the **equations of equilibrium of all forces and moments** acting on the separated part [1 - 4].

Two kinds of stresses can be distinguished: **normal stress**  $\sigma$ , acting in the direction normal to the section, and **shear** or **tangential stress**  $\tau$  in the direction tangential to this plane. Both stresses have the same dimension ( $\text{N/m}^2$  or Pa, MPa or GPa), their effects, however, are different. Normal stress is positive (tensile), if it acts out of the material and tries to enlarge the distance between the adjacent layers of atoms. Compressive normal stress (negative) presses the adjacent layers of atoms together. Shear stress causes mutual sliding of the neighbouring layers. These stresses endanger the component in different way. Normal tensile stress contributes to brittle fracture by tearing off, while shear stress promotes plastic deforming.

Both normal and shear stresses act nearly always together in the loaded component, even if it is not obvious at first sight. For example, if we consider a long rod loaded by tensile force (Fig. 1.1), we know immediately that at places distant from the ends normal tensile stress acts of magnitude

$$\sigma_0 = F / S ; \quad (1.1)$$

$F$  is the axial force and  $S$  is the area of the cross section. We have tacitly assumed that the section is perpendicular to the axis (as denoted in the formula by subscript 0). What is the situation in an inclined cut?



**Fig. 1.1.** Rod loaded by tensile force – dimensions and deformations.

This situation is depicted in Fig. 1.2. The cut is inclined by angle  $\alpha$ . The normal force  $N$  acts perpendicularly to it, and the tangential force  $T$  acts in the plane of the cut. Both forces are in equilibrium with axial force  $F$ , and it holds

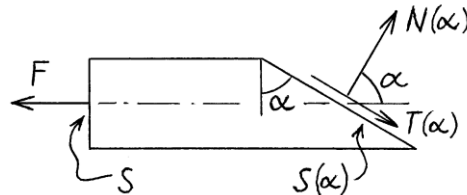
$$N(\alpha) = F \cos \alpha , \quad T(\alpha) = F \sin \alpha . \quad (1.2)$$

These forces generate normal and tangential (shear) stress. These stresses are obtained by dividing the force  $N$  or  $T$  by the area of the inclined cut. This area,  $S_\alpha$ , is related with the area  $S$  of the perpendicular cut as

$$S_\alpha = S / \cos \alpha . \quad (1.3)$$

The combination of Eqs. (1.2) and (1.3) yields (with respect to Eq. 1.1) stresses

$$\sigma(\alpha) = N_\alpha / S_\alpha = \sigma_0 (\cos \alpha)^2 , \quad \tau(\alpha) = T_\alpha / S_\alpha = \sigma_0 \sin \alpha \cos \alpha . \quad (1.4a, b)$$



**Fig. 1.2.** Forces in an inclined cut.

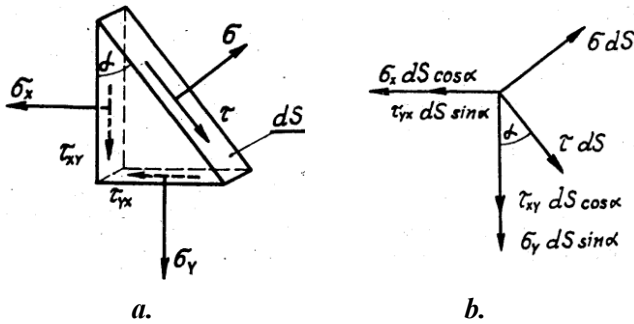
## 1.2 Plane stress, Mohr's circle

Let us look at the stresses in an oblique cut if in the directions  $x$  and  $y$  normal stresses  $\sigma_x$  and  $\sigma_y$  act, and shear stresses  $\tau_{xy}$  and  $\tau_{yx}$ . The subscript at normal stress denotes the direction of the stress and of the normal to the oblique plane. The first subscript at the shear stress shows the normal direction to the pertinent plane, while the second subscript denotes the direction of the stress itself.

The situation in an infinitesimal element is depicted in Fig. 1.3. After writing the equations of equilibrium in the direction normal and tangential to the oblique cut, one obtains (with respect to the relationships between the size of the inclined area  $dS_\alpha$  and vertical and horizontal areas  $dS_x$   $dS_y$ ) the following expressions:

$$\sigma(\alpha) = \frac{\sigma_x + \sigma_y}{2} + \frac{\sigma_x - \sigma_y}{2} \cos 2\alpha + \tau_{xy} \sin 2\alpha , \quad (1.5a)$$

$$\tau(\alpha) = \frac{\sigma_x - \sigma_y}{2} \sin 2\alpha - \tau_{xy} \cos 2\alpha . \quad (1.5b)$$

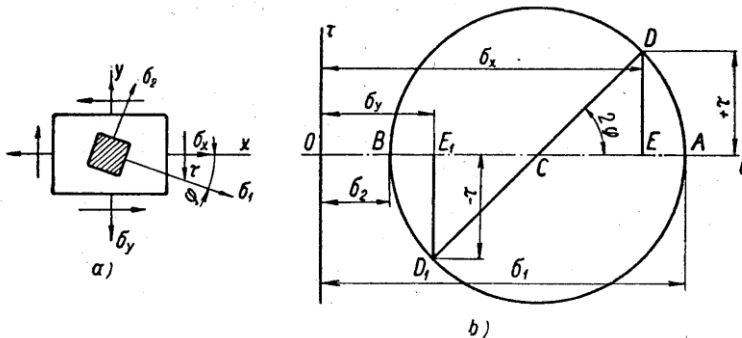


**Fig. 1.3.** Plane state of stress – stresses in an inclined cut.  
*a – stress components, b – equilibrium of forces.*

In the derivation of these equations the **rule of complementary shear stresses** was used: *If at some point shear stress acts in certain plane, then shear stress of the same magnitude acts also in the perpendicular plane. Both vectors are oriented towards the intersection line of both planes, or away from it.* For directions  $x, y$ ,

$$\tau_{xy} = \tau_{yx} . \tag{1.6}$$

Equations (1.5a), (1.5b) enable calculation of normal and shear stress in any cut, if the stress components  $\sigma_x, \sigma_y, \tau_{xy}$  in some coordinate system  $x, y$  are known. A pair of values  $\sigma(\alpha), \tau(\alpha)$  can be depicted by a point in the plane  $\sigma - \tau$ . Such points for all angles  $\alpha$  lie on a circle (Fig. 1.4), called **Mohr's circle** [1 – 4]. In the past, it was used for the geometrical determination of characteristic stresses. Today, this is no more necessary, as every computer program for stress analysis can calculate the



**Fig. 1.4.** Mohr's circle. *a) – stress components, b) construction of the circle.*



stress components in any section. Nevertheless, Mohr's circle remains a very useful tool that gives a good idea on mutual relationships of stress components in various directions and on the character of stressing. It also enables easy evaluation of safety of components from brittle or ductile materials, and the orientation of strain gauges for experimental determination of stresses in components and constructions. It is also useful in the analysis of fractures. We shall therefore look at it in detail.

**Mohr's circle** has a centre at point  $C [(\sigma_x + \sigma_y)/2; 0]$  and radius

$$\bar{R} = \sqrt{\left(\frac{\sigma_x - \sigma_y}{2}\right)^2 + \tau_{xy}^2} \quad (1.7)$$

The mutual magnitudes of the normal and shear stress depend on the orientation  $\alpha$  of the investigated cut. Two sections, containing angle  $\alpha$ , are represented in the Mohr's circle by rotation of the radiusvector by angle  $2\alpha$ . Two perpendicular sections ( $90^\circ$ ) correspond in this circle to the straight angle ( $2 \times 90 = 180^\circ$ ) and to two end points of the diameter. When constructing the Mohr's circle, we plot the shear stress as positive if it tries to rotate the element clockwise, and as negative, if it rotates the element anticlockwise. Always at least two mutually perpendicular directions exist, in which the shear stress equals zero, and normal stress has extreme value (Fig. 1.4). These directions and stresses are called **principal directions** and **principal stresses**,  $\sigma_1, \sigma_2$ . Stress  $\sigma_1$  is always the principal stress far right in the Mohr's circle. **Maximum shear stress**  $\tau_{\max}$  acts in the sections containing angle  $45^\circ$  with the directions of principal stresses; the corresponding rotation of the radiusvector in the Mohr's circle is  $90^\circ$ . It holds

$$\sigma_{1,2} = \bar{C} \pm \bar{R} = \frac{\sigma_x + \sigma_y}{2} \pm \sqrt{\left(\frac{\sigma_x - \sigma_y}{2}\right)^2 + \tau_{xy}^2} \quad (1.8a,b)$$

$$\tau_{\max} = \bar{R} = \sqrt{\left(\frac{\sigma_x - \sigma_y}{2}\right)^2 + \tau_{xy}^2} = \frac{\sigma_1 - \sigma_2}{2} \quad (1.8c)$$

The angle between the plane of the cut with stresses  $\sigma_x, \tau_{xy}$  and the principal plane with stress  $\sigma_1$  can be determined from the relationship

$$\varphi_0 = \frac{1}{2} \operatorname{arctg} \frac{2\tau_{xy}}{\sigma_x - \sigma_y} . \quad (1.9)$$

The knowledge of principal directions is important for the orientation of reinforcement, for example steel bars in concrete or fibers in a composite material, and also for orientation of strain gauges.

The construction of Mohr's circle will be shown on the following example.

**Example.**

In coordinate system  $x, y$  normal stresses  $\sigma_x = 120$  MPa,  $\sigma_y = 60$  MPa, and shear stress  $\tau_{xy} = 40$  MPa act. Determine the principal stresses  $\sigma_1, \sigma_2$  and their directions.

Solution. After inserting the input values into equations (1.7) – (1.9) we obtain:

$$\sigma_1 = \frac{120+60}{2} + \sqrt{\left(\frac{120-60}{2}\right)^2 + 40^2} = 90 + 50 = 140 \text{ MPa}$$

$$\sigma_2 = 90 - 50 = 40 \text{ MPa}$$

$$\tau_{\max} = \bar{R} = \sqrt{\left(\frac{120-60}{2}\right)^2 + 40^2} = 50 \text{ MPa}$$

$$\varphi_0 = \frac{1}{2} \operatorname{arctg} \frac{2 \times 40}{120 - 60} = 26,56^\circ .$$

The construction of Mohr's circle is obvious from Fig. 1.4.

Now, we shall look at several simple, but important cases. For each, the element with acting stresses is shown together with the corresponding Mohr's circle, and also the values of principal stresses and maximum shear stress are given.

**Simple (uniaxial) tension** (Fig. 1.5a)

Normal stress  $\sigma$  acts in the investigated section, but no shear stress acts here. This means that the stress  $\sigma$  is the principal stress  $\sigma_1$ , which makes the first point of the Mohr's circle. No stress acts in the perpendicular section, so that the corresponding point (0,0) forms the second point of the circle, and represents the second principal stress  $\sigma_2 (= 0)$ . The maximum shear stress corresponds to the radius of this circle (i.e.  $\tau_{\max} = \sigma/2$ ), and is inclined against the direction of stress  $\sigma$  by  $45^\circ$ .

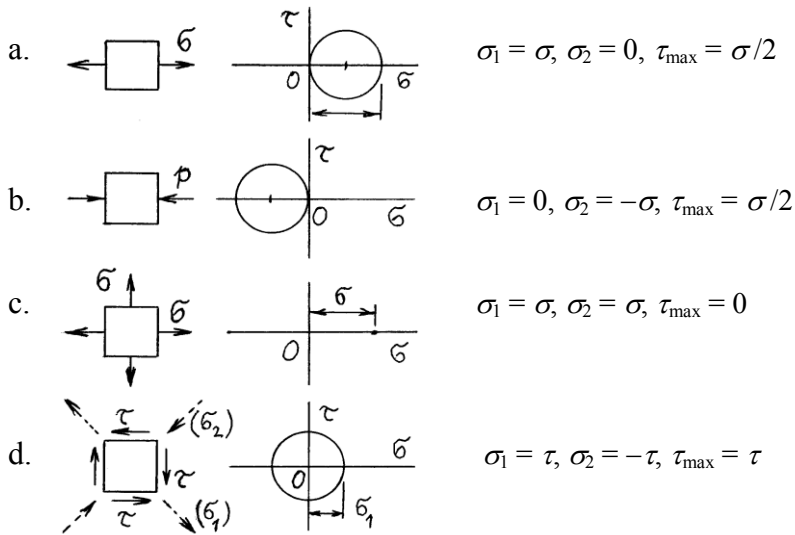


Fig. 1.5. Mohr's circles - examples.

### Uniaxial compression (Fig. 1.5b)

The situation is similar to the previous case, but the circle lies now in the half-plane of negative stresses. The principal stresses are  $\sigma_2 = -p, \sigma_1 = 0$  (the corresponding point of the Mohr's circle for  $\sigma_1$  is lying at right from  $\sigma_2$ ).

### Isotropic tension (Fig. 1.5c)

The values of stress in two mutually perpendicular directions are the same, and shear stresses are equal zero. Both points in the plane  $\sigma$ - $\tau$  have merged together, and the Mohr's circle has degenerated to a single point. No shear stress acts in this plane ( $\tau = 0$ ). The real situation, however, is more complex, as we shall see in the section about triaxial state of stress.

### Simple shear (Fig. 1.5d)

In this case, the center of Mohr's circle lies in the origin of coordinate system. No normal stresses act in the considered sections of the element, but only shear stresses, one positive and the other negative. The situation is the same as if in the cut inclined by  $45^\circ$  tensile stress  $\sigma_1 = \tau$  acts, and compressive stress  $\sigma_2 = -\tau$  in the perpendicular cut. The stresses  $\sigma_1, \sigma_2$  are the principal stresses.

This state of stress exists, e.g., in a rod of circular cross section, loaded by twist.

A rod or shaft from brittle material breaks in this case due to normal stress, as it is witnessed by oblique fracture surface (Fig. 1.6). Similarly, when wet washing is twisted, the water flows out of it thanks to compressive stress acting in the inclined sections. In the past, before reliable safety ski binding was developed, torsion fractures of skiers' shin-bones were rather common.

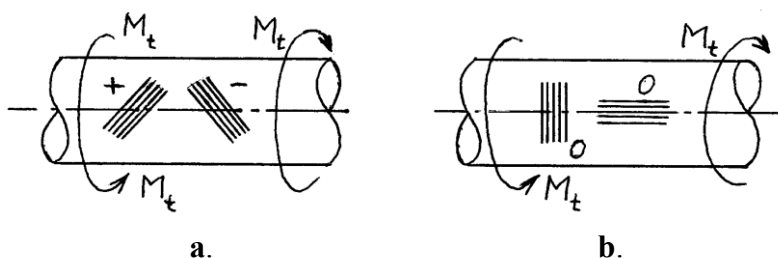


**Fig. 1.6.** Torsion fracture of a bar from brittle material.

As we shall see later, plastic deformations arise if the maximum shear stress attains the yield strength in shear; the plastic flow occurs by mutual sliding of material layers in the direction of shear stresses. This can be seen sometimes in a sheet of soft steel loaded by axial tension. Due to plastic flow systems of tiny lines appear at the edges of the sheet, which are inclined by  $45^\circ$  to the sheet axis (so-called Lüders lines, generated by the material slipping due to shear).

**Remark.** If twisting moment in a shaft should be measured by strain gauges, it is necessary to orientate them into the directions of maximum normal stresses, i.e. in the angle  $45^\circ$  to the shaft axis (Fig. 1.7a). If they were oriented in the direction of shaft axis or perpendicular to it (Fig. 1.7b), nothing could be measured, as the sensors react only to length changes. The arrangement of two strain gauges according to Fig. 1.7a, one loaded by tension and the other by compression, doubles the sensitivity, and, moreover, compensates the influence of temperature changes.

The Mohr's circle is useful also in the analysis of fractures, as we shall see later.

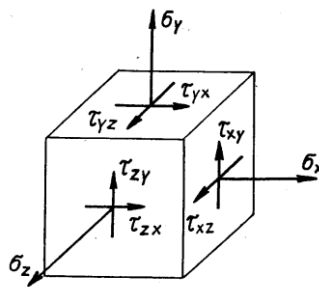


**Fig. 1.7.** Shaft loaded by twist, with strain gauges.

*a - suitable orientation of gauges, b - these sensors will measure nothing.*

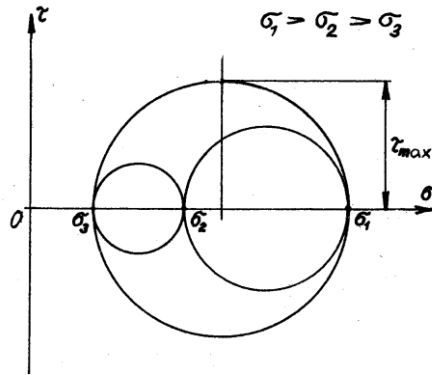
### 1.3 Triaxial state of stress

We have seen Mohr's circle for stresses acting in the plane  $x, y$ . Similarly, normal and shear stresses can act in the planes  $x, z$  and  $y, z$ . Every stress state is generally tri-axial (Fig. 1.8). In coordinate system  $x, y, z$ , three normal stresses exist:  $\sigma_x, \sigma_y, \sigma_z$  and six components of shear stresses:  $\tau_{xy}, \tau_{yx}, \tau_{yz}, \tau_{zy}$ , and  $\tau_{zy}, \tau_{xz}$ . Shear stresses are characterised by two subscripts; the first shows the direction normal to the plane of shear stress, and the other subscript shows the direction of the shear stress itself. This distinguishing is necessary: it is obvious from Fig. 1.8 that the shear stress in one plane (e.g.  $x$ ) can act in direction  $y$  or  $z$ . Normal stress acts always perpendicularly to the plane, so that one subscript is sufficient. (In theory of elasticity, two subscripts are sometimes used, as well). The description of stress state at a certain point needs nine stress components in general. With respect to the rule of complementary shear stresses it follows  $\tau_{xy} = \tau_{yx}, \tau_{yz} = \tau_{zy}$  and  $\tau_{zx} = \tau_{xz}$ , so that six values are sufficient: three for normal and three for shear stresses [1 – 4].



**Fig. 1.8.** Triaxial state of stress. Coordinate system and stress components.

Some stress components can equal zero. Principal stresses can be found in every plane. Always **three** mutually perpendicular directions exist, in which only normal stress acts, and shear stress equals zero. These are the **principal directions**, and the corresponding stresses are **principal stresses**, denoted  $\sigma_1, \sigma_2, \sigma_3$ . Generally, three Mohr's circles can be plotted, with  $\sigma_1 \geq \sigma_2 \geq \sigma_3$ ; the stress far right is always  $\sigma_1$  (Fig. 1.9). One circle corresponds to the plane  $x-y$ , the second to the plane  $y-z$ , and the third to the plane  $z-x$ . If the state of stress is defined by nine (or 6) stress components, the principal stresses and their directions can be obtained by solution of a cubic equation (see [1 – 3]); a common software for stress analysis can do it. The situation is simpler, if certain principal direction is known, for example from the symmetry of the body or from the character of load. Some principal directions



**Fig. 1.9.** Mohr's circles for triaxial state of stress.

are „natural“: radial and circumferential direction for a rotational body with axisymmetrical load, axial, circumferential and radial direction for a cylindrical pressure vessel. For a spherical pressure vessel, any tangential direction is also circumferential, and the stress state is isotropic; the third principal direction is radial. The axial direction in long bars, shafts and beams, loaded by axial force or bending moment is the principal direction. In plates, thin shells and plane problems, one principal direction is perpendicular to the surface; the same holds for unloaded surface of a body. In such cases the formulae given above (or Mohr's circle) are sufficient for finding the principal stresses.

The knowledge of principal directions is very important for the orientation of fibers in some composites, for orientation of reinforcement in concrete (the steel bars serve for transfer of tensile stresses and should be oriented in their directions), and for the proper orientation of strain gauges (Fig. 1.7). Their knowledge helps also in the analysis of fractures and identification of the causes of failures in machines or buildings, as we shall see later.

## 1.4 Strain

### Hooke's law

Components are deformed by acting stresses. The strain intensity is described by relative elongations  $\varepsilon$  and changes  $\gamma$  of the initially right angles (Fig. 1.1, 1.10),

$$\varepsilon = \Delta l / l, \quad u/a = \operatorname{tg} \gamma. \quad (1.10)$$

The angles  $\gamma$  are small for small strains, so that  $\operatorname{tg} \gamma \approx \gamma$ ;  $\gamma$  is called shear strain.

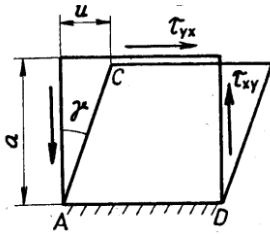


Fig. 1.10. Shear strain (a schematic).

Direct proportionality between normal stresses and strains exists for small strains in elastic bodies (till the proportionality limit). This is called Hooke's law, and its form for uniaxial load is

$$\varepsilon = \sigma / E \quad \text{or} \quad \sigma = \varepsilon E ; \quad (1.11)$$

$\sigma$  is normal stress and  $E$  is Young's tensile modulus of elasticity, defined as

$$E = \sigma / \varepsilon . \quad (1.12)$$

It corresponds to the stress, which would cause doubling of the initial length of the specimen (i.e.  $\varepsilon = 1$ ). It is thus measure of material stiffness.

Every state of stress is, in general, triaxial, with stresses and strains in all directions, and general Hooke's law is

$$\begin{aligned} \varepsilon_x &= [\sigma_x - \mu(\sigma_y + \sigma_z)] / E , \\ \varepsilon_y &= [\sigma_y - \mu(\sigma_z + \sigma_x)] / E , \\ \varepsilon_z &= [\sigma_z - \mu(\sigma_x + \sigma_y)] / E ; \end{aligned} \quad (1.13)$$

the subscript indicates the direction.  $\mu$  is the coefficient of transverse contraction, so-called Poisson's number, which expresses the ratio of shortening in transverse direction to the elongation in the load direction (Fig. 1.1):

$$\mu = \Delta D / D . \quad (1.14)$$

Hooke's law for shear strains is

$$\gamma_{xy} = \tau_{xy} / G , \quad \gamma_{yz} = \tau_{yz} / G , \quad \gamma_{zx} = \tau_{zx} / G ; \quad (1.15)$$

$\tau$  is shear stress, and  $G$  is the shear modulus, related to the tensile modulus as

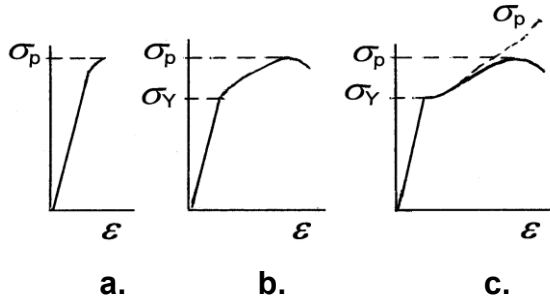
$$G = E / [2(1 + \mu)] , \quad \text{or} \quad E = 2(1 + \mu)G . \quad (1.16)$$

The stresses  $\sigma_x$ ,  $\sigma_y$  in plane stress can be expressed as functions of strains  $\varepsilon_x$ ,  $\varepsilon_y$ :

$$\sigma_x = \frac{E}{1-\mu^2} (\varepsilon_x + \mu\varepsilon_y), \quad \sigma_y = \frac{E}{1-\mu^2} (\varepsilon_y + \mu\varepsilon_x). \quad (1.17)$$

These formulae are used for the determination of stresses in constructions by means of strain gauges, which measure strains.

Fig. 1.11 shows tensile test diagrams of various materials. Brittle material (Fig. 11.1 a) breaks suddenly if the stress has reached the tensile strength  $\sigma_p$ . In ductile materials, the deformations start growing faster after the yield strength  $\sigma_Y$  has been attained, and permanent deformations remain after unloading. The yield strength is sometimes obvious by a dwell in the stress-strain diagram (Fig. 11.1c). Sometimes it is not visible (Fig. 11.1b); then it is defined as the stress, that causes permanent relative elongation  $0,2\% = 0,002$ . Various symbols are used. In material standards,  $R_e$  is used for pronounced yield stress and  $R_{p, 0,2}$  for imperceptible;  $f_Y$  is used in the codes for metallic structures; here we shall use  $\sigma_Y$  (in Czech literature also  $\sigma_k$ ). The ultimate tensile strength is denoted  $R_m$  or  $f_u$  (ultimate); in Czech literature (and here) also  $\sigma_p$ . Plastic deformations will be treated in detail in Chapter 4.



**Fig. 11.1.** Tensile tests of various materials. a - brittle materials, b, c - elastic-plastic materials.  $\sigma$  - stress,  $\varepsilon$  - strain.

### Mohr's circle for strains

Relative deformations depend on the orientation of the investigated plane. The pertinent expressions are similar to those for stresses:

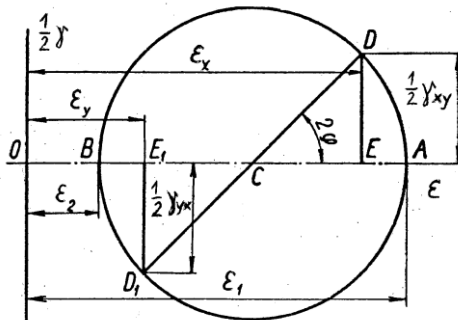
$$\varepsilon(\alpha) = \frac{\varepsilon_x + \varepsilon_y}{2} + \frac{\varepsilon_x - \varepsilon_y}{2} \cos 2\alpha + \frac{1}{2} \gamma_{xy} \sin 2\alpha, \quad (1.18a)$$

$$\frac{1}{2} \gamma(\alpha) = -\frac{\varepsilon_x - \varepsilon_y}{2} \sin 2\alpha + \frac{1}{2} \gamma_{xy} \cos 2\alpha. \quad (1.18b)$$



The term  $\frac{1}{2}$  at  $\gamma$  in (1.18) follows from the fact that  $\frac{1}{2} \gamma$  expresses the angle of rotation of the line of direction  $\alpha$ . The shear strain  $\gamma$  expresses the change of the right angle, and is created by the sum of rotations ( $\frac{1}{2}\gamma$ ) of two perpendicular lines.

The points  $\alpha(\alpha)$ ,  $\frac{1}{2} \gamma(\alpha)$  plotted in the system  $\varepsilon, \frac{1}{2} \gamma$  for various orientations of fictitious cuts lie on a circle similar to the Mohr's circle (Fig. 1.12). Similarly with stresses, we can also say for deformations that two mutually perpendicular directions exist, in which the shear strain equals 0 and strains are extreme. These are **principal strains** ( $\varepsilon_1, \varepsilon_2$ ) and lie in the **principal directions of elongation**.



*Fig. 1.12. Mohr's circle for strain.*

The principal directions of strains in isotropic materials coincide with the principal directions of stress. Their knowledge facilitates the orientation of strain gauges; if possible, they should lie in principal directions. It is thus reasonable to make general analysis of stress state in the component before gluing the strain gauges.

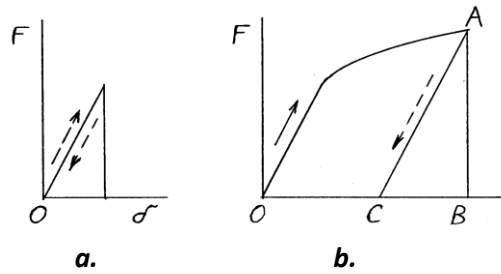
### 1.5 Work of loading forces and strain energy

A compliant body is deformed, when loaded. This causes movement of the acting forces, which do work. This work is positive, if the displacement occurs in the direction of force, and negative, if the displacement direction is opposite. (Work is also done by the moments during their rotation.) The work performed by constant force equals the product of the force and displacement,  $W = F\delta$ . If the force  $F$  varies during deforming (Fig. 1.13), the work must be calculated as the integral

$$W = \int_{(L)} F d\delta. \quad (1.19)$$

In elastic bodies with direct proportionality between the force and deformation,

$$F = k \delta, \quad (1.20)$$



**Fig. 1.13.** Deformation work. *a* – elastic deforming, *b* – deforming elastic-plastic. *OABO* – work expended during loading, *ACB* – energy released during unloading.

the work equals

$$W = \frac{1}{2} F \delta = \frac{1}{2} k \delta^2 = \frac{1}{2} F^2 / k; \quad (1.21)$$

$k$  is the stiffness, corresponding to the force needed for causing the deformation of unit magnitude. If an elastic body is deformed, the *work of loading forces is transformed into potential energy of elastic strains*,

$$W = U. \quad (1.22)$$

This is the **law of energy conservation**. The potential energy can be expressed by means of forces and displacements, and then by means of stresses and strains.

For example, the energy accumulated in a rod of length  $l$  and section area  $S$ , loaded by axial force  $F$ , is

$$U = \frac{1}{2} \sigma S \times \varepsilon l = \frac{1}{2} \sigma^2 / E \times Sl = \frac{1}{2} \varepsilon^2 E Sl. \quad (1.23)$$

All these expressions contain the term  $Sl$ , which is the volume of the rod. Division of the expressions (1.23) by the volume yields energy per unit volume, called **strain energy density  $\mathcal{A}$** . This is used for the evaluation of the possibility of fracture or plastic deformations (see Chapter 8).

If the body is unloaded, the deformations and accumulated energy disappear.

The energy conservation law enables sometimes a very quick estimation of forces or stresses in a body, for example under impact, as it will be shown further.

### Example.

A vehicle with an elastic bumper hits a massive wall by velocity  $v = 10$  km/h. Determine the maximum force, if the vehicle has the mass  $m = 1000$  kg, and the

stiffness of the bumper is  $k = 500 \text{ N/mm} = 500000 \text{ N/m}$ .

Solution. The maximum force at impact can be obtained easily from the law of energy conservation. At the beginning the vehicle has kinetic energy  $E_{kin}$ , which is gradually changed into the potential energy  $U_{pot}$  in the bumper spring. The initial velocity is  $v = 10000/3600 = 2,78 \text{ m/s}$ , so that the kinetic energy  $E_{kin} = \frac{1}{2} mv^2 = 3865 \text{ J}$ . Rearrangement of Equation (1.21) gives

$$F_{max} = \sqrt{2kE_{kin}} = \sqrt{2 \times 500000 \times 3865} = 62169 \text{ N}.$$

This force can be used for the determination of the path and time to stopping. The pertinent expressions and results are presented in Chapter 4 of the book [5].

Loads often cause permanent deformations (Fig. 1.13b). The direct proportionality between deformation and force is no more valid, and the work must be calculated according to the general formula (1.19). The total work of deforming equals the sum of the potential energy of elastic stresses and of the dissipated work. During unloading, only elastic part of the deformation and work disappears, as obvious from Fig. 1.13b. The energy is spent irreversibly for plastic deforming and for the friction or for creation of new fracture surfaces in fracture processes. Equation (1.19) is valid also in these cases. The energy spent in irreversible processes is often much larger than the accumulated energy of elastic stresses.

### References to Chapter 1.

1. Höschl, C.: Pružnost a pevnost ve strojnictví. SNTL, Praha, 1971. 375 p.
2. Kolektiv: Pružnost a pevnost I. Skriptum ČVUT, Fakulta strojní, Praha, 1965. 272 p.
3. Novák, O. a kolektiv: Nauka o pružnosti a pevnosti ve stavitelství. Technický průvodce, sv. 3. SNTL, Praha, 1963. 536 p.
4. Timošenko, S. P.: Soprotivlenije materialov I. Fizmatgiz, Moskva, 1960. 380 p. (Timoshenko, S. P.: Strength of materials. Part I. Elementary theory and problems. D. van Nostrand Company, Inc., Princeton, New Jersey, 1955.)
5. Menčík, J.: Impacts and vibrations. University of Pardubice, Pardubice, 2018. 132 p. ISBN 978-80-7560-165-0. Available freely after writing the book title into the search engine Google, or via web: <https://hdl.handle.net/10195/70531>.

## 2. Finite element method, analytical and numerical methods

### 2.1 Finite element method

The analysis of stresses and deformations in complex construction and components is done mostly by the finite element method (FEM). Various commercial programs exist for this method, which are used by design engineers and researchers. This section will be, therefore, limited to basic information.

The **finite element method** is a numerical method, which, after the first steps in the second half of the last century, has proven as very powerful, and was gradually developed for solution of problems in mechanics of bodies, heat transfer, flow of liquids and gases, magnetic fields, and other areas [1 – 5]. We shall use a brief interpretation from the mechanics of elastic bodies, where the method is based on the Lagrange principle: *In stable equilibrium, the total potential energy of the system, consisting of the deformation energy and the decrease of the potential energy of the loads, is minimum,*

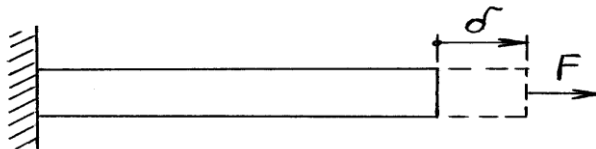
$$\Pi = \Pi_{\delta} + \Pi_z = \min ! \quad (2.1)$$

This principle will be illustrated here on a simple body – a rod with one end fixed and the other loaded by axial force  $F$  (Fig. 2.1). This force is related with the displacement  $\delta$  of the free end by the formula

$$F = K \delta; \quad (2.2)$$

$K = F/\delta$  is the rod stiffness in tension; here  $K = F/[FL/(ES)]$ , where  $L$  is the length of the rod,  $S$  is the area of its cross section, and  $E$  is the modulus of elasticity in tension. During deforming, strain energy was accumulated in the bar

$$\Pi_{\delta} = \frac{1}{2} F \delta = \frac{1}{2} K \delta^2. \quad (2.3)$$



**Fig. 2.1.** Rod loaded by axial force.

The force  $F$  moves by  $\delta$  and its potential energy decreases by  $\Pi_z = F\delta$ . The total energy of the system equals

$$\Pi = \frac{1}{2} K\delta^2 - F\delta. \quad (2.4)$$

According to the Lagrange principle this energy will be minimum for such displacement  $\delta$ , for which its derivative (with respect to the path) will be zero. Differentiating Equation (2.4) by  $\delta$  gives

$$d\Pi/d\delta = K\delta - F = 0. \quad (2.5)$$

This expression can be rewritten into the form

$$K\delta = F, \quad (2.6)$$

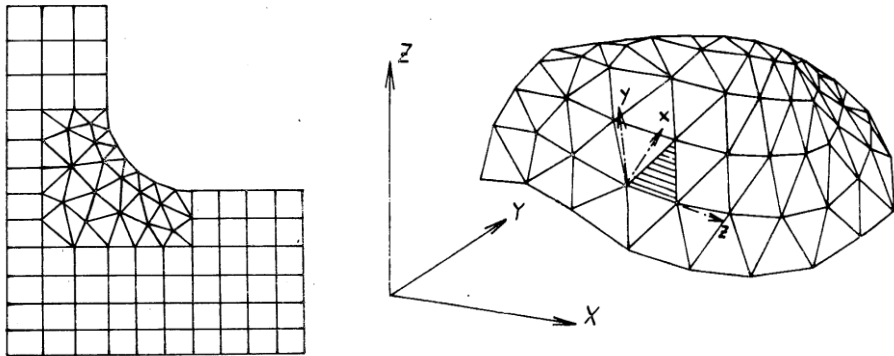
which says „**force  $F$  equals the product of deformation  $\delta$  and stiffness  $K$** “. Vice versa, the solution of Eq. (2.6) for the known load and stiffness yields the value  $\delta$ . For the above rod of stiffness  $K = ES/L$ , the known formula for elongation,  $\delta = F/K = FL/(ES)$ , is obtained.

The Lagrange principle was applied first on simple bodies, in the form of so-called Ritz method. With this method, the deformations of the body are expressed by means of simple functions, e.g. polynomials:  $w = a_0 + a_1x + a_2x^2 \dots$ . Then, Hooke's law is used for the determination of deformations and stiffness from the strains and elastic properties. Since the displacements depend on (yet unknown) values of constants  $a_0, a_1, a_2, \dots, a_{n-1}$ , the minimum of potential energy is sought so that the expression (2.6) is differentiated by each of them,  $d\Pi/da_j$ , and each derivative is put equal zero. This gives a system of  $n$  linear equations. Its solving yields the unknown constants, and the deformations and stresses in the body.

A disadvantage of the Ritz' method is that it always works with only one approximation function  $w = f(x)$  for the whole body. Therefore, it cannot be adjusted to a more complicated body shape or load distribution. Fortunately, in the sixties it was only one step from here to the finite element method, the more so that this was the time of advent of computers, which are indispensable for it. At that time, moreover, also the use of matrix methods for the analysis of large truss structures became common.

With the finite element method, the analysed body is divided by fictitious cuts into high number of small parts, so-called finite elements, which are connected together

in nodal points (Fig. 2.2). The mesh of elements is created so that the loads act in nodes. The solution finds the displacements of the individual nodes, from which the strains, internal forces and stresses in various places are calculated. The work with high numbers of these values is facilitated by their arrangement into matrices.



**Fig. 2.2.** Finite element method – examples of simple meshes [4].

The displacements within individual elements are usually expressed by polynomials; for example, a polynomial of second degree for the  $j$ -th element is:  $w_j = a_{0j} + a_{1j}x + a_{2j}x^2$ . It is important that the deformations of individual elements can be approximated by various functions, provided that the conditions of equilibrium and boundary conditions are satisfied. The displacements are then used for the creation of strain and stiffness matrices of the individual elements. In the following step these matrices are composed together so that the **stiffness matrix** of the whole body is created. Load matrix and node displacements matrix for the whole body are created in similar way. The advantage of matrix notation is its simplicity and clear arrangement. The **basic equation of the finite element method** looks identically to Equation (2.6) for the deformation of a spring loaded by force  $F$ . The difference between them is that  $\mathbf{K}$ ,  $\mathbf{F}$  and  $\boldsymbol{\delta}$  in the finite element method represent matrices of the body stiffness, load and displacements of all nodes. The arrangement of the individual values into the pertinent matrices is a matter of a mathematician or programmer. The final task is the solution of a large system of equations with several hundreds to several hundred thousands of unknowns.

Programs for the finite element method consist of three parts: preprocessor, processor (solver), and postprocessor.

**Preprocessor** serves for the definition of the body geometry, prescription of material properties, loads and boundary conditions. Every commercial FEM program offers ample choice of elements and material models. Some programs are suitable especially for certain problems, such as plastic deformations or contact problems, analysis of elastomeric materials, dynamic problems, etc.

**Solver (processor)** contains tools for the solution of large systems of linear equations. It was just the finite element method and its big potential for solution of problems in automotive and aircraft industry, which have contributed to the development of efficient methods for solution of large systems of equations.

**Postprocessor** processes large amounts of calculated values, for example node displacements, and from them it calculates strains, stresses and forces. It also calculates the values of equivalent stresses according to various failure hypotheses. For better illustration it presents them in graphic form and in colours.

The well-known finite element method (FEM) programs are (in alphabetical order) Abaqus [6], Ansys [7], Cosmos [8], LS Dyna [9] and Marc [10]. They also enable solution of nonlinear problems, for example large deformations, plasticity and contact problems, dynamic or flow problems, and other. Some programs are integrated into systems for computer aided design CAD.

More information on the individual programs can be found via the pertinent web pages.

## **2.2 Use of numerical and analytical methods for problems in mechanics**

Computers have changed solution of many problems. The analysis of stresses and deformations of complicated components is today done mostly by the finite element method. This method and the pertinent programs are universal – suitable software can solve nearly everything. This is a big difference compared to the pre-computer time, when a specific method of solution existed for every kind of problem. The deflection of beams was obtained by integration of the differential equation of deflection curve, by the Mohr's method, by means of Castigliano's theorem, or by other methods. Twist of rods was solved by means of differential equations ordinary or partial, but also in experimental way using so-called membrane analogy. The solution for circular plates was obtained by integration of

simple differential equation. Rectangular plates, on the other hand, needed the finite differences (mesh) method or the use of Fourier series. With elastic-plastic deformations, only the simplest material models and geometries could be analysed.

On the other hand, the algorithm for the use of the FEM is the same for the solution of any problem: proposal of the element types and creation of the corresponding mesh in the investigated body, definition of suitable material models, boundary conditions and loads, and „letting the computer to do its job“. Then, „only“ the analysis of results and interpretation of them follow. No wonder that if a design engineer has got some experience with the finite element method, he is no more willing to solve the problems by older „classic“ ways. However, each of them confirms that he (or she) needed a lot of time to master the FEM, and made many mistakes at the beginning, such as defining the boundary conditions, creation of the mesh, or description of the loads. Sometimes he also admits that he faced to a problem, which even recognised software was unable to solve. We should not forget that also the FEM codes have been gradually improved, partly thanks to solving problems from actual practice, and this often revealed their weak places, which were gradually removed.

The computers take the burden of the routine calculations from the design engineer, and give him a space for better understanding the problem and considering all possible loads, actual shape of the structure, boundary conditions and material properties, and, therefore, give the space for general increase of technical level and reliability of the designed object. This, however, needs also some theoretical knowledge. And, as E. Becker has said,

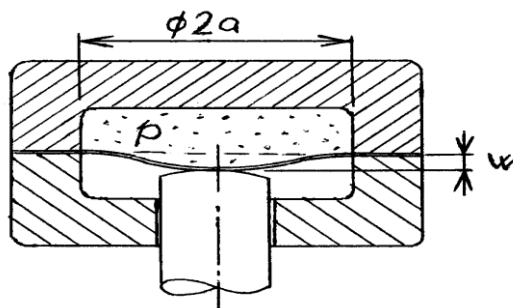
***computation without a good theory is nothing else than production of rubbish.***

The statistics from the past show that about 30% of failures of civil engineering structures were due to “misunderstanding of their static action” during the design stage. A good design engineer must understand the terms “force equilibrium” and the “method of fictitious cut”, understand the difference between the normal and shear stress, know the main features of stresses in uniaxial and multiaxial loads, and understand the origin and effects of thermal stresses. He should understand the term strain energy density, and know the criteria of material failure both brittle and ductile. He (or she) must also be aware that real structures contain some imperfections and that the computations are often done under simplifications regarding the geometry, loads, and material models. The analytical (or technical)



science on the strength of materials is very important even in this „computer age“. It provides the engineer with general view on the matter and with the terminology and concepts. It also shows the solutions of basic problems, which can be used for testing of new procedures and programs. In certain sense of the word, these solutions are asymptotical, similar to beacons in the unknown sea, in which we sail. The simple analytical solutions have also other advantages. They show illustratively, which factors influence the result, and enable very easy and vivid assessment of the influence of the individual factors. (Of course, one must always be aware of the conditions and limitations of validity of these solutions.) The analytical solution for small deflections of thin beams teaches us the engineering way of thinking. It was here that the preliminary analysis enabled neglecting of insignificant terms, and this then markedly simplified the solution. Also, the approximate models used in some finite elements are based on simplified analytical models. Analytical formulae can also be transformed easily to nondimensional expressions, corresponding to similarity criteria (cf. Chapter 14). Therefore, they enable - similarly to the mentioned beacons - to direct the design proposal in the right direction in the early stages of design. As an example, a problem from technical practice will be shown here.

**Example.** The force pushing the movable part of vulcanisation press is generated by the pressure of compressed air on a circular membrane (Fig. 2.3). A steel membrane was used in the original design (as usual in mechanical appliances), but it broke after short time of operation. Despite of several attempts to improve the shape using demanding FEM computations, with changes of the shape at places of stress concentration, the stresses remained always very high. Therefore, general analysis of stresses in a circular elastic plate was done. The basic formulae for the deflection  $w$  of a plate of thickness  $h$  and radius  $a$ , loaded by pressure  $p$ , and for the



*Fig. 2.3. Pressure chamber of the mechanism in a vulcanisation press.*

maximum stress acting in radial direction at clamping are [5]:

$$w_{\max} = \frac{pa^4}{64D} = \frac{3}{16} \frac{p(1-\mu^2)}{Eh^3} \left(\frac{a}{h}\right)^3 a ; \quad \sigma_{\max} = \frac{3}{4} \left(\frac{a}{h}\right)^2 p, \quad (2.7)$$

The combination of these equations gives, after a rearrangement, the following expression for maximum stress:

$$\sigma_{\max} = 4 \frac{E}{1-\mu^2} \frac{h}{a} \frac{w_{\max}}{a} ; \quad (2.8)$$

$E$  and  $\mu$  are Young modulus and Poisson's number of the plate material. It is obvious that the stress, corresponding to the prescribed deflection  $w$  (needed for the demanded motion of the movable part of the mould), could be significantly reduced only by reduction of the bending stiffness of the membrane, especially by significant lowering the modulus of elasticity. The simplest solution, which then appeared as successful, was the replacement of the original steel membrane by a membrane from a special polymer. Its elastic modulus, lower by four orders, has ensured that, despite of much larger thickness of the membrane, the operation stresses were lower than fatigue strength of this elastomer.

Equations (2.7) and (2.8) can be expressed in nondimensional form, in which they would be more general. Dimensional analysis and similarity will be addressed in Chapter 15.

The presented example has shown that general analytical relationships can sometimes show direction to very efficient solutions, even with the use of less traditional materials. (As regards materials selection, the excellent book [12] by M. F. Ashby can be recommended.) For similar reasons and with the aim to support the engineering way of thinking, simple analytical approach will be used also in this book.

## References to Chapter 2.

1. Španiel, M., Horák, Z.: Úvod do metody konečných prvků. ČVUT, Praha, fakulta strojní, 2011, 158 p. Available (14. 2. 2019) at:  
[http://www.fsiforum.cz/upload/soubory/knihy/mechanika/uvod\\_do\\_metody\\_konecn\\_ych\\_prvku.pdf](http://www.fsiforum.cz/upload/soubory/knihy/mechanika/uvod_do_metody_konecn_ych_prvku.pdf)

2. Kolář, V., Němec, I., Kanický, V.: FEM principy a praxe metody konečných prvků. Computer Press, 2001. 401 p.
3. Höschl, C.: Úvod do metody konečných prvků. (Cyklus Stavba strojů XXXVIII.) DT ČSVTS, Praha, 1976. 123 p. Available (11. 3. 2019) at: [http://www.it.cas.cz/files/skripta/04\\_UVOD%20DO%20METODY%20KP-ocr150.pdf](http://www.it.cas.cz/files/skripta/04_UVOD%20DO%20METODY%20KP-ocr150.pdf)
4. Teplý, B.: Maticová analýza konstrukcí. Metoda konečných prvků. VUT, Brno, 1984. 98 p.
5. Höschl, C.: Pružnost a pevnost ve strojnictví. SNTL, Praha, 1971. 375 p.
6. ABAQUS. 6.13; Getting started with Abaqus interactive edition. Dassault Systemes Simulia Corp., Providence, RI, 2013.
7. Ansys: <https://en.wikipedia.org/wiki/Ansys>, <https://www.ansys.com/>  
<https://www.techsoft-eng.cz/software/ansys-fluent>,  
<https://www.svsfem.cz/produkty/explicit/ansys-ls-dyna>
8. Cosmos: <http://www.swmath.org/software/4289>
9. LS DYNA: <https://en.wikipedia.org/wiki/LS-DYNA>,
10. MARC a další produkty ze skupiny MSC:  
<http://www.mssoftware.com/products>
11. Kolektiv: Pružnost a pevnost II. Skriptum ČVUT, Fakulta strojní, Praha, 1985. 214 p.
12. Ashby, M. F.: Materials selection in mechanical design. Pergamon Press, Oxford – New York, 1992.

### 3. Failure hypotheses and criteria

If a component should be dimensioned, one needs to know the load that would cause failure, either by fracture or by plastic deforming. The state of stress is often multiaxial, with various stress components ( $\sigma$ ,  $\tau$ ) in various directions. The ultimate strength and the yield stress are usually measured in uniaxial tension or compression. We thus need to have rules for the determination of equivalent stress (from the known stress components), which could be compared with the yield or ultimate strength. The **equivalent stress** is such *uniaxial normal stress, which has the same effect on the possible failure, as the investigated triaxial stress state*.

Several criteria have been proposed for the evaluation of possible failure by brittle fracture (i.e. without observable change in shape), and for the creation of permanent (plastic) deformations. Some of these strength hypotheses will be described here.

#### 3.1 Brittle fracture

##### Hypothesis of maximum normal stress (Rankine)

*The component fails if the maximum tensile stress attains (or exceeds) the tensile strength  $\sigma_{p,t}$ , or if the maximum compressive stress attains the uniaxial strength in compression  $\sigma_{p,d}$ .* It is always principal stress, so that the conditions are

$$\sigma_{eq} = \sigma_1 \geq \sigma_{p,t} \text{ , or } \sigma_{ekv} = |\sigma_3| \geq \sigma_{p,d} . \quad (3.1)$$

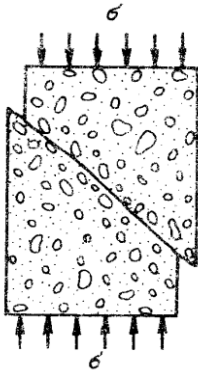
##### Hypothesis of maximum shear stress (Guest)

It was formulated from the observation that a brittle specimen, loaded by uniaxial compression, fails by shear under  $45^\circ$ , that is in the direction of maximum shear stress (Fig. 3.1). It says: *Fracture occurs if the maximum shear stress attains the shear strength,*

$$\tau_{max} \geq \tau_p . \quad (3.2)$$

Two stress states are equivalent if they have the same value of maximum shear stress. This stress equals the radius of the largest Mohr's circle (Fig. 1.9). For triaxial stress,  $\tau_{max} = (\sigma_1 - \sigma_3)/2$ . For uniaxial stress state,  $\tau_{max} = \sigma_1/2 = \sigma_{eq}/2$ . Comparison of shear stresses in both cases gives, after a rearrangement,

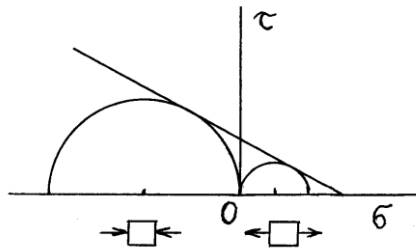
$$\sigma_{eq} = \sigma_1 - \sigma_3 \geq \sigma_{p,t} . \quad (3.3)$$



**Fig. 3.1.** Shear failure under compression.

### Mohr – Coulomb hypothesis

The compressive strength of brittle materials is usually several times higher than the tensile strength, and the above hypotheses do not consider sufficiently the simultaneous action of tensile and (higher) compressive stress in various directions. According to O. Mohr, *failure occurs if the largest Mohr's circle touches certain limit curve, constructed as the envelope of Mohr's circles corresponding to failures at various combinations of tensile and compressive stresses*. Coulomb then proposed the limit curve as the straight line touching the Mohr's circles for uniaxial tension and uniaxial compression (Fig. 3.2).



**Fig. 3.2.** Mohr – Coulomb failure criterion.

## **3.2 Onset of plastic deformations**

### Hypothesis of maximum shear stress (Tresca)

*Plastic flow of material occurs if the highest shear stress reaches the yield strength in shear* (Fig. 1.9). This hypothesis is similar to Guest's one, and similar also is the expression for equivalent stress:

$$\sigma_{\text{eq}} = \sigma_1 - \sigma_3 \geq \sigma_Y . \quad (3.4)$$

### Hypothesis of distortion energy density (von Mises, HMM)

Beltrami has proposed a hypothesis saying that failure occurs if the density of strain energy  $\Lambda$  attains certain critical value. This hypothesis, however, is not universal, because a homogeneous material can sustain any high hydrostatic pressure without failure. Richard von Mises has proposed to split the stress state (and the strain energy densities) into two components: one, corresponding to the change of volume, and the other, corresponding to the shape change. According to von Mises, *ductile material starts deforming permanently, if the strain energy density corresponding to the shape change attains a critical value*. Comparison of the energy densities for shape change in a triaxial case and in the uniaxial tension by equivalent stress gives the following expression for the equivalent stress [1 – 5]:

$$\sigma_{\text{ekv}} = \sqrt{\sigma_x^2 + \sigma_y^2 + \sigma_z^2 + \sigma_x\sigma_y + \sigma_y\sigma_z + \sigma_z\sigma_x + 3(\tau_{xy}^2 + \tau_{yz}^2 + \tau_{zx}^2)} . \quad (3.5a)$$

This expression shows strong influence of shear stresses on the onset of plastic deforming. If, for example, only shear stress  $\tau_{xy}$  acts (and all other stress components are equal zero), its influence is the same as if uniaxial tensile stress of magnitude  $\sigma_x\sqrt{3}$  would act, which is by 73% higher! The equivalent stress (3.5a) can also be expressed by means of principal stresses:

$$\sigma_{\text{ekv}} = \frac{\sqrt{2}}{2} \sqrt{(\sigma_1 - \sigma_2)^2 + (\sigma_2 - \sigma_3)^2 + (\sigma_3 - \sigma_1)^2} . \quad (3.5b)$$

The expressions in brackets correspond to diameters of Mohr's circles, and the diameter of each circle equals two times the maximum shear stress in the pertinent plane (Fig. 1.9). We thus see that the influence of shear stresses is present even in the criterion based on the strain energy density; moreover the influence of all three shear stresses, in contrast to only maximum shear stress in Tresca's criterion. However, it is impossible to say which criterion is better. They both are used.

Comment. The symbol HMM gives the first letters of the names of three persons who contributed to the formulation of this criterion: Huber, Mises, Hencky.

Remark. Equivalent stress, defined by Eq. (3.5a) or (3.5b) is also called **stress intensity**.

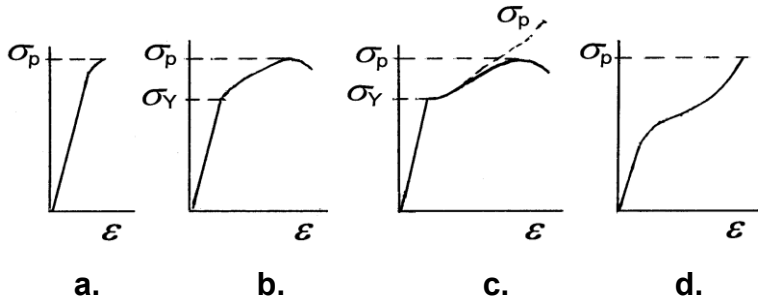
The values of equivalent stress determined by both criteria coincide in some cases (e.g. uniaxial tension), while they differ in others. The largest difference is for pure shear. The equivalent von Mises stress is  $\sigma_{eq} = \sqrt{3} \tau$ , while Tresca's stress is  $\sigma_{eq} = 2\tau$ , that is by 15% more. Also these differences (and the impossibility to decide, which criterion is more correct) are one of the reasons for the use of the **factor of safety** in design. Another reason is insufficient knowledge of strength or yield stress of the material. (Caution ! The minimum strength, as given in material data sheets, corresponds to 5% quantile of strength. This is such value, that probability 5% exists of occurrence of weaker products. If the design engineer would like to ensure safety of its products only by dimensioning them according to this "minimum" strength, every 20-th piece would fail!) Further reason for the use of safety factor is insufficient knowledge of loads, which are related to the conditions of operation (for example weight and distribution of cargo in the vehicle, its velocity, conditions of the road and also condition of the suspensions and damping), and other factors.

### References to Chapter 3.

1. Höschl, C.: Pružnost a pevnost ve strojnictví. SNTL, Praha, 1971. 375 p.
- 2, Kolektiv: Pružnost a pevnost I. Skriptum ČVUT, Fakulta strojní, Praha, 1965. 272 p.
3. Novák, O. a kolektiv: Nauka o pružnosti a pevnosti ve stavitelství. Technický průvodce, sv. 3. SNTL, Praha, 1963. 536 p.
4. Němec, J., Dvořák, J., Höschl, C.: Pružnost a pevnost ve strojírenství. SNTL, Praha, 1989. 600 p.
5. Pešina, E.: Základy užití teorie plasticity. SNTL, Praha, 1966. 188 p.

## 4. Basics of plasticity

Figure 4.1 shows diagrams of tensile tests of various materials. Brittle materials fail suddenly (Fig. 4.1a) if the stress attains the ultimate strength  $\sigma_p$ , while ductile (metallic) materials can sustain also permanent change of shape. Figures 4.1b, c show work diagrams of elastic-plastic materials, for example steels.



**Fig. 4.1.** Tensile test diagrams of various materials. a - brittle materials, b, c - elastic-plastic materials, d - elastomeric materials (e.g. rubber).

$\sigma$  - stress,  $\varepsilon$  - strain,  $\sigma_p$  - tensile strength,  $\sigma_Y$  - yield strength.

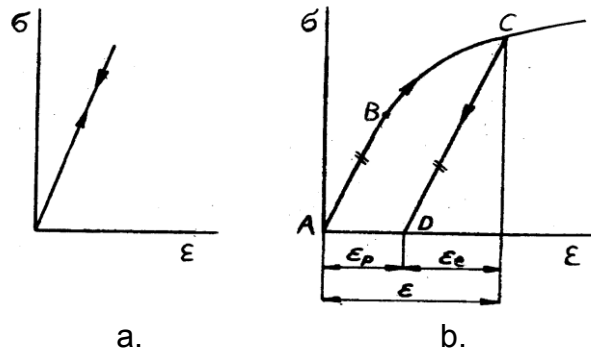
If the stress is lower than the yield strength  $\sigma_Y$ , the deformations are reversible and disappear after unloading. Until the proportionality limit  $\sigma_e$  linear relationship (Hooke's law) exists between stress  $\sigma$  and strain:

$$\varepsilon = \sigma/E ; \quad (4.1)$$

$\varepsilon$  is strain, and  $E$  is the modulus of elasticity in tension. Hooke's law is valid in similar form also for multiaxial state of stress, and also for shear deformations.

The situation during loading and unloading of elastic-plastic materials is depicted in Fig. 4.2. If the stress has not exceeded the yield limit, during unloading the record returns back along the initial curve, and the deformation disappears (Fig. 4.2a). If the stress exceeds the yield strength (point B in Fig. 4.2b), deformations start increasing faster. The following unloading (from point C in Fig. 4.2b) proceeds in the diagram along the straight line parallel to its initial part, and permanent deformations remain in the material (point D). During new loading, the deforming proceeds first along the straight line DC. If the load increases further, the loading curve proceeds from the point C along the initial solid line.





**Fig. 4.2.** Stress-strain diagram of a material: elastic (a) and elastic-plastic (b).  
 $\varepsilon$  - strain,  $\varepsilon_e$  - elastic component of strain,  $\varepsilon_p$  - plastic component of strain.

If residual stresses remained in the body from the previous load, they are summed with the stress from new loading.

Reaching the yield stress does not mean end of use of the component. Everybody has seen a car whose metal body showed permanent traces of previous collision with another vehicle or obstacle. If the deformations are not too large, the vehicle can fulfil its task further, though in limited extent. Metal constructions for civil engineering tolerate small plastic strains if they do not endanger the safety and proper function of the structure. This brings better utilisation of the material and reduces the costs. However, the designer must know what he can afford. Especially he (or she) must have sufficient knowledge on material properties.

#### 4.1 Material properties

The basis is the **stress-strain diagram of the material**, obtained in a tensile test. For better understanding, these diagrams are often approximated by simple expressions. Three most usual approximations are shown in Fig. 4.3 [1 – 6]:

1) Bilinear function (Fig. 4.3a):

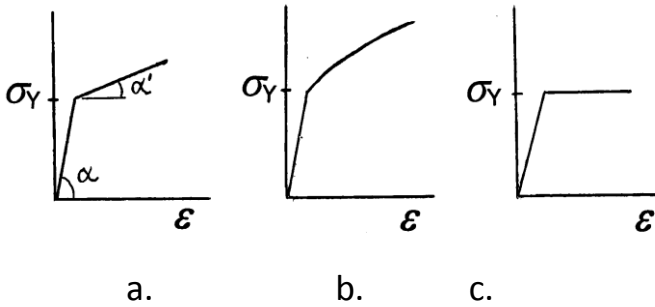
$$\sigma \leq \sigma_Y, \quad \varepsilon = \sigma/E \quad \sigma_Y \text{ is the yield strength} \quad (4.2a)$$

$$\sigma > \sigma_Y, \quad \varepsilon = \varepsilon_Y + (\sigma - \sigma_Y)/E'; \quad E' \text{ is the strain-hardening modulus} \quad (4.2b)$$

2) Power-law function (Fig. 4.3b),

$$\sigma \leq \sigma_Y, \quad \varepsilon = \sigma/E \quad (4.3a)$$

$$\sigma > \sigma_Y, \quad \varepsilon = K\sigma^m; \quad K, m \text{ are constants} \quad (4.3b)$$



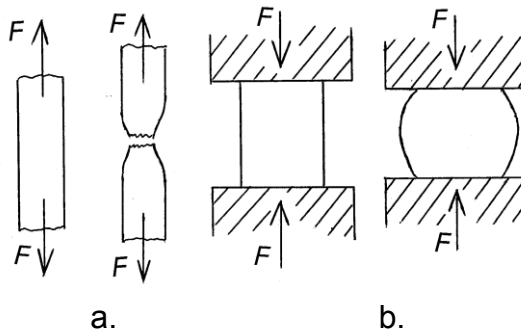
**Fig. 4.3.** Idealised stress-strain diagrams. *a* – bilinear function,  $\operatorname{tg} \alpha = E$ ,  $\operatorname{tg} \alpha' = E'$ , *b* – power-law function, *c* – ideal elastic-plastic material without strain hardening.

3) Ideal elastic-plastic material without strain-hardening (Fig. 4.3c).

$$\sigma \leq \sigma_Y, \quad \epsilon = \sigma/E \quad (4.4a)$$

$$\epsilon > \epsilon_Y, \quad \sigma = \sigma_Y \quad \epsilon_Y \text{ is the strain for } \sigma = \sigma_Y \quad (4.4b)$$

These expressions and diagrams are valid only for small strains. Stress in common tensile tests is usually calculated as the load divided by the nominal area of the cross section,  $\sigma = F/S$ , and such **diagrams** are called **conventional**. The fact, that also the size of cross section changes, is neglected. This is acceptable for strains smaller than several percent. At larger deformations the changes of the cross section area are not negligible, and the true stress starts differing significantly from the nominal one. The relationship between the true stress and strain at tensile test of a soft steel is shown in Fig. 4.1c by dashed line. The differences increase especially at stresses approaching the ultimate strength, when a neck is formed at the place of the future fracture (Fig. 4.4a).



**Fig. 4.4.** Large deformations of ductile materials under: *a* – tension, *b* - compression

The opposite situation exists under compression: the cross section area becomes larger (Fig. 4.4b) and the true compressive stress lower than the nominal ones. Very ductile material could sustain uniaxial compressive load nearly without limits. For example, thin Al foils are produced by rolling from massive blocks.

In some materials, for example low-carbon steels, the yield strength is easily recognisable by the dwell in the stress-strain diagram (Fig. 4.1c). This limit is denoted in material data sheets [7] as  $R_e$ . If the stress-strain curve is smooth (Fig. 4.1b), the yield stress is defined as such stress, which causes permanent relative elongation  $0,2\% = 0,002$ . This value, denoted  $R_{p,0,2}$ , was chosen for practical reasons. It can be revealed from the diagram of tensile test without extreme demands on measuring technology, and usually does not preclude the use of the component. The ultimate strength is denoted  $R_m$ ; here, symbol  $\sigma_p$  will be used.

Remark. In codes for steel structures, yield stress is denoted  $f_Y$  and ultimate strength  $f_u$ .

Several words must be said here to the approximations of stress-strain diagrams. The first two (Figs 4.3a,b) are easily understandable, as they correspond to the stress-strain diagrams for metals without pronounced yield limit (Fig. 4.1b). The approximation shown in Fig. 4.3c, i.e. ideal elastic-plastic material without strain hardening, seems to be unrealistic. However, it corresponds acceptably to the left part of the stress-strain diagram of material with pronounced yield limit, such as low-carbon structural steel (Fig. 4.1c). We must not forget that even if plastic deformations will be allowed, they are usually acceptable only to very small extent, up to several percent; that means before the curve  $\sigma$ - $\varepsilon$  starts again increasing. From the safety point of view: if the component appears safe in the check based on the material model without strain hardening, the more so the component from real material will be safe, because this material gets stronger during plastic deforming, and the ultimate strength is higher than the yield strength.

The standard for metallic constructions [7] allows plastic deformations, but only under the following conditions:

- 1) ultimate strength must be at least 20% higher than the yield strength ( $f_u \geq 1,2 f_Y$ ),
- 2) material must have sufficient ductility; elongation at rupture A5 at least 15%.

The first condition is here because the quantities  $f_u$  and  $f_Y$  were measured with certain dispersion, and also the load is usually not known accurately. The second

condition wants to ensure that the material does not start breaking due to larger plastic strain. For ensuring higher safety, and with respect to the uncertainties in design, the mentioned standard [7] allows creation of only such number of plastic hinges (see later), that the initially statically indeterminate construction becomes statically determinate. Higher load is not allowed here.

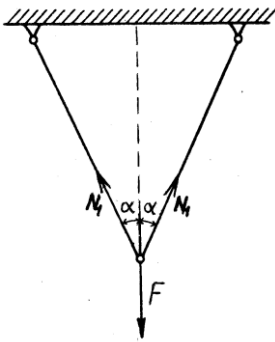
If the standards do not need to be considered, or with components that would be cold formed, higher strains and larger permanent deformations may be allowed. The relevant material properties are, however, necessary; especially high ductility.

Now we shall look at some features typical for elastic-plastic deforming. For simplicity, they will be illustrated on simplest problems.

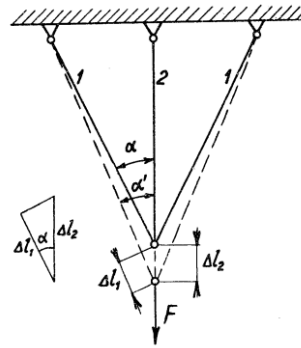
#### 4.2 System of rods loaded by tension

Figure 4.5 shows **two rods**, loaded by tensile force  $F$ . Using the method of fictitious cut, the equation of equilibrium forces in the vertical direction gives, after a rearrangement, the forces in the rods:

$$N_1 = \frac{F}{2 \cos \alpha} \quad (4.5)$$



**Fig. 4.5.** System of two rods.



**Fig. 4.6.** System of three rods.

Vertical displacement  $\delta$  of the connecting pin (see also  $\Delta l_2$  in Fig. 4.6) is:

$$\delta = \frac{\Delta l_1}{\cos \alpha} = \frac{F l_1}{2ES \cos^2 \alpha} \quad (4.6)$$

The same stress acts in both rods of the same area of cross section:

$$\sigma_1 = \frac{N_1}{S} . \quad (4.7)$$

This stress reaches the yield strength at the load

$$F_Y = \sigma_Y (2S \cos \alpha) = F_m . \quad (4.8)$$

If the rods were made of ideal elastic-plastic material without strain hardening, they could (after reaching the yield stress, corresponding to the load  $F_Y$ ) flow without limitations. As plastic deforming proceeds under constant stress, the volume of the rods is also constant. Their cross section becomes smaller during their elongation, so that the true stress,  $\sigma_{\text{true}} = N_1/S_{\text{true}}$ , increases. The process thus becomes instable, and after a while the rods break. The force, corresponding to the onset of yield, is, therefore, the **limit load**, and can be denoted  $F_m$ .

Now we can look at the **system of three rods** (Fig. 4.6). The side rods have length  $l_1$ , and the rod in the middle  $l_2$ . This problem is statically indeterminate and its solution is more complicated; a deformation condition must be used that all rods connected by a pin will be deformed as a whole. The forces in rods are, therefore, mutually related. After several steps, one obtains the forces in elastic deforming [1, 2, 8]:

$$N_1 = F \frac{\cos^2 \alpha}{1 + 2 \cos^3 \alpha} , \quad (4.9)$$

$$N_2 = F \frac{1}{1 + 2 \cos^3 \alpha} . \quad (4.10)$$

If all rods have the same cross section area  $S$ , the stresses in them will be

$$\sigma_1 = N_1/S , \quad \sigma_2 = N_2/S . \quad (4.11)$$

The stress in the central rod 2 is higher (the exception is for  $\alpha = 0$ ). This rod starts deforming plastically as soon as the stress here attains the yield strength. This is at the total load of the system

$$F_Y = \sigma_Y S (1 + 2 \cos^3 \alpha) . \quad (4.12)$$

From this instant the stress in rod 2 remains constant, equal the yield limit (non-strain-hardening material is assumed), and carries the force

$$N_2 = \sigma_Y S . \quad (4.13)$$

The problem has become statically determinate, and its solution is simpler. The situation is the same as with the system of two rods according to Fig. 4.5, but loaded by the force  $F - N_2$ . The stress in the edge rods is still lower than the yield stress, so that the system can carry higher force. Any load increase is transmitted only by the edge rods, with the following force in each

$$N_1 = \frac{F - N_2}{2 \cos \alpha} = \frac{F - \sigma_Y S}{2 \cos \alpha} . \quad (4.14)$$

As soon as the yield strength is achieved also in them, they start flow plastically without limitation, and the system collapses. The corresponding limit load is

$$F_m = \sigma_Y S (1 + 2 \cos \alpha) . \quad (4.15)$$

This load for  $\alpha < 90^\circ$  is higher than  $F_Y$ ; the system can thus be overloaded. Let us see how many times the limit load  $F_m$  is higher than the load  $F_Y$  at the onset of plastic flow in rod 2. A rearrangement of the ratio of Eqs. (4.15) and (4.12) gives:

$$\frac{F_m}{F_Y} = \frac{1 + 2 \cos \alpha}{1 + 2 \cos^3 \alpha} \geq 1 . \quad (4.16)$$

This ratio shows the possible overloading (till failure) from the instant that the stress in the most loaded rod has attained the yield limit. For giving an idea, it is shown here for several values of angle  $\alpha$ :

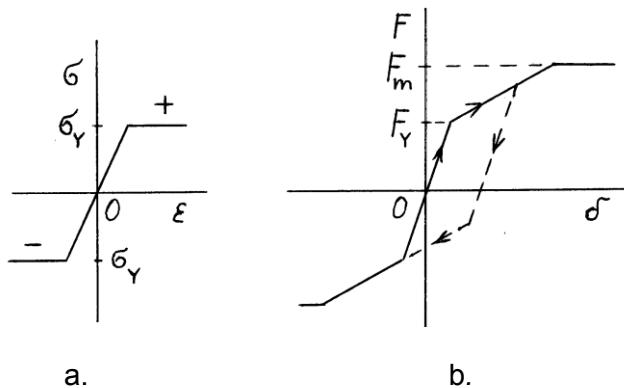
$\alpha$	$0^\circ$	$30^\circ$	$45^\circ$	$60^\circ$	$75^\circ$
$F_m/F_Y$	1	1,19	1,41	1,60	1,47

As we can see, the utilisation of plastic properties enables certain degree of safe overloading. Or, vice versa, the bars dimensioned for certain load may be thinner, and this means material savings. The deformations on attaining the limit state are only slightly larger than at the load corresponding to the onset of plastic flow (the exception being large angles  $\alpha$ ).

### 4.3 Deformations in elastic-plastic state

Until the limit state is reached, the deformations of the body can be determined by means of such part, which is still deformed only elastically (with respect to the links between the individual parts). Figure 4.7b shows displacement of the connecting pin as a function of the load  $F$ . It is the **work diagram of the body**, in

contrast to the work diagram of the material (Fig. 4.7a). Diagram 4.7b has three parts. The first part, for the loads from 0 to  $F_Y$ , corresponds to the situation when all rods are deformed elastically; the displacement of the pin can be calculated as the elongation of rod 2. In the second part, for  $F_Y < F \leq F_m$ , the deformations grow faster, as the rod 2 is now unable to transmit higher load than  $\sigma_Y S$ . The deformations could be calculated from the elongation of rod 1, corresponding to the force  $N_1$  according Eq. (4.14). As soon as the limit load  $F_m$  is attained, the deformations can increase without limitations (horizontal part of the broken line in Fig. 4.7b).



**Fig. 4.7.** a – work diagram of the material,  
b – work diagram of the system according Fig. 4.6.

There is no direct proportionality between the load and deformations of the body, so that the principle of superposition cannot be used. The deformations must always be calculated for the actual load!

#### 4.4 Situation after unloading

As long as the stresses everywhere are lower than the yield strength, all deformations are elastic and disappear after unloading (Fig 4.6). However, if the load has exceeded  $F_Y$ , the rod 2 is deformed plastically, and if it were free, it would remain longer after unloading. The rods 1 would like to shrink to the initial length. They all are, however, connected by the pin. The permanently elongated rod 2 prevents the rods 1 in full shrinking, and generates permanent tensile stress in them. Vice versa, the rods 1 generate permanent compressive stress in the rod 2.

The deformations are depicted in Fig. 4.8. The unloading proceeds along the straight line parallel to the initial part of the work diagram 4.7b. It holds generally:

**Residual forces, deformations and stresses after unloading can be determined as the difference of the actual values in elastic-plastic state, and the values determined for the same load under the assumption of only elastic deforming.**

Also:

**After unloading, the residual stress in the part, where the plastic flow occurred first, will have the opposite sign than under load.**

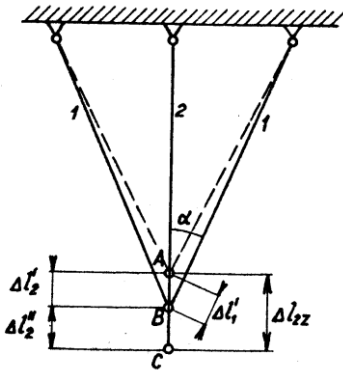


Fig. 4.8. Three rods after unloading.

The residual forces in the system will have the following values:

$$N_{1,res} = N_{1,ep} - N_{1,fict,el} , \quad N_{2,res} = N_{2,ep} - N_{2,fict,el} . \quad (4.17)$$

Subscript  $ep$  corresponds to elastic-plastic state under load, subscript  $fict,el$  denotes fictive elastic forces, which would act in the body, if the material had much higher yield strength and no plastic flow occurred.

Expression of the individual quantities by Equations (4.17) and (4.9, 4.10) gives

$$N_{2,res} = \sigma_Y S - F \frac{1}{1 + 2 \cos^3 \alpha} , \quad (4.18a)$$

$$N_{1,res} = \left( F \frac{1}{1 + 2 \cos^3 \alpha} - \sigma_Y S \right) \frac{1}{2 \cos \alpha} . \quad (4.18b)$$

The residual forces  $N_{1,res}$  and  $N_{2,res}$  are mutually in equilibrium, because no external forces act. The residual stresses are obtained if the residual forces are divided by the cross section area  $S$ .



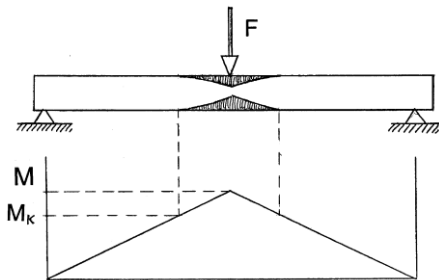
Under load, tension acted in all rods. The residual stress in our case will therefore be compressive in rod 2 and tensile in rods 1. This is obvious from the equations

$$2 N_{1,res} + N_{2,res} = 0, \quad \text{or} \quad N_{2,res} = -2 N_{1,res}. \quad (4.19)$$

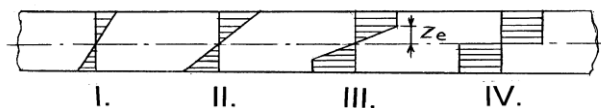
The residual stresses act in the body permanently. During new loading, these stresses and deformations superimpose with the elastic deformations and stresses from the new load, until they attain the maximum value from the previous loading cycle. This means that the previous plastic deforming has increased the load till which the body is deformed elastically (Fig. 4.7). However, in components with the same yield stress in tension and compression, the plasticising and creation of residual stresses can also lower the limit of plastic deforming of the opposite sense! Repeated loading by tension and compression then can cause plastic flow and energy dissipation in each cycle, and nucleation of a fatigue crack after some time.

#### 4.5 Elastic-plastic bending

It will be shown first how the stress distribution develops with increasing load. Figure 4.9 shows a beam on two supports loaded in the middle by transverse force. The following Figure 4.10 shows gradual changes of stress distribution in the most loaded section in the middle of the span. For simplicity, the analysis will be limited to rectangular cross section and ideal elastic-plastic material without strain hardening (Fig. 4.3c), with the same value of yield stress  $\sigma_Y$  in tension and compression. It is an idealisation, but it is useful for obtaining a general idea.



**Fig. 4.9.** Elastic-plastic bending. Plastically deformed region and distribution of moments.  $M$  – bending moment,  $M_K$  – the moment, at which the stresses in the outer fibres attain the yield strength.



**Fig. 4.10.** Gradual development of distribution of bending stresses in the rectangular cross section. I – elastic bending, II – elastic bending - maximum stress has attained the yield strength, III – elastic-plastic bending, IV – elastic-plastic bending, the cross section was fully plasticised.

At the beginning (Fig 4.10 I.), the material is deformed only elastically, and the stresses in the cross section increase proportionally with the distance  $z$  from the neutral axis. Tensile stress acts in one half of the cross section, and compressive in the other half, and their values are

$$\sigma(z) = \frac{M}{J} z ; \quad (4.20)$$

$M$  is the bending moment in the investigated section, and  $J$  is the moment of inertia of the cross section in bending. For rectangular cross section,  $J = bh^3/12$ ;  $h$  is the height of the cross section in the load direction, and  $b$  is its width. Similar stress distribution exists till the instant when the maximum stress in the surface layer attains the yield stress  $\sigma_Y$  (Fig. 4.10 II.). The corresponding moment and load are

$$M_Y = \sigma_Y W_0 = \sigma_Y \frac{bh^2}{6} ; \quad F_Y = \frac{4M_Y}{l} , \quad (4.21)$$

$W_0$  is the section modulus in bending, and  $l$  is the distance between the supports. During further load increase the stress distribution changes. The stress does not increase at places where the yield stress has been attained (the material is without strain hardening, Fig. 4.3c). The increase of bending moment above  $M_Y$  is thus carried by the material in the regions with the stress still lower than  $\sigma_Y$ . Deformations will, therefore, increase faster. Near the neutral axis elastic core exists with linear stress distribution (Fig. 4.10 III.). The material in larger distances is fully plasticised, and the stress here is constant, equal  $\sigma_Y$ . The transition between the elastic core and the plastic region is at the distance from neutral axis [1, 2, 5]:

$$z_e = \sqrt{3 \left( \frac{h^2}{4} - \frac{M_{el-pl}}{\sigma_Y b} \right)} ; \quad (4.22)$$

$M_{el-pl}$  is elastic-plastic moment, higher than  $M_Y$ . With increasing load, the thicknesses of plasticised layers increase, and the thickness of elastic core decreases. It finally disappears at the limit magnitude of bending moment

$$M_m = \sigma_Y \frac{bh^2}{4} ; \quad (4.23)$$

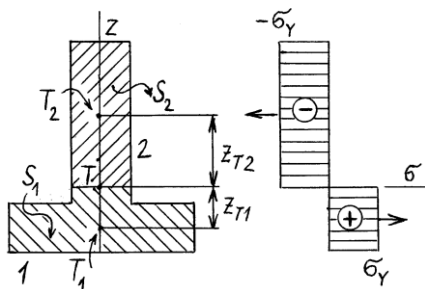
The cross section is now fully plasticised (Fig 4.10 IV.). The limit moment for rectangular cross section is 50% higher than the moment  $M_Y$  at the onset of plastic

flow. We can see again that if plastic properties of the material are utilised, the component can carry much more. (Or, its cross section may be smaller.) The beam deflection at reaching the limit moment is not large. Attaining of the limit moment  $M_m$  in the material without strain hardening could, however, lead to unlimited rotation of both arms of the beam and to the collapse of the structure. (In real materials, certain strain hardening occurs.) As the deformations are concentrated in the region of maximum moment, the term **plastic hinge** is used (Fig. 4.9).

Similar situation is with other shapes of cross section. The limit elastic-plastic moment can be determined directly if stress distribution similar to that in Fig. 4.10 IV is assumed. The situation for general shape of cross section is depicted in Fig. 4.10. The limit moment is obtained by integration over the whole section  $S$ . Considering that the stress for full plasticisation of the cross-section is constant, equal the yield strength, we can calculate it as

$$M_m = \int_{(S)} z \sigma(z) dS = \sigma_Y [z_{T1} S_1 + z_{T2} S_2] = \sigma_Y z_{T1T2} (S/2) \quad (4.24)$$

$S_1$  and  $S_2$  are areas of the individual halves of the cross section, and  $z_{T1}$ ,  $z_{T2}$  are the distances of their centroids from the neutral axis of the whole cross section;  $S$  is the total area of the cross section, and  $z_{T1T2}$  is the distance between the centroids of its






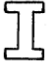
**Fig. 4.10.** Fully plasticised cross section. a – geometry, b – stress distribution.

halves. The neutral axis halves the area of fully plasticised cross section. In unsymmetrical profiles this does not need to be in the centroid. The limit moment can be expressed simply as

$$M_m = \sigma_Y W_{pl} \quad (4.25)$$

where  $W_{pl}$  is so-called plastic section modulus. The formulae for some shapes are shown in Table 4.1 on the next page. The table also gives the values of the ratio of the limit moment  $M_m$  and moment  $M_Y$  at the onset of plastic deformations. This ratio says how much the beam could be overloaded from the beginning of plastic flow to attaining the limit state.

**TABLE 4.1.** Section moduli for bending of various profiles.

PROFILE	$W_{\text{elast}}$	$W_{\text{plast}}$	$M_{o,m}/M_{oY} = W_{\text{pl}}/W_{\text{elast}}$
	$1/6 bh^2$	$1/4 bh^2$	$3/2 = 1,5$
	$\pi d^3/32$	$d^3/6$	$16/(3\pi) = 1,7$
	$\sqrt{2} a^3/12$	$\sqrt{2} a^3/6$	2
			$\approx 1,15$

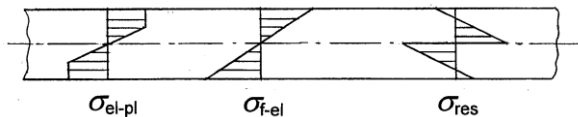
We see that higher overloading (compared to the onset of plastic flow) is possible for profiles with more material near the neutral axis. In contrast, the rolled I-profile has only thin web, and only small reserve after plasticisation of the flanges.

**Remark.** Profiles with high load reserve after the onset of plastic deforming are often those with relatively early start of plastic flow.

If plastic flow occurred during loading, **permanent deformations** remain in the body after unloading. The elastic deformations disappear. If the stress was distributed nonuniformly in the cross section (for example in bending), **residual stresses** will act in the material permanently. Their magnitude at certain point is obtained as the difference of the real elastic-plastic stress and the fictitious stress, which would act here if the material was deformed only elastically (i.e. as if it had much higher yield strength):

$$\sigma_{\text{res}} = \sigma_{\text{el-pl}} - \sigma_{\text{f-el}} \quad (4.26)$$

Figure 4.11 shows the distribution of residual stresses in the cross section after elastic-plastic stress distribution corresponding to Fig. 4.10 III. Again it holds:



**Fig. 4.11.** Elastic-plastic bending. Determination of residual stress.  $\sigma_{\text{el-pl}}$  – stress in elastic-plastic state,  $\sigma_{\text{f-el}}$  – fictitious elastic stress due to the load corresponding to  $\sigma_{\text{el-pl}}$ .  $\sigma_{\text{res}} = \sigma_{\text{el-pl}} - \sigma_{\text{f-el}}$ : residual stress.

***The residual stresses acting after unloading at places, where plastic deforming occurred first, have the opposite sign than under load.***

During plastic flow much more energy is absorbed than in elastic deforming. Therefore the materials for components that should mitigate impact effects by plastic deforming must sustain large permanent deformations and must have high ductility. This is more important than high strength. Metal elements for absorbing energy at impact are often bent [5], and must therefore sustain very intensive bending without fracture.

Some other features of plastic deforming and limit state will be shown on a thick-walled cylindrical pressure vessel.

#### **4.6 Elastic-plastic deforming of thick-walled cylindrical pressure vessel**

In the wall of a cylindrical thick-walled pressure vessel (Fig. 4.12), loaded by internal pressure  $p_1$ , circumferential stress ( $\sigma_t$ ) and radial stress ( $\sigma_r$ ) act. If the vessel is closed, also axial stress  $\sigma_a$  acts here. As long as the load is elastic, the circumferential and radial stress are [1, 8]

$$\sigma_t(r) = A + \frac{B}{r^2}; \quad \sigma_r(r) = A - \frac{B}{r^2}, \quad \sigma_t(r) = 2A - \sigma_r(r), \quad (4.27a)$$

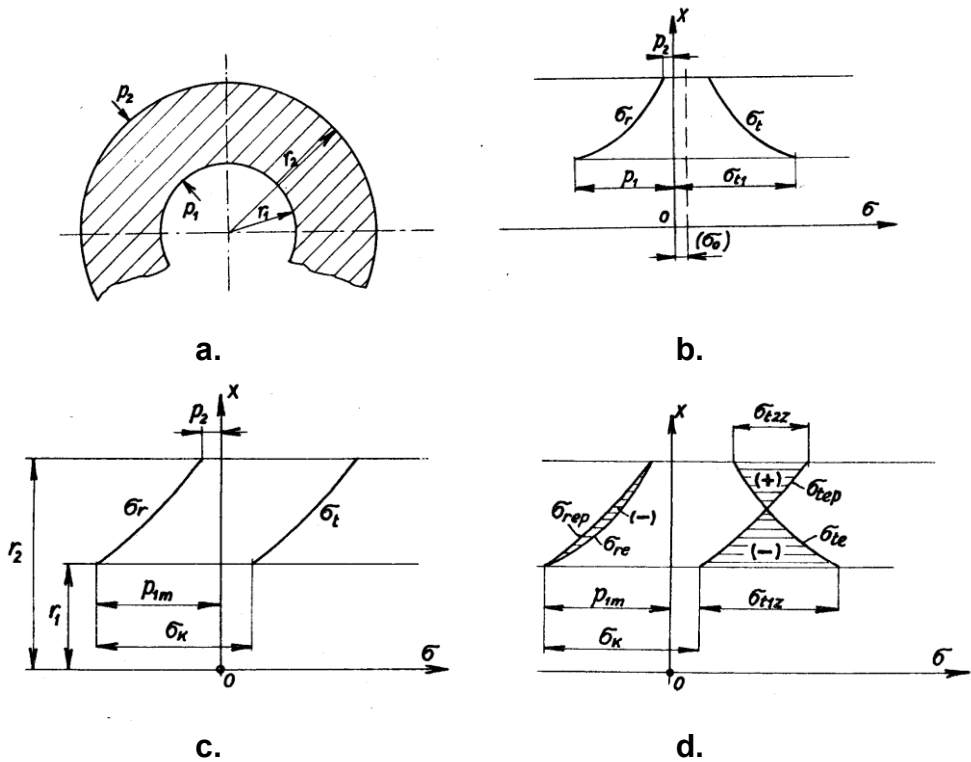
$$A = \frac{p_a a^2}{b^2 - a^2} = \sigma_a; \quad B = p_a \frac{a^2 b^2}{b^2 - a^2}; \quad (4.27b)$$

$a$  is the internal radius, and  $b$  the outer. The constant  $A$  has the same value as the axial stress in a closed vessel. The stress distribution is shown in Fig. 4.12b.

The vessel from brittle material breaks if the maximum stress, i.e. the circumferential stress in the inner surface, reaches the material strength. A vessel from ductile material starts deforming in plastic manner if the equivalent stress reaches the yield strength. We shall look at this situation. For simplicity, ideal elastic-plastic material without strain hardening will be assumed, and also the Tresca's condition for plastic flow, with equivalent stress

$$\sigma_{ekv} = \sigma_1 - \sigma_3 = \sigma_t(a) - \sigma_r(a) = \sigma_Y = \text{const}. \quad (4.28)$$

If no plastic flow should occur, the equivalent stress must be lower than the yield stress. Equations (4.27) – (4.28) can yield the necessary wall thickness, or the outer



**Fig. 4.12.** Thick-wall cylindrical vessel loaded by pressure on the inner and outer surface. **a** – geometry, **b** – elastic stresses, **c** – stresses in fully plasticised wall, **d** – stresses after unloading.  $p_1, p_2$  – pressures on inner and outer surface,  $\sigma_r$  – radial stress,  $\sigma_t$  – circumferential stress,  $e$  – elastic,  $ep$  – elastic-plastic,  $z$  – residual.

radius  $b$  of the wall, with respect to the inner radius  $a$ :

$$b = a \sqrt{1 / \left( 1 - \frac{2p_a}{\sigma_Y / k} \right)} ; \quad (4.29)$$

$k (\geq 1)$  is the demanded degree of safety. For simplicity,  $k = 1$  can be assumed here. The pressure, under which the material of the wall with radii  $a, b$  starts flowing, is

$$p_{a,Y} = \frac{\sigma_Y}{2} \left[ 1 - \left( \frac{a}{b} \right)^2 \right] . \quad (4.30)$$

The necessary wall thickness thus increases with increasing pressure  $p_a$ . As  $2p_a/\sigma_Y$  approaches to 1, the denominator in (4.29) approaches to zero, and the necessary outer radius  $b$  approaches to infinity. This would be attained for  $2p_a/\sigma_Y = 1$ . This means that for  $p_a > \sigma_Y/2$  plastic flow occurs for any wall thickness!

At the beginning this flow happens only in a thin layer at the inner surface. Nothing special happens yet, because it is surrounded by much thicker layer of material, which is still deformed only elastically. With increasing pressure in the vessel the thickness of the plasticised layer grows, and with respect to the condition of plastic flow (4.28) also the distribution of stresses changes. They are distributed in this layer according the logarithmic function:

$$\sigma_r(r) = \sigma_Y \ln \frac{r}{a} - p_a ; \quad \sigma_t(r) = \sigma_r(r) + \sigma_Y \cdot \quad (4.31)$$

If the overpressure in the vessel attains the limit value

$$p_{a,m} = \sigma_Y \ln \frac{b}{a} \quad , \quad (4.32)$$

the whole wall is plasticised. The distribution of radial and circumferential stress is shown in Fig. 4.12c. Plastic flow (of material without strain-hardening) continues under this pressure till the wall bursts;  $p_{a,m}$  is the actual limit pressure.

Now we shall look at the possible overloading from the onset of plastic flow to the limit state. The corresponding ratio  $p_{a,m}/p_{a,Y}$  is obtained as the ratio of Equations (4.32) a (4.30):

$$k_{m,Y} = \frac{p_{a,m}}{p_{a,Y}} = \frac{2 \ln \frac{b}{a}}{1 - (a/b)^2} \quad . \quad (4.33)$$

Note that the overloading capacity  $k_{m,Y}$  for materials without strain hardening does not depend on the yield strength. We shall show how  $k_{m,Y}$  depends on the ratio of inner and outer radius:

$b/a$	1,1	1,2	1,5	2	3	10	100
$k_{m,Y}$	1,098	1,19	1,46	1,85	2,47	4,65	9,21

It is obvious that the onset of plastic flow does not mean, especially for vessels with thick wall, any danger of attaining the limit state.

If the pressure  $p_a$  is higher than  $p_{a,Y}$  and lower than the limit pressure  $p_{a,m}$ , the wall is **partly plasticised**. The material is fully plasticised from the radius  $a$  till the radius  $c$ , and the stresses are distributed according to Eqs. (4.31) and Fig. 4.12c. From the radius  $c$  till the outer radius  $b$  the material is deformed elastically (Fig. 4.12b), with stresses according to Eq. (4.27). The radius  $c$  of the boundary between both regions can be obtained by solving the equation

$$p_a = \sigma_Y \left\{ \ln \frac{c}{a} + \frac{1}{2} \left[ 1 - \left( \frac{c}{b} \right)^2 \right] \right\}, \quad (4.34)$$

obtained from Eqs. (4.27) and (4.32), in which  $b$  and  $a$  were replaced by radius  $c$ .

Residual stresses after unloading, which can be calculated via Eq. (4.26), are depicted in Fig. 4.12d. Similarly to previous cases, compressive circumferential stress will act permanently in the layer at the inner surface also in the partly plasticised thick-wall pressure vessel. This process is sometimes used for increasing fatigue resistance of cyclically loaded pressure appliances, such as hydraulic cylinders of gun barrels. Another example, how plasticity can be used, will be shown in section 4.8.

#### 4.7 Criterion of plastic flow under multiaxial stress state

Plastic deforming under multiaxial state of stress can be studied using intensity of stresses and strains. **Stress intensity** was defined earlier:

$$\sigma_i = \sqrt{\sigma_x^2 + \sigma_y^2 + \sigma_z^2 + \sigma_x\sigma_y + \sigma_y\sigma_z + \sigma_z\sigma_x + 3(\tau_{xy}^2 + \tau_{yz}^2 + \tau_{zx}^2)}, \quad (4.36)$$

$$\sigma_i = \frac{\sqrt{2}}{2} \sqrt{(\sigma_1 - \sigma_2)^2 + (\sigma_2 - \sigma_3)^2 + (\sigma_3 - \sigma_1)^2}. \quad (4.37)$$

**Strain intensity** is defined similarly:

$$\varepsilon_i = \frac{\sqrt{2}}{3} \sqrt{(\varepsilon_1 - \varepsilon_2)^2 + (\varepsilon_2 - \varepsilon_3)^2 + (\varepsilon_3 - \varepsilon_1)^2}; \quad (4.38)$$

The strain intensity in plastic deforming is generally a function of stress intensity,

$$\varepsilon_i = f(\sigma_i). \quad (4.39)$$

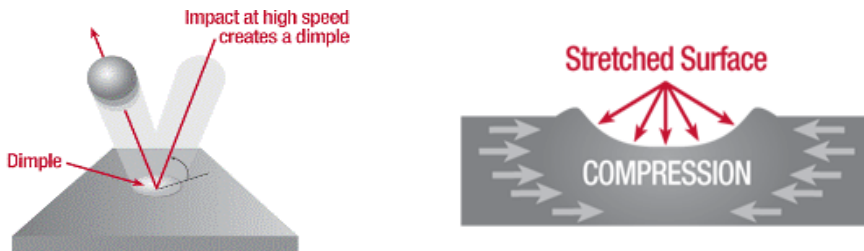
Various theories exist for extensive plastic deformations. More information can be found, for example, in [1 – 4].



#### 4.8 Increasing the fatigue resistance of metallic components

The growth of fatigue cracks can be slowed down or stopped by creation of compressive prestress in the surface layer. The most common method for ductile materials is local plastic deforming, for example by shot peening or rolling. In these processes, a hard tool with small diameter and rounded surface is pressed point after point into the surface of the treated component. One process is so-called shot peening: a stream of hard balls is thrown (by the air flow or by blades of a blasting appliance), or a hard cylinder of small diameter is rolled under pressure along the surface, or the surface is impacted by a system of hard pins or needles that are put into motion by an electric hammer or by an ultrasound generator.

The principle of creation of compressive prestress is as follows. Pressing a hard ball or similar hard body into the strengthened object causes high local contact stresses in its surface layer, whose material is deformed plastically. The thickness of the plastically deformed layer (on the elastic core) becomes smaller and its width becomes larger – the material flows in radial directions (Fig. 4.13). The material out of this layer adjusts to its permanent widening by elastic stretching. After the ball jumps away and the pressure on the surface is released, the elastically deformed material tries to shrink to its original dimensions. It thus compresses the central plastically extended part of the contact area, in which therefore compressive permanent (residual) stress appears. This process occurs at all places hit by the balls. In this way, compressive prestress is created on the whole surface layer.



**Fig. 4.13.** Increasing the fatigue resistance of ductile materials by shot peening. Left – the process, Right – creation of compressive prestress in the surface layer.

The fatigue resistance of components with a notch is sometimes increased by the preloading, controlled so that certain plastic flow occurs in the notch [9]. After unloading, permanent compressive stress arises here.

#### **References to Chapter 4.**

1. Kolektiv: Pružnost a pevnost II. Skriptum ČVUT, Fakulta strojní, Praha, 1985. 214 p.
2. Pešina, E.: Základy užití teorie plasticity. SNTL, Praha, 1966. 188 p.
3. Kuliš, Z.: Plasticita a creep I. ČVUT, Praha, 1986.
4. Hill, R.: The mathematical theory of plasticity. Clarendon Press, Oxford, 1950.
5. Menčík, J.: Impacts and vibrations. University of Pardubice, Pardubice, 2018. 132 p. ISBN 978-80-7560-147-6. Available at: <https://hdl.handle.net/10195/70531>, or after putting the book title into the search engine Google.
6. Veles, P.: Mechanické vlastnosti a skúšanie kovov. ALFA, Bratislava, 1985. 408 p.
7. ČSN 73 1401. Navrhování ocelových konstrukcí. Český normalizační institut, 1998. 134 p.
8. Höschl, C.: Pružnost a pevnost ve strojnictví. SNTL, Praha, 1971. 375 p.
9. Fuchs, H. O., Stephens, R. I.: Metal Fatigue in Engineering. J. Wiley and Sons, New York, 1980.

## 5. Thermal stresses

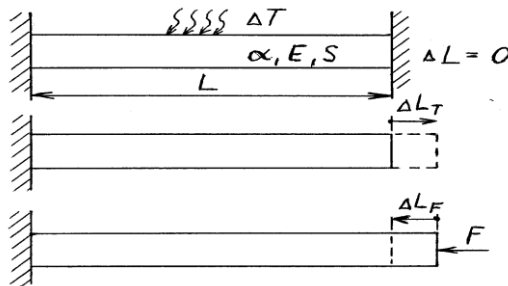
### 5.1 Principal equations

If a body cannot change dimensions during a temperature change, thermal stresses arise in it. These stresses and corresponding forces or deformations can worsen or make impossible the operation of a certain object, or damage or destroy it. The principal features will be explained on a rod of elastic material (Fig. 5.1).

If the temperature of a free rod increases from  $T_0$  to  $T$ , its length changes from  $L_0$  to  $L$ . The increase in length,  $\Delta L = L - L_0$ , is

$$\Delta L = \alpha L \Delta T, \quad (5.1)$$

where  $\Delta T = T - T_0$ , and  $\alpha$  is the coefficient of thermal expansion ( $\text{K}^{-1}$ ), which gives the relative length increase corresponding to the temperature increase by 1 K. We shall consider so small changes of temperature, that the coefficient of thermal expansion can be assumed constant. Also the changes of the cross section will be negligible, and the forces and stresses will be calculated for the initial dimensions.



**Fig. 5.1.** Thermal stresses – principle of determination

**Remark.** It is recommended to calculate any increment as the difference of the actual and initial value. For example, the temperature distribution in a body can be complicated, and it cannot be said immediately whether the stress at a certain point will be tensile (i.e. positive) or compressive (negative). Adherence to the sign convention facilitates the answer, which will be clear from the numerical values. If the result is positive, we know that the stress will be tensile (and vice versa).

If both ends of the rod are clamped in a rigid structure, its length cannot change due to temperature change (that is,  $\Delta L = 0$ ), and stress appears in the rod. Its magnitude can be obtained by the following thought experiment done in two steps [1]. In the first step, one end of the rod is released, and the rod is heated by  $\Delta T$ . Its length increases by  $\Delta L$  according Eq. (5.1), but no forces appear in it. In the second step, a compressive force  $F$  is applied to the rod and slowly increased. This causes shortening of the rod. At certain time the free elongation  $\Delta L$  is eliminated. The corresponding force is such that will act in the heated rod with clamped ends. It can be written for the total change in length

$$\Delta L = \Delta L_T + \Delta L_F = 0 . \quad (5.2)$$

The subscripts at the individual components denote the length increment from temperature (T) or from the force (F). With respect that the increase of the rod length from the (tensile) force  $F$  is generally  $\Delta L_F = FL/(ES)$ , where  $E$  is modulus of elasticity of the rod in tension, and  $S$  is its cross section, one obtains after a rearrangement

$$\Delta L = \alpha L \Delta T + FL/(ES) = 0 , \quad (5.3)$$

so that

$$F = -\alpha \Delta T E S . \quad (5.4)$$

If the temperature was increased,  $\Delta T$  is positive. For common materials, which expand at temperature increase,  $\alpha$  is also positive. The force  $F$  causes in the rod normal stress of magnitude

$$\sigma = -\alpha \Delta T E . \quad (5.5)$$

The sign minus says that temperature increase ( $\Delta T > 0$ ) causes compressive stress and force in the rod.

Equation (5.5) is very important, as it shows the principal quantities, which influence thermal stresses at temperature change, if free dilatations of the body are precluded:

1. temperature change ( $\Delta T$ ),
2. coefficient of thermal expansion of the material ( $\alpha$ ),
3. material stiffness ( $E$ ).

For example, if we want to reduce thermal stresses, we can use the material with

lower thermal expansion ( $\alpha$ ) or lower modulus of elasticity  $E$  (i.e. more compliant) or reduce the temperature difference  $\Delta T$ , for example by thermal insulation of the body if the heat transfer between it and the environment lasts only limited time. Other examples are glass oven-ware or electric cooking plates. During their use sudden temperature changes can be expected. Therefore they are produced from a special glass or glass-ceramics with extremely low thermal expansion coefficient  $\alpha$ ,

Expression (5.5) can also be used for finding the necessary value of thermal expansion coefficient, elastic modulus, or admissible temperature change, if the body should not be destroyed.

The total force, acting in the body with precluded thermal dilatations, is given by Equation (5.4), which differs from stress (5.5) by the area of cross section  $S$ . This force will be higher for larger cross section area of the rod. The consequences of high force can be critical. For example, decrease of temperature causes tensile force in the rod, and if it exceeds the strength of the joints, the rod can be torn off from the structure; high tensile stress can cause fracture of the rod.

Until now, uniform distribution of temperatures and stresses was assumed. If the temperature of the environs changes, the temperature of the body starts changing gradually from the surface to depth. The situation is depicted in Fig. 5.2. In the first instants, only thin surface layer is influenced. The material here wants to expand or shrink, according to whether the body is heated or cooled. The dimensions inside the body with the initial temperature are still without a change and prevent changes of the dimensions of surface layer. It means that compressive stress will act during

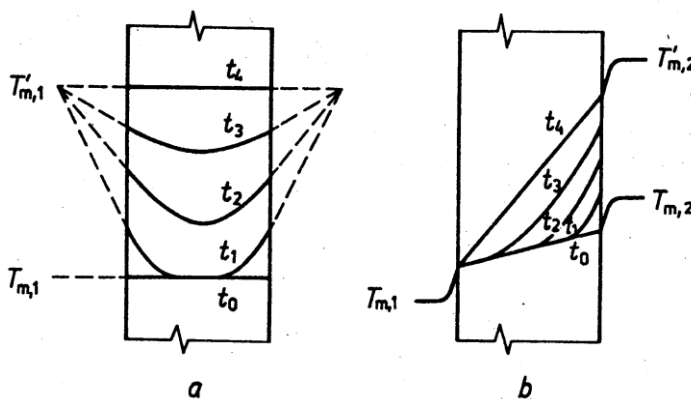


Fig. 5.2. Temperature development in a plate heated from: a – both sides, b – one side.

heating in the directions parallel with the surface. During cooling, tensile stress appears in the surface. This can even cause cracks in teeth enamel, if this comes – after hot tea – into contact with very cool liquid.

Quantitative idea can be obtained from the sudden temperature change on the surface of a plate, if the thickness of the influenced layer is so small that the plate dimensions in the directions of acting stresses remain practically unchanged. The stress in the surface layer at depth  $z$  below the surface will be

$$\sigma(z) = -\alpha \Delta T(z) E / (1 - \mu) ; \quad (5.6)$$

$\Delta T(z)$  is the difference between the instantaneous temperature at depth  $z$  and the initial temperature of the plate. In contrast to Eq. (5.5), the term  $(1 - \mu)$  is here in the denominator, because plane strain state exists now in the plate, where the stresses at certain depth have the same value in all directions parallel to the surface.

The resultant of compressive stresses in the surface layer must be in equilibrium with the resultant of tensile stresses inside the body. As long as the thickness of the surface layer is negligible compared to the interior thickness, the stresses inside are also negligible. As the thickness of the influenced region grows, also the force caused by the compressive stress grows, and also the reaction tensile force below it. Also the mean temperature of the plate changes. The equilibrium of all forces is

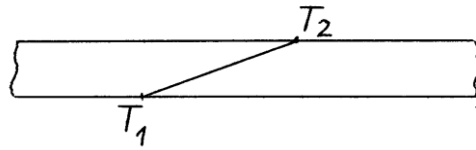
$$\int_{(h)} \sigma(z) dz = 0 , \quad (5.7)$$

where  $h$  is the plate thickness.

If the conditions for heating or cooling at each surface are different, unsymmetrical stress distribution appears in the plate. This can lead to its deflection, and sometimes also to generation of stresses. Let a thin plate be heated from one side so that the temperature distribution across the thickness is linear (Fig. 5.3). If the plate is free, it can deflect into the shape of a part of spherical surface with radius [2]

$$R = h / (\alpha \Delta T) ; \quad (5.8)$$

$h$  is the plate thickness,  $\alpha$  is the coefficient of thermal expansion, and  $\Delta T$  is the difference of both surface temperatures,  $\Delta T = T_1 - T_2$ . No stresses occur in it. (Equation (5.8) is valid under the assumption that the deflection is small.)



**Fig. 5.3.** Linear distribution of temperature across the wall.

If the plate is fixed so that it cannot deflect, thermal stresses arise in it. These stresses will be distributed linearly across the thickness. We can thus speak of them as of bending stresses. The highest stress acts on the surface, and its magnitude is

$$\sigma_{\max} = \pm \alpha \Delta T E / 2(1 - \mu) ; \quad (5.9)$$

The positive sign, which means tensile stress, pertains to the half of thickness with temperature lower than the mean temperature  $T_s = (T_1 + T_2)/2$ . In the opposite half, compressive stress acts. The stress in the mean plane equals zero.

These and other situations are discussed in detail in books [3 – 8].

### Example.

Determine the stress magnitude on the surface of glass plate in the first instant after its surface was cooled suddenly from 100°C to 10°C. Thermal expansion coefficient  $\alpha = 8,5 \times 10^{-6} \text{ K}^{-1}$ ,  $E = 72 \text{ GPa}$ ,  $\mu = 0,2$ .

Inserting these values into Eq. (5.6) gives the tensile stress

$$\sigma(0) = 8,5 \times 10^{-6} \times (100 - 10) \times 72000 / (1 - 0,2) = 68,85 \approx 69 \text{ MPa}.$$

## 4.2 Procedures for strength increasing by thermal treatment

Thermal stresses can lead to the damage of the body. However, sometimes they can be useful, for example in strengthening of glass. A drawback of glass is its low tensile strength. This drawback can be mitigated by a suitable thermal treatment, so called tempering. (Another case is strengthening by ion exchange, which will be explained later.) Glass is an amorphous material that has no fixed temperature of solidification, but during cooling its viscosity increases gradually to the values when it behaves like a solid. **Glass tempering** [4, 7, 8] is done so that the glass object is heated to the temperature at which the glass starts soften, then it is let on this temperature so that the temperatures get equalised in the whole volume, and then it is quickly cooled, for example by the stream of air. During cooling,

temperature gradient is formed between the cooler surface and the hotter interior (Fig. 5.4). At the same time glass shrinks, more on the surface and less inside. As long as the glass is soft, these deformations are compensated by the viscous flow, and the glass remains without any stress. On crossing the glass transformation temperature  $T_g$ , the individual layers become successively rigid and an arrangement is built in the glass, which corresponds to temperature distribution given. If the cooling continues with a constant rate, the body remains without stress until its surface temperature drops to the ambient temperature. At this time, the inner warmer layers continue to cool and contract. This contraction is, however, opposed by the cold surface layers. This gives rise to a system of stresses, compressive at the surface and tensile in the interior. As the glass is already rigid, these stresses cannot be released and remain in the glass permanently.

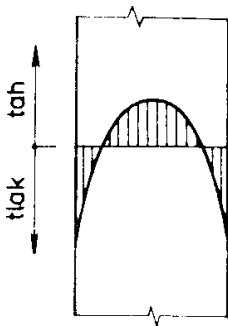
The stress distribution in tempered glass corresponds to the temperature distribution during the passage across the transformation region. If a glass plate of thickness  $h$  was cooled from both sides with not very high intensity, its temperatures will have parabolic distribution according to Fig. 5.4:

$$T(x, t) = T_0(t) \left(1 - x^2/h^2\right) ; \quad (5.10)$$

$T_0$  is the temperature in time  $t$  in the central plane, and  $x$  is the distance from it. After cooling the permanent stresses parallel with the surface will act:

$$\sigma(x) = \frac{\alpha E}{1 - \mu} T_g k \left(1 - 12 \frac{x^2}{h^2}\right) ; \quad (5.11)$$

$k$  is a parameter characterising the intensity of cooling. Equation (5.11) shows that the maximum compressive stress acts in the surface ( $x = h/2$ ) and has the magnitude



**Fig. 5.4.** Stress distribution in tempered glass.



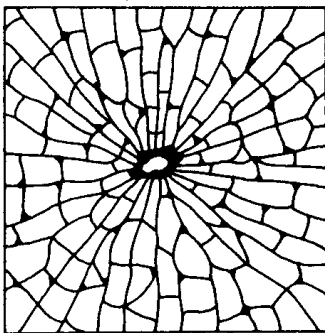
$$\sigma(h/2) = -2 \frac{\alpha E}{1-\mu} T_g k \cdot \quad (5.12)$$

This stress is twice as high as the tensile stress inside the plate ( $x = 0$ ), and the thickness of the compressed layer is approximately one fifth of the wall thickness.

Equations (5.10) – (5.12) correspond to the places remote from edges. If the influence of edges should be considered, numerical solution and suitable software must be used.

Strengthening by creation of compressive prestress in the surface layer also has its limits. Higher compressive prestress in the surface layer and its larger thickness mean higher tensile force in the interior. Thickness of the inner part must therefore be sufficient to equalise the compressive force. It means that strengthening by tempering cannot be used for very thin glass products, as usually also certain requirements exist for the minimum thickness of the compressive layer, able to prevent its easy breaking through.

Thermal stresses also mean the accumulation of potential energy in the body. Tempered glasses are used in vehicles (windows of railway carriages, side windows in cars). If the compressed layer, hit by a small stone with sharp edges, was broken through into the inner part with permanent tensile stresses, cracks start propagating spontaneously in all directions from the point of damage. If the residual stresses were high, these cracks branch: the released energy changes into fracture energy. The higher the prestress, the higher the accumulated energy released during the process, and a higher number of smaller pieces, into which the glass plate disintegrates. Typical appearance of a damaged glass plate is in Figure 5.5. Thanks to suitable distribution of stresses in the tempered glass the individual fragments have not sharp edges, and are not as dangerous as common splinters.

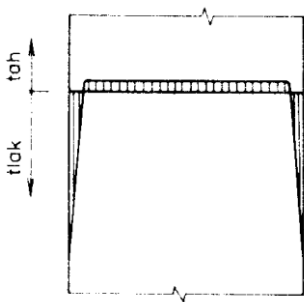


*Fig. 5.5. Fracture of tempered glass plate broken through by a sharp body.*

In the past, tempered glasses were used in cars for all windows. Because the dense network of cracks makes the view through the glass impossible, or the damaged glass is spilled, the front glasses are made today from laminated glass. Usually, two panes of non-toughened glass are connected by a layer of polyvinylbutyral (PVB). In this case, a flying small stone can break out a small piece of glass, or the window fractures on the side of tensile stress, but the damage does not penetrate through the PVB layer. Everybody perhaps has seen such damaged glass in a bus.

Glass can be strengthened also by **ion exchange** [4, 8]. Here, compressive prestress is created in a very thin surface layer (several mm) by putting the glass for some time into a hot bath of melted salts. Ions of the pertinent salt diffund into the glass and remain built-in here. As they have larger diameter than the original ions of the glass network, they generate permanent compressive prestress (Fig. 5.6). This process proceeds below the glass transformation temperature, so that the stress cannot be released by viscous flow. The very high compressive stress (several hundred MPa) in the surface layer is in equilibrium with the very low tensile stress inside the body. Certain advantage is that damaging of this layer does not cause destruction of the object, in contrast to failure of tempered glass.

Thermal stresses arise also in welding of metals by flame or electric arc. The temperatures in the weld region are very high, and the material expands here. The melted or soft material adjusts itself to the dimensions in the vicinity and remains without stresses. They appear in it only during solidification and remain then in the body permanently. They can be mitigated by annealing.



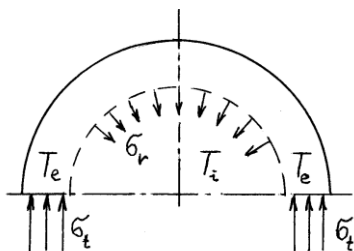
**Fig. 5.6.** Distribution of stresses in a glass plate strengthened by ion exchange

Other examples of permanent stresses in steel components are nitriding, surface hardening, or cementing and quenching. In the last process martensite arises in the surface layer rich on carbon. Martensite has specific volume larger than the original

pearlite that remained in the untransformed interior. As a consequence, favourable compressive prestress acts in the very hard surface layer.

Thermal stress can appear also in composite materials or structures, whose components have different coefficients of thermal expansion. The importance of knowledge of thermal expansion can be illustrated on one lawsuit from the past. The glass cover of airtight lamps for mines was joined with metallic body by gluing with an epoxy glue, and this arrangement worked well for many years. After some time, the glass manufacturer has decided to reduce the range of produced glasses, and to produce only „glass with better thermal resistance“ (i.e. glass with better resistance to sudden changes of temperature). The lamp manufacturer has not realised that this „resistance“ was higher due to lower thermal expansion of new glass in comparison with the original glass, and agreed with the change. And the lamps started to break, because the stress arising after gluing the glass to the lamp body at higher temperature was higher than the glass strength. In this case, the magnitude of forces between the glass and the fitting depended on the difference between the high temperature at the beginning of curing and the common temperature, and on the difference of thermal expansion coefficients of both parts. And the latter difference has become larger.

Let us look at the following feature of cooling or heating of rounded surfaces. For example, when a long cylinder or a sphere is heated, its warmer surface layer wants to become longer, and, therefore, to increase its radius. The cooler interior hampers it. In the surface layer compressive stress therefore arises in the circumferential direction, and also in axial direction in a cylinder (Fig. 5.7). Moreover, radial tensile stress appears between this layer and the still cold interior. (During cooling, radial compressive stress and tensile circumferential stress in the surface layer would arise.) For obtaining simple idea we can assume that the surface layer is very thin, with the thickness  $h$  very small compared to the radius of curvature  $R$  at



**Fig. 5.7.** Thermal stresses during heating a massive shaft.  $T_i$  – temperature of the interior,  $T_e$  – temperature of the surface layer,  $\sigma_r$  – radial stress between warmer layer and the interior,  $\sigma_t$  – circumferential stress,

the boundary between the layer and interior, and its temperature (assumed constant in the whole thickness of the layer and equal to the average value) differs from the temperature of the interior (also assumed constant) by  $\Delta T$ .

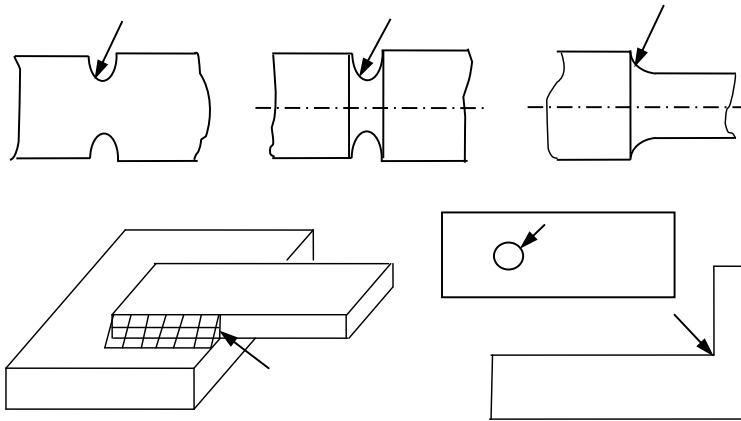
### References to Chapter 5.

1. Höschl, C.: Pružnost a pevnost ve strojnictví. SNTL, Praha, 1971. 375 p.
2. Timošenko, S. P.: Strength of materials, Part II. D. van Nostrand Company, Inc., Princeton, New Jersey, 1956.
3. Timoshenko, S. P., Goodier, J. N.: Theory of elasticity. 3rd ed., McGraw-Hill, New York, 1970.
4. Menčík, J.: Strength and fracture of glass and ceramics. Elsevier, Amsterdam, 1992. 357 p.
5. Menčík, J.: Výpočty strojních součástí s povrchovými úpravami na pevnost a životnost. (Cyklus Stavba strojů, č. DT01-211-91) DT ČSVTS, Praha, 1991. 120 s.
6. Menčík, J.: Mechanics of Components with Treated or Coated Surfaces. Kluwer Academic Publishers, Dordrecht, 1996.
7. Schill, F.: Chlazení skla a kontrola pnutí. SNTL, Praha, 1968. 194 p.
8. Novotný, V.: Zpevnování skla. (Hutní sklářská příručka). SNTL, Praha, 1972.

## 6. Stress concentration

### 6.1 Introduction

Failure of a component starts often at a place with sudden change of cross section or shape, such as a hole, notch or a crack (Fig. 6.1). These places are sources of higher stress, and are called **stress concentrators**. Transfer of forces in a loaded body between atoms can be represented by means of force-lines, analogous to stream lines in flowing liquid. The density of force lines is proportional to the stress. If the cross section is constant or changes slowly, the force-lines are distributed uniformly, and so is also the stress. At a sudden change of cross section or shape, generally at a stress concentrator, the continuity of the force flow is disturbed, and the force lines here become denser and the stress higher. Complicated three-axial stress state arises here; the stress is maximal on the surface of notch root and decreases with depth (Fig. 6.2); faster for a sharper notch.

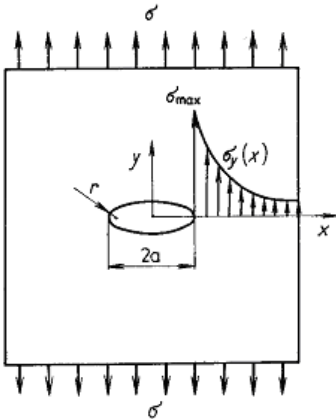


**Fig. 6.1.** Examples of notches in components. The arrows show dangerous places.

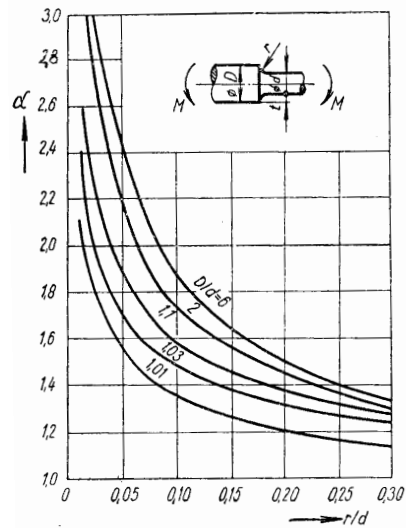
The stress analysis in notches is demanding. Today, suitable computer programs (e.g. FEM) can determine detailed distribution of stresses in bodies of complex shape, including notches. In the past, such analysis was possible only for simple shapes, and the evaluation of notch effects was limited to simple obtaining the maximum stress  $\sigma_{\max}$  in the notch root as

$$\sigma_{\max} = \alpha \sigma_{\text{nom}} , \quad (6.1)$$

where  $\alpha$  is the **stress concentration factor**, and  $\sigma_{\text{nom}}$  is the nominal stress in the notch region. The values of shape factors  $\alpha$  were determined for technically important notch shapes and loads, and can be found in various handbooks, for example [1 – 4]; an example is shown in Fig. 6.3. Also this approach is useful, as it yields simple illustrative idea, important for practical applications.



**Fig. 6.2.** Plate with an elliptic hole and stress distribution at its apex.



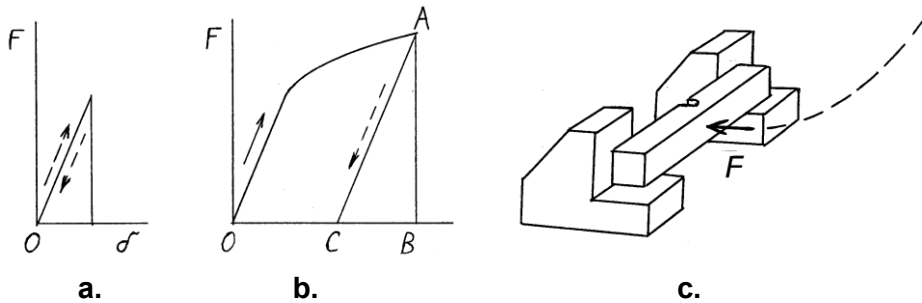
**Fig. 6.3.** Stress concentration factor  $\alpha$  for a stepped shaft loaded by bending [2].

For example, a component from brittle material breaks if the maximum stress at certain point attains the ultimate strength  $\sigma_p$ . It follows from Eq. (6.1) that a brittle component with a notch fails if the nominal stress attains the value

$$\sigma_{\text{nom}} = \sigma_p / \alpha . \tag{6.2}$$

It means that the **notch reduces the technical strength**  $\alpha$ -times! In components from ductile materials loaded slowly the notches are not so dangerous, because if the maximum stress somewhere attains the yield strength, the material starts flowing plastically, the stress here does not increase so fast, and the increasing load can be transferred by areas where the stress is still lower and can therefore increase, as it was explained in Chapter 4. Despite of it, every notch means a danger, especially at impact load (see further). A fatigue crack, generated under periodical load, usually starts also at a stress concentrator; however, the reduction of fatigue limit is smaller than that given by Equation (6.2).

If the body should not fail under impact load, it must be able to absorb the energy of impact. If it deforms elastically, the energy consumption is small (Fig. 6.4a). If the stress exceeds the yield limit, the material deforms plastically, and more energy is absorbed (Fig. 6.4b). Plastic flow in a component with a notch is limited (due to



**Fig. 6.4.** Deformation work. **a** – elastic deforming, **b** – elastic-plastic deforming.  $OABO$  – work expended during loading,  $CAB$  – energy released during unloading. **c** - test of notch toughness by a pendulum hammer (Charpy).

nonhomogeneous stress distribution) only to a small volume of material in this region. The stresses at larger distances are lower than the yield strength, and the material is deformed only elastically. The total consumption of impact energy is therefore smaller than in a similar body without a notch, with homogeneous stress distribution and thus with better condition for plastic flow in larger volume. (Let us compare in Fig. 6.4b the area corresponding to elastic deforming with the area of the whole diagram.) In a body of simple shape, the impact energy can be distributed in a large volume, and the corresponding stresses will be relatively low, while the same energy, passed onto a body with a notch, is concentrated in much smaller volume, and causes much more intensive plastic flow here; after the material's plastic ability is exhausted, a fracture follows. The influence of a notch can be illustrated on an example of impact on a smooth beam and on a similar specimen with a notch, as common in tests of notch toughness (Fig. 6.4c). If the smooth specimen has the thickness equal the minimum thickness of a notched specimen, the falling hammer bends it, while the specimen with a notch breaks, despite of the fact that it is more massive in general – with the exception of the notch. Addition of material alone does not increase the strength, if the material was not added at the proper place. (See also Chapter 14, the part on the effect of ribs.)

Further, we shall look at the stress concentration at holes in components.

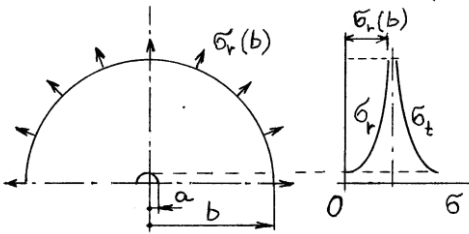
## 6.2 Stresses around holes

The main features will be shown on several typical cases.

1) The first case is a small circular opening of radius  $a$  in the centre of a circular plate of radius  $b \gg a$  (Fig 6.5). The outer circumference of the plate is loaded by uniformly distributed radial tensile stress  $\sigma_r(b) = \sigma_{rB}$ . At the distance  $r$  from the axis the circumferential stress  $\sigma_t$  and radial stress  $\sigma_r$  act [3 – 6]

$$\sigma_t(r) = \sigma_{rB} \left( 1 + (a/r)^2 \right), \quad \sigma_r(r) = \sigma_{rB} \left( 1 - (a/r)^2 \right). \quad (6.3a,b)$$

On the surface of the opening ( $r = a$ ) no radial stress act,  $\sigma_r(a) = 0$ , and circumferential stress here is  $\sigma_t(a) = 2\sigma_{rB}$ ; that is two times higher than the stress on the loaded outer edge. The stress concentration factor is thus  $\alpha = 2$ . If no hole were in the plate, the stress  $\sigma_{rB}$  would act here in all directions. The presence of the hole means the local increase of stress here by 100 %..



**Fig. 6.5.** Stress around the circular hole in a plate loaded by isotropic tension.

The same increase of stress will exist around a small opening in a large square plate, loaded on all edges by the same tensile stress  $\sigma_{rB}$ . The stress state also in this plate is biaxial isotropic, similarly to a circular plate.

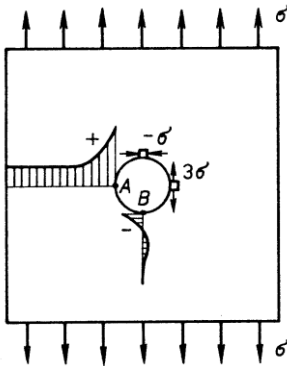
2) The second case is a small circular hole of radius  $a$  in a large square plate loaded by uniaxial tensile stress  $\sigma_0$  (Fig. 6.6). The circumferential stress here is [3, 6]

$$\sigma_t(r, \varphi) = \frac{\sigma_0}{2} \left( 1 + \frac{a^2}{r^2} \right) + \frac{\sigma_0}{2} \left( 1 + 3 \frac{a^4}{r^4} \right) \cos 2\varphi \quad ; \quad (6.4)$$

$\varphi$  is the angle between the direction of tensile stress and the point on the radius  $r$ , in which the stress is determined. The circumferential stress is highest on the surface (i.e. at  $r = a$ ), where it changes with the angle  $\varphi$  as

$$\sigma(\varphi) = \sigma_0 (1 + 2 \cos 2\varphi) \quad . \quad (6.5)$$



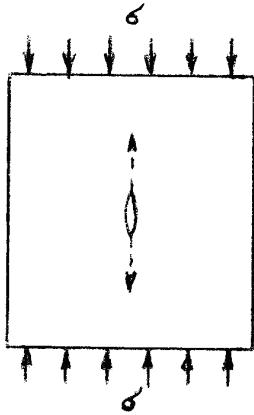


**Fig. 6.6.** *Stress around a circular hole in a large plate loaded by tension in vertical direction. On the circumference of the hole maximum tensile stress  $3\sigma$  acts at points A and compressive stress  $-\sigma$  at points B.*

At points A maximum tensile stress  $\sigma_t(A) = 3\sigma_0$  acts, so that the stress concentration factor is  $\alpha = 3$ . From here the circumferential stress changes continuously to compressive stress  $-\sigma_0$  at point B. This has several interesting consequences. If this plate is also loaded at the edge by the stress  $\sigma_0$  in perpendicular direction, isotropic stress state has arisen with the stress  $\sigma_0$  in all directions. Everywhere along the surface of the opening tensile stress in circumferential direction  $2\sigma_0$  will act, similarly to the previous paragraph. For example, in vertical direction the stress  $3\sigma_0 + (-\sigma_0) = 2\sigma_0$  acts, and it holds for any direction in the plate plane.

3) The third case pertains to the loading of the plate by pure shear. Such load acts in components loaded by torsion. As it follows from Mohr's circle (Fig. 1.5d), this stress state arises also if the component is loaded by tensile stress  $\sigma_0$  acting at angle  $45^\circ$  and simultaneously by perpendicular compressive stress  $-\sigma_0$  (Fig. 1.5d). Tensile load causes tensile stress  $3\sigma_0$  on the surface at point A. The perpendicular compressive load causes at the point A also tensile stress  $\sigma_0$ . The resultant stress is thus tensile of magnitude  $4\sigma_0$ , so that the stress concentration factor is  $\alpha = 4$ . The hole in a hollow shaft transmitting twisting moment is therefore more dangerous than in a rod loaded by tension, or in a shaft or a bend beam.

4) Interesting situation is in Fig. 6.7. A crack emanating from the top of a hole in the plate loaded by compressive force will grow in the load direction. This looks paradoxically. However, it is so because the crack is at the place with tensile stress perpendicular to its plane (see point B in Fig. 6.6). If the plate is wide, the crack stops as soon as the crack arrives at the region where the tensile stress is low. Vice



**Fig. 6.7.** Crack propagation in the direction of acting stress.

versa, a relatively long crack emanating from a hole in a relatively narrow strip could grow further, if the strip halves can buckle.

5) Figure 6.2 shows an elliptical opening in a large elastic plate loaded perpendicularly to the long axis of the ellipse [3]. The maximum stress at the ends of the long axis is

$$\sigma_{\max} = \sigma_{\text{nom}} \left( 1 + 2 \sqrt{\frac{a}{\rho}} \right); \quad (6.6)$$

$\sigma_{\text{nom}}$  is the nominal stress in the plate,  $a$  is the length of its longer semi-axis, and  $\rho$  is the radius of curvature of the ellipse at this point. The maximum stress is higher for a narrower ellipse. For very high ratios  $a/\rho$  Equation (6.6) simplifies to

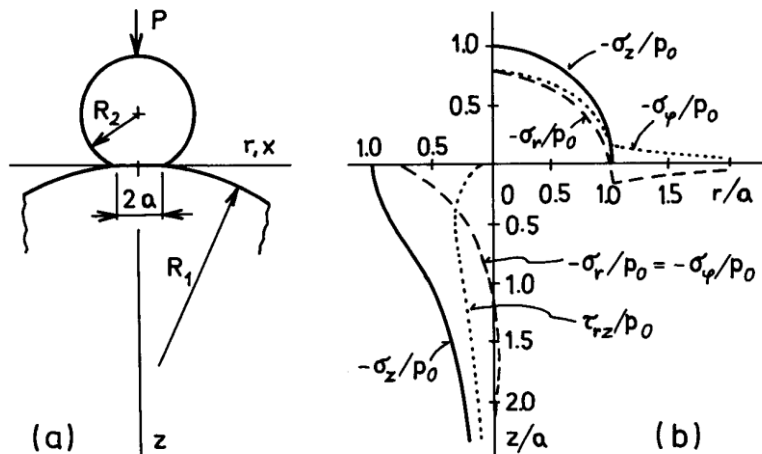
$$\sigma_{\max} = \sigma_{\text{nom}} 2 \sqrt{\frac{a}{\rho}}. \quad (6.7)$$

For  $\rho$  approaching to 0 the elliptic opening approaches to a crack, and the maximum stress  $\sigma_{\max}$  grows above all limits. This case will be addressed in the chapter on fracture mechanics.

Besides openings also many further stress concentrators exist. Any sudden change in shape or size of the cross section acts as a notch. Generally, the stress increase is higher if the notch is deeper (or if the change of diameter or thickness of a shaft is larger), and if the radius of notch root is smaller. A significant role is played by the shape of the notch. Even small shape change can result in significant reduction of maximum stress. These questions will be treated in more detail in Chapter 14 on the shape optimisation.

### 6.3 Stress state at concentrated contact

Local high stresses act sometimes at mutual contact of two bodies. The situation will be illustrated on the contact of bodies with rounded surfaces. The forces are transferred between the bodies over a small contact region. The stress state here is complex: the stresses act in three directions and decrease quickly with the distance from the contact area. Under low loads, both bodies are deformed only elastically, and the stresses and deformations can be determined according to the theory developed by Heinrich Hertz and other scientists. Here, we shall look on the contact of two spheres, pressed together by normal force  $P$  (Fig. 6.8). The initial contact is in one point. As the force increases, circular contact area of radius  $a$  is formed here, and becomes larger with higher force. Therefore the relationship between the load and the stresses or deformation in elastic contact is nonlinear.



**Fig. 6.8.** Contact of two spheres. **a** – geometry, **b** – contact stresses. Above horizontal axis: stresses in the contact area, below the axis: stresses beneath the surface in the contact axis. After [7].

The distribution of pressure on the contact surface is parabolic (the upper part of Fig. 6.8b), with the maximum value  $p_0$  in the centre [6 – 9]:

$$p_0 = \frac{3}{2} \frac{P}{\pi a^2} = \frac{1}{\pi} \sqrt[3]{\frac{6PE_e^2}{R_e^2}} ; \quad (6.8)$$

the equivalent curvature  $1/R_e$  of the contact (= the reciprocal of the radius of curvature) equals the sum of their curvatures:

$$\frac{1}{R_e} = \frac{1}{R_1} + \frac{1}{R_2} ; \quad (6.9)$$

$R_1$  and  $R_2$  are radii of curvatures of their surfaces at the contact.  $R_j$  is positive for convex surface, and negative for concave surface. If the surface is plane, the curvature  $1/R_j$  equals zero.  $E_e$  is the equivalent modulus of elasticity of both materials, calculated as

$$\frac{1}{E_e} = \frac{1-\mu_1^2}{E_1} + \frac{1-\mu_2^2}{E_2} . \quad (6.10)$$

In this case, reciprocal values of the moduli, i.e. the compliances, were summed, similarly to two springs in series. The Poisson's numbers  $\mu_1, \mu_2$  are here because the deformations in two perpendicular directions are mutually related.

The centres of both bodies get nearer by the value

$$w = \sqrt[3]{\frac{9P^2}{16RE_e^2}} = CP^{2/3} ; \quad (6.11)$$

$C$  is a constant expressing the contact compliance. Equation 6.11 is nonlinear, so that the principle of superposition cannot be used; the problem must always be solved for the actual load.

The radius of contact area is

$$a = \sqrt[3]{\frac{3PR_e}{4E_e}} . \quad (6.12)$$

The distribution of contact stresses is shown in Fig. 6.8b. At the edge of contact area tensile stress acts in radial direction, i.e. perpendicularly to its edge,

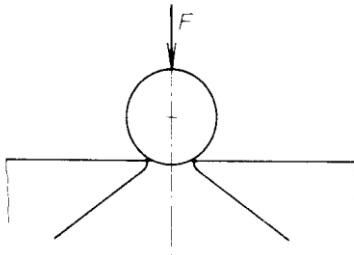
$$\sigma_{r,\max} = \frac{1-2\mu}{3} p_0 . \quad (6.13)$$

In the contact region also shear stress acts. It attains the maximum value at the depth  $a/2$ ; for  $\mu = 0,3$  it is

$$\tau_{\max} \approx 0.31 p_0 . \quad (6.14)$$

The state of stress has similar features also for other shapes of contacting surfaces. The formulae of similar kind for contact pressure, stress and deformations can be used also in contact of cylinders and other bodies, and it is sufficient if the surfaces in the contact region can be approximated by a part of a spherical or cylindrical surface, or – in more complex shapes – by means of two semi-ellipsoids; the pertinent formulae can be found in [6, 8, 9].

High stresses in the contact region can cause failure. If the tensile radial stress on the edge of contact area in a brittle material attains its tensile strength, a small ring-shaped crack is generated here. As the pressure on the contact surface increases, the material below it is pressed in the direction of force  $P$ , and the surrounding material prevents it. Shear stresses therefore act between the material outside the contact and inside it (that is beneath the loading force), and also at the edge of the crack, which gradually extends into a conical surface (Fig. 6.9; the corresponding tensile stress that opens the crack, is everywhere inclined to the axis by  $45^\circ$ ). In contact of ductile materials the material starts flowing plastically below the surface, in depth  $a/2$ , as soon as the maximum shear stress here attains the value  $\sigma_y/2$ . The plasticised region grows gradually, and at several times higher load it spreads to the surface [7].



**Fig. 6.9.** *Creation of a conical crack at concentrated contact (so-called Hertz' conical fracture).*

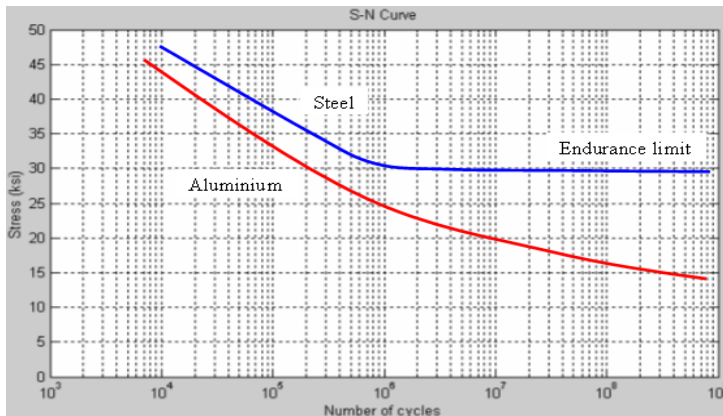
A fatigue crack in ductile material can be created below the surface under repeated contact, for example in metallic ball bearings. Such crack grows gradually, and after some time it penetrates onto the surface, and a small particle of material is peeled off. This gradual deterioration of surface is called pitting.

### References to Chapter 6.

1. Höschl, C. a kol.: Tabulky pro konstruktéry. 2.vyd. SNTL, Praha, 1961. 23 p. + 156 free sheets.
2. Černoch, S.: Strojně technická příručka. 12. vydání, díl 1, kapitola 5.11. SNTL, Praha, 1968. 1183 p.
3. Höschl, C.: Pružnost a pevnost ve strojnictví. SNTL, Praha, 1971. 375 p.
4. Peterson, R. E.: Stress Concentration Factors. J. Wiley and Sons, New York, 1974.
5. Kolektiv: Pružnost a pevnost II. Skriptum ČVUT, Fakulta strojní, Praha, 1985. 214 p.
6. Timoshenko, S. P., Goodier, J. N.: Theory of elasticity. 3rd Ed., McGraw-Hill, New York, 1970.
7. Menčík, J.: Strength and fracture of glass and ceramics. Elsevier, Amsterdam, 1992. 357 p.
8. Němec, J., Dvořák, J., Höschl, C.: Pružnost a pevnost ve strojnictví. SNTL, Praha, 1989. 600 p.
9. Birger, I. A., Panovko, Y. G.: Pročnosť, ustojčivost', kolebanija. Tom 2. Mašinostrojenije, Moskva, 1968.

## 7. Response under alternating load; fatigue

Metal parts loaded cyclically or periodically sometimes fail due to fatigue. This phenomenon appears in railway and other transport means, in various machines with rotating parts, but also in civil engineering constructions. Figure 7.1 depicts schematically the relationship between the stress amplitude and number of cycles to failure, so-called  $S-N$  or Wöhler curve. The number of cycles to failure increases with decreasing stress amplitude  $\sigma_a$ ; if  $\sigma_a$  is lower than so-called **endurance** (or fatigue) **limit**  $\sigma_c$ , the component can sustain unlimited number of loading cycles. However, the situation is more complex; some aluminium alloys, for example, do not exhibit fatigue limit at all. A role is also played by characteristic load.

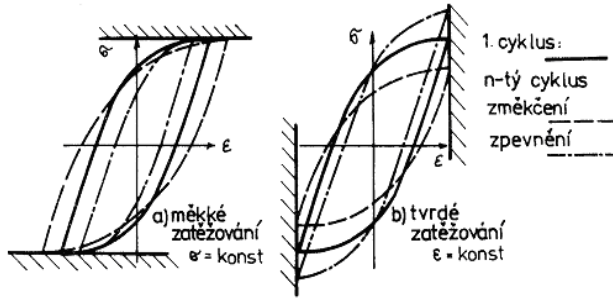


**Obr. 7.1.**  $S-N$  (Wöhler) curve [1].  $1 \text{ ksi} = 6,89 \text{ MPa}$ .

Fatigue process has four stages: 1) Change of mechanical properties 2) Creation of a crack, 3) Slow crack growth till the critical size, and 4) Fast fracture. Here, the first two stages will be discussed; the crack growth will be dealt with in Chapter 8.

### 7.1 Change of mechanical properties

Dislocations in a material start moving at very low stresses (MPa), but it is not obvious in the static stress-strain diagram yet. Under alternating loading new dislocations are generated; some block mutually and some disappear. All this is demonstrated by gradual change of properties (Fig. 7.2). One speaks about cyclical

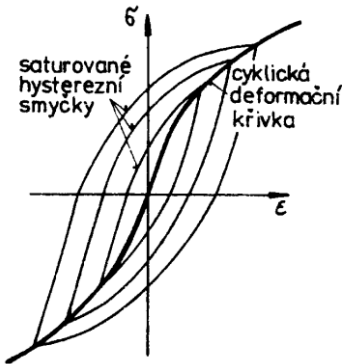


**Obr. 7.2.** Examples of cyclic softening and strengthening [2].

strengthening or softening. The first case occurs, e.g., in annealed steels, with small number of dislocations; softening occurs in high-strength steels. After several tens or hundreds of loading cycles the properties do not change any more; the hysteresis loop is saturated. Connecting the extreme values of these loops for various ranges of stress or strain gives so-called cyclic deformation curve (Fig. 7.3). This curve is usually described by

$$\varepsilon_a = \varepsilon_{a,el} + \varepsilon_{a,pl} = \frac{\sigma_a}{E} + \left( \frac{\sigma_a}{K'} \right)^{1/n'} ; \quad (7.1)$$

$K'$  and  $n'$  are constants, which are found in experimental way.



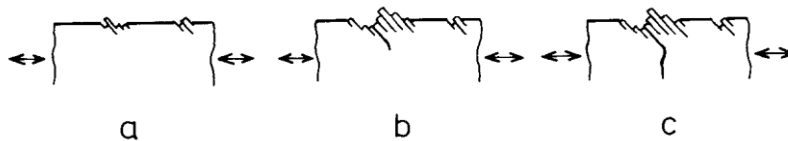
**Fig. 7.3.** Cyclic deformation curve [2].

## 7.2 Initiation and growth of fatigue cracks

Fatigue fracture usually starts at some stress concentrator. However, even without it a fatigue crack can be nucleated in a metallic material if the stress amplitude is higher than its fatigue limit [2 – 8]. In polycrystalline materials microplastic deformations and slips occur in oblique planes where the highest shear stresses act.



The easiest situation is in the surface layer, as here the slips are less restricted than inside the body (Fig. 7.9). During repeated loading dislocations are generated here, and the surface relief changes. The dislocations are gradually accumulated. All this damages the material, and since certain instant this place appears as a small crack. At the beginning the crack grows in the direction of maximum shear stress, which is inclined  $45^\circ$  to the direction of tensile force in a rod loaded by periodical axial force. Similarly fatigue cracks can be nucleated on the surface of any notch. After



**Fig. 7.4.** Nucleation and growth of a fatigue crack. *a* – slips in the surface layer due to shear stress, *b* – nucleation of fatigue crack in the direction of maximum shear stress, *c* – crack tip turning into the direction perpendicular to the maximum tensile stress.

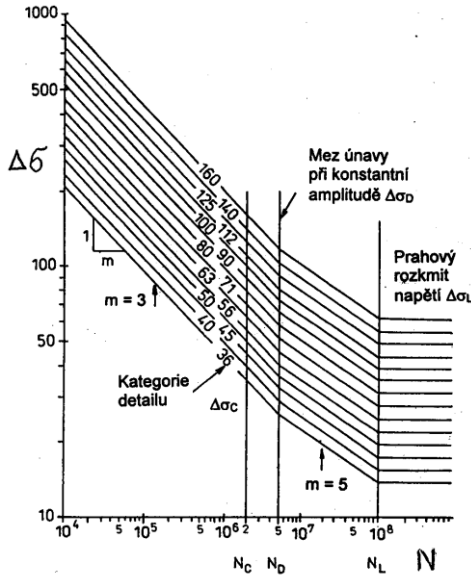
a while, the influence of macrostress prevails and the fatigue crack turns gradually into the direction perpendicular to the maximum tensile stress (Fig. 7.4c). Such crack can grow further only if tensile stress acts in its plane at least for a part of the loading cycle. In contrast, if the crack gets into the region of compressive stress, it can stop. This is used for increasing of fatigue resistance by shot peening, as it was shown in Chapter 4.8.

### 7.3 Time to fatigue failure

Under relatively low stresses (and very high number of cycles to failure) one speaks on high-cycle fatigue. This is well characterised by means of stress amplitude. Various expressions exist for the number of cycles to failure  $N_f$  [2 – 8]. The simplest one is the Wöhler curve (Fig. 7.1):

$$N_f = A \sigma_a^{-m}; \quad (7.2)$$

$A$ , and  $m$  are constants, found by measurement, and  $\sigma_a$  is the stress amplitude. In logarithmic form Eq. (7.2) changes to a straight line ( $\log N_f = \log A - m \log \sigma_a$ ). At higher amplitudes and lower number of cycles Equation (7.2) is not sufficiently accurate. Therefore the standard for metallic constructions uses a broken line (Fig. 7.5). This is due to the fact that the time to fatigue failure has two principal stages:

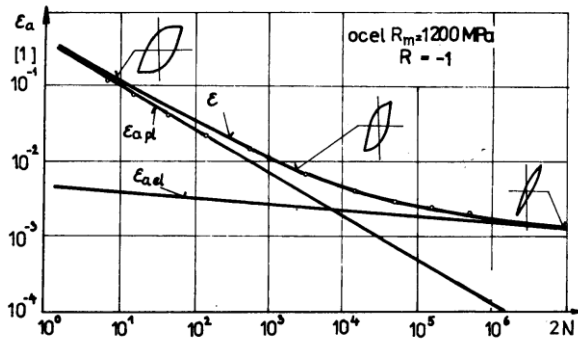


**Fig. 7.5.** Fatigue curves for steel parts according to the code [9]. Exponent of low-cycle fatigue  $m = 3$ , exponent of high-cycle fatigue  $m = 5$ . Category (detail No.) – see the code.

1) till the crack nucleation, and 2) the slow crack growth, and each is characterised by different exponent. At higher loads the Hooke's law is not accurate, and strain amplitude or range are more suitable for the determination of the time to failure. Here, one speaks about low-cycle fatigue. Both high-cycle and low-cycle fatigues are better described by the universal fatigue curve (Fig. 7.6):

$$\varepsilon_a = \frac{\sigma_f'}{E}(2N)^b + \varepsilon_f'(2N)^c \quad (7.3)$$

It has two asymptotes, which correspond to elastic and plastic component of strain in Eq. (7.1). The first component, prevailing at high-cycle fatigue, is the Wöhler



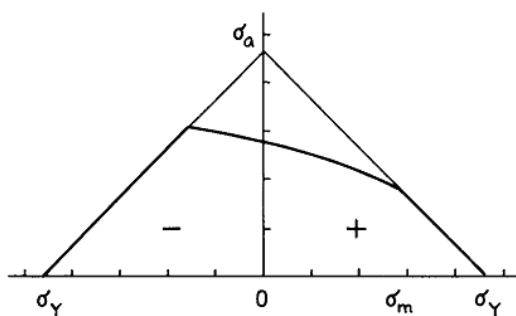
**Fig. 7.6.** Universal curve for low- and high cycle fatigue [2].

curve (7.2) divided by the Young modulus. The other component, so-called Manson-Coffin, expresses the dependence of the number of cycles to failure on the plastic component of the amplitude ( $\varepsilon_{\text{apl}}$ ). This is characterised by the names of the individual constants in Eq. (7.3):  $\sigma_f'$  is the fatigue strength coefficient,  $b$  – fatigue strength exponent,  $\varepsilon_f'$  – fatigue ductility coefficient, and  $c$  – fatigue ductility exponent. At left from the intersection of both asymptotes one speaks about the low-cycle fatigue, and right of it about high cycle fatigue.

**Remark.** The term  $2N$  in Eq. (7.3) expresses the number of half-cycles. These are more suitable for the evaluation of irregular or random loading, similarly as the stress range  $\Delta\sigma$  instead of amplitude ( $\Delta\sigma = 2\sigma_a$ ), because it is easily determined from the  $\sigma(t)$  record as the difference between the local maximum and minimum.

#### 7.4 Factors influencing the fatigue endurance

In addition to the stress amplitude or range a role is also played by the mean stress in the loading cycle, surface roughness, the component size and notches. The influence of mean stress is depicted in the Haigh diagram (Fig. 7.7, thick lines); also Smith diagram is used; see [2 – 6]. Tensile stress reduces the fatigue limit, while compressive stress increases it. The unfavourable influence of tensile stress is understandable, because a part of the fatigue process is spent by crack growth, and the crack is opened by tensile stress. Vice versa, compressive stress hinders the crack and can it even stop; remember the increasing of the life endurance by shot peening. The traces after machining and also any other surface unevenness act



**Fig. 7.7.** Haigh diagram.  $\sigma_a$  – amplitude,  $\sigma_m$  – mean stress in the cycle,  $\sigma_Y$  – yield strength, + tension, – compression. If the operation point ( $\sigma_m, \sigma_a$ ) lies below the limit line, the component does not fail.

as smaller or larger notches. The component size plays a role in two ways. A larger body has larger surface area, with higher probability that a larger material defect can exist here, which can act as a fatigue crack initiator. The stress gradient (from the surface inwards) in larger components loaded by bending is smaller, so that larger is the thickness of the surface layer, where some defect can play a role. The influence of a notch is characterised by so-called notch factor  $\beta$ , which is calculated from the stress concentration factor  $\alpha$ . The simplest formula for the **fatigue limit**  $\sigma_c^*$  of certain place is

$$\sigma_c^* = -\sigma_c \frac{\eta_p v}{\beta}; \quad (7.4)$$

$\sigma_c$  is the basic fatigue limit,  $\eta_p$  is the factor for the surface quality, and  $v$  is the size factor [2 – 6]. Similar recalculation is used for the timed fatigue limit, corresponding to certain number of cycles to failure (7.2). Several procedures exist for the prediction of the fatigue limit of various components; see, e.g. [4 – 8].

Certain problem for metal constructions is caused by residual stresses due to welding, as they cannot be released by annealing. The code [9] for steel constructions uses therefore a different approach. It gives fatigue curves for various construction details (Fig. 7.5), which were obtained by measurement on samples created by similar procedure as in reality, and contain also the residual stresses.

## 7.6 Damage accumulation

Fatigue curves show the relationship between characteristic load and the number of cycles to failure with the same character of loading. In reality, the stress amplitude often varies during the operation. The evaluation of the number of cycles to failure is not necessary if the largest amplitude is smaller than the fatigue limit. If it is higher, it is necessary to determine the number of cycles to failure, or to dimension the component appropriately. In such cases, a suitable hypothesis of damage accumulation is used. The simplest one, Palmgren-Miner hypothesis of linear damage accumulation, assumes that each loading cycle depletes certain part of the component life. So-called (relative) damage  $D$  is calculated, defined as the ratio of the number  $N$  of loading cycles undergone to the number  $N_f$  of cycles to failure under the same way of loading:  $D = N/N_f$ . The resultant damage at complex loading is calculated as a sum of damages during the individual processes:

$$D = \sum_j N_j / N_{f,j} \quad (7.5)$$

Failure can be expected for  $D = 1$ . If damage  $D_1$  for one day of operation is known, the component should sustain  $N_f = 1/D_1$  days. However, one must be aware of high dispersion of the number of cycles to failure, so that failure can also occur at  $D \leq 1$ .

Material fatigue is often a source of serious failures. Many procedures have been proposed for its evaluation, including random loading, and various commercial programs exist. For further study, Refs [4 – 8, 10 – 13] can be recommended.

### References to Chapter 7.

1. Wikipedia, the term Fatigue limit; 20. 4. 2019.
2. Růžička, M., Hanke, M., Rost, M.: Dynamická pevnost a životnost, ČVUT, Praha, 1987. 212 p.
3. Höschl, C.: Pružnost a pevnost ve strojnictví. SNTL, Praha, 1971. 375 p.
4. Höschl, C.: Únava materiálu při periodickém zatěžování. Dům techniky ČSVTS, Praha, 1981. 125 p. Volně na <http://www.it.cas.cz/cs/hoschl/skripta>.
5. Kolektiv: Pružnost a pevnost II. ČVUT Praha, SNTL, Praha, 1985. 214 p.
6. Růžička, M., Havlíček, V.: Výpočet strojních částí na únavu za normálních a zvýšených teplot I. Dům techniky ČSVTS, Praha, 1988. 88 p.
7. Fuchs, H. O., Stephens, R. I.: Metal Fatigue in Engineering. J. Wiley and Sons, New York, 1980.
8. Holzmann, M., Klesnil, M.: Křehký a únavový lom materiálů a konstrukcí. VUT Brno, SNTL Praha, 1972. 207 p.
9. ČSN 73 1401. Navrhování ocelových konstrukcí. Český normalizační institut, 1994, 1998. 134 p.
10. Höschl, C.: Únava materiálu při náhodném zatěžování. Dům techniky ČSVTS, Praha, 1982. 87 p. Available at <http://www.it.cas.cz/cs/hoschl/skripta>.
11. Růžička, M., Havlíček, V.: Výpočet strojních částí na únavu za normálních a zvýšených teplot II. Dům techniky ČSVTS, Praha, 1989. 84 p.
12. Růžička, M., Hanke, M.: Výpočet strojních částí na únavu za normálních a zvýšených teplot III. Dům techniky ČSVTS, Praha, 1990. 114 p.
13. Vlk, M.: Dynamická pevnost a životnost. VUT, Brno, 1992. 223 p.

## 8. Principles of fracture mechanics

### 8.1 Situation in bodies with cracks, principles of fracture mechanics

Figure 8.1 shows cracks in a bituminous pavement, which emanate from the corners of a metal hatch. This hatch prevents free dilatations of the asphalt during daily temperature changes. Stresses therefore arise here, highest at the cover corners. During heating, the bitumen wants to expand. It cannot, but as it is softer thanks to higher temperature, the thermal stresses relax. During the decrease of temperature, tensile stresses arise in the bitumen due to its effort to shrink. In cold brittle bitumen these stresses caused the formation of cracks. Their roots acted as strong stress concentrators, so that the cracks continued growing during changes of temperature despite of the large distance of their tips from the hatch corners.

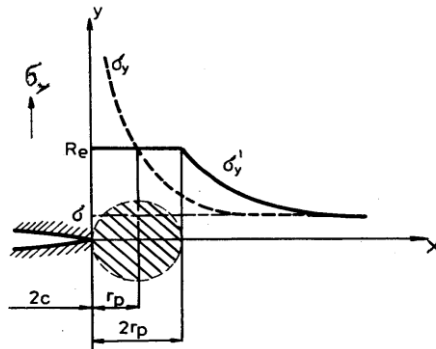


*Fig. 8.1. Cracks in a bitumen pavement at the corners of a metal cover, which have arisen due to thermal stresses.*

From the fracture point of view, the situation in bodies with one or more sharp cracks is worse than in case of notches, described in the previous chapter. The cracks could have been generated during manufacture or operation, for example due to fatigue under repeated loading. A body with a crack breaks more easily in a brittle manner, especially under impact. Thanks to a sharp root, the crack represents a very strong stress concentrator, which significantly limits the plastic deforming, and thus also the energy absorption at the region. According to theoretical analysis, the stress in front of a sharp crack in an elastic body is

$$\sigma(r) = \sigma_{nom} C \sqrt{\frac{a}{r}} ; \quad (8.1)$$

$\sigma_{nom}$  is the nominal stress,  $C$  is a constant,  $a$  is the crack length or another characteristic dimension, and  $r$  is the distance from the crack tip (Fig. 8.2).



**Fig. 8.2.** Stress distribution and plastic zone in front of the crack.  $\sigma_y$  – stress perpendicular to the crack plane,  $\sigma_y'$  – stresses corrected for the plastic zone of radius  $r_p$  (hatched),  $2c$  – crack length,  $Re$  – yield strength of the material.

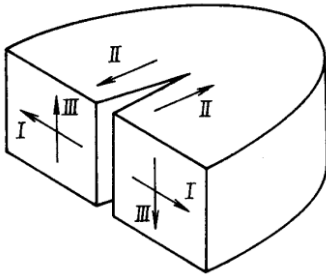
This solution gives infinitely high stress at the crack root ( $r \rightarrow 0$ ), which is impossible. This contradiction made big problems initially in the investigation of the conditions for fracture. Later, two approaches were proposed, which have overcome the problem [1 – 4]. The first one, formulated by Irwin and Orowan, uses the concept of **stress intensity factor  $K$** . This factor characterises simultaneously the influence of nominal stress and the crack size in the following way

$$K_i = \sigma_{nom} Y \sqrt{a} ; \quad (8.2)$$

$Y$  is a shape factor that includes the influence of the shape and position of the crack, its relative size with respect to cross section area in the investigated place, and also the character of the stress distribution (tension, bending, etc.) The dimension is  $\text{Pa}\cdot\text{m}^{1/2}$  or  $\text{MPa}\cdot\text{m}^{1/2}$ . (Caution when using mm instead of m, as  $\sqrt{1000} = 31,6$ , so that the value is different !) The subscript  $i$  at the stress intensity factor (I, II or III) denotes the mode of crack opening (Fig. 8.3). Note that Eq. (8.2) is similar to Eq. (8.1) for the stress at unit distance in front of the crack, i.e. for  $r = 1$ .

The crack grows quickly if the stress intensity factor attains the critical value, i.e.

$$K \geq K_C . \quad (8.3)$$



**Fig. 8.3.** Principal modes of crack opening.

The most important case is simple opening (mode I). The corresponding critical value is denoted  $K_{IC}$  and called **fracture toughness**. It is measured on standard specimens. A suitable specimen with a crack, for which the relationship between load  $F$ , crack length  $a$  and the value of stress intensity factor,  $K_I = f(F, a)$ , is loaded by continuously growing force till the start of fast crack growth. The corresponding load and crack length are used for the determination of the value of  $K_I$ , which represents the fracture toughness  $K_{IC}$ . A possibility of fast fracture of another body can be assessed if the value of  $K_I$  for this body with actual crack and load is compared with the value of fracture toughness  $K_{IC}$  for the same material. This approach has overcome the necessity to know accurately the true magnitude of the highest stress at the crack root.

Formulae or diagrams for the determination of stress intensity factor can be found in various handbooks [5, 6, 3], or they can be obtained by means of a suitable computer model. Figure 8.4 presents two examples, and one specimen for the determination of fracture toughness is shown in Fig. 8.5.

A component with a crack fails if the stress intensity factor at certain place attains the critical value (and does not drop below  $K_{IC}$  soon). It follows from Eqs. (8.2) and (8.3) that a component with a crack breaks if the nominal stress attains the critical value

$$\sigma_{cr} \geq \frac{K_C}{Y\sqrt{l_{cr}}} \quad (8.4)$$

Vice versa, critical crack length for certain nominal stress  $\sigma_{nom}$  can be determined,

$$l_{cr} = \left( \frac{K_C}{Y\sigma_{nom}} \right)^2, \quad (8.5)$$



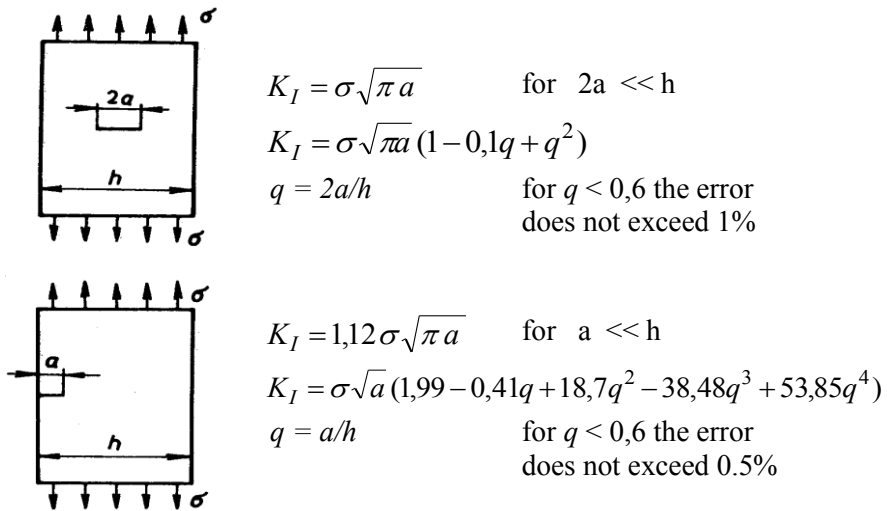


Fig. 8.4. Stress intensity factor for plates with central and edge crack [3 - 6].

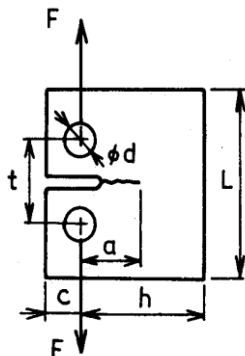


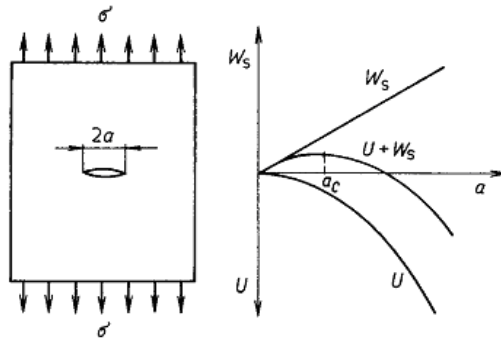
Fig. 8.5. Compact Tension (CT) specimen for the determination of fracture toughness [3].

$$K_I = \frac{F a^{1/2}}{bh} (29,6 - 185,5q + 655,7q^2 - 1017q^3 + 638,9q^4)$$

$$q = a/h$$

and it can be checked (or ensured) that cracks larger than  $l_{cr}$  cannot appear in the product. As the shape factor  $Y$  of longer cracks depends also on their size, it is sometimes necessary to find the critical length by iteration procedure.

The other approach to the assessment of a body with a crack, as proposed by A. Griffith, is based on energy principles. The body with a crack contains accumulated energy of elastic stresses. If the crack grows, this energy is released. On the other hand, the crack growth consumes energy, especially for plastic deforming of the material in the region of high stresses in front of the crack. The situation is depicted in Fig. 8.6. The energy, consumed for the creation of new fracture surfaces is directly proportional to the crack length. The released energy is proportional to the square of this length; for simplicity we can imagine that the creation of a crack



**Fig. 8.6.** Plate with a crack – energy balance [1].

$U$  – energy of elastic stresses, released by the crack growth,

$W_s$  – energy consumed by the crack growth,  $a_c$  – critical length.

releases the stresses and energy from the circular area of the same diameter as the crack. At the beginning more energy is consumed for crack growth than released, but from certain instant (corresponding to crack length  $a_c$ ), the energy released by this growth prevails, and the fracture process becomes unstable. The description of this process uses so-called **strain energy release rate**  $G$ , defined as the energy released by the increase of fracture surface by unit of area ( $\text{J/m}^2$ ), and **specific fracture energy**  $\Gamma$ , which expresses how much energy is needed for the creation of fracture surface of unit area ( $\text{J/m}^2$ ). The condition of spontaneous fast crack growth is

$$G \geq \Gamma, \quad \text{or} \quad G \geq G_C, \quad (8.6)$$

where  $G_C$  means critical value of energy release rate.

Both approaches are equivalent if fracture of brittle character is judged. For simple crack opening, for example,

$$G_I = K_I^2 / [E/(1 - \mu^2)] . \quad (8.7)$$

The formulae for other modes of crack opening are similar. Table 8.1 shows the values of fracture toughness and specific fracture energy for some materials.

Remark. Other approaches are used for ductile materials [1].

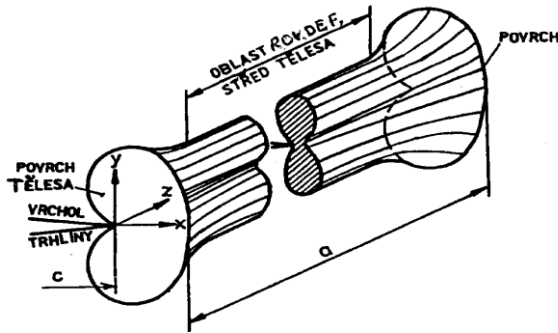
If the possibility of failure should be judged, usually the stress intensity factor is used. However, it is useful to look always on the matter from the energy point of view. At impact, for example, certain amount of energy is delivered into the body. And the fracture can be expected only if this amount is higher than the value  $\Gamma \times S$ ,

**Table 8.1.** Fracture toughness  $K_{IC}$  and specific fracture energy  $\Gamma_C$  of several materials [3, 4]. *r.b.* – reaction bonded, *h.p.* – hot pressed.

Material	$K_{IC}$ (MPa m <sup>1/2</sup> )	$\Gamma_C$ (J/m <sup>2</sup> )
steel	30 – 140	4000 – 85000
grey cast iron	10 – 25	860 – 5400
ceramics r.b.	1,5 – 3,5	2 – 50
ceramics h.p.	2,5 – 5,0	12 – 80
glass-ceramics	1,8 – 4,5	30 – 210
glass	0,6 – 1,0	6 – 10
epoxy resins	0,5 – 2,0	50 – 200

$\Gamma$  being the specific fracture energy and  $S$  the area of the remaining part of the cross section. Similarly it is possible to predict the enlargement of the existing crack by impact, and the corresponding strength degradation.

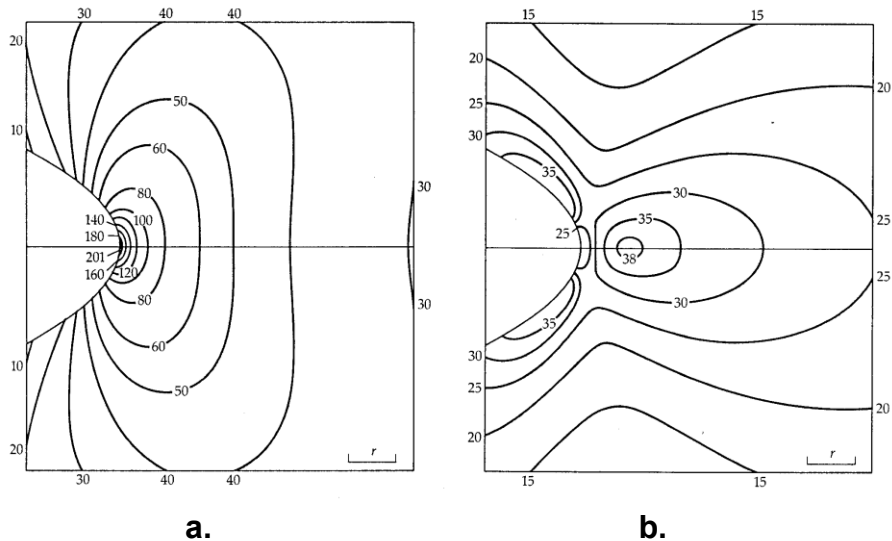
Fracture toughness of common technical materials is determined according to standards, which also prescribe dimensions of the specimens. Thickness is very important for metallic materials. This is related to the ductility of metals. High stresses cause plastic flow in the vicinity of crack tip. The boundary between the elastic and plastic region can be determined according the von Mises hypothesis of the density of strain energy responsible for shape change, or according to the Tresca's hypothesis of maximum shear stress [1]. Both approaches give similar results. Figure 8.7 shows the shape of plastic zone in front of a crack in a plate. The plane stress state is on the side surfaces: the stress acts only in the plane of surface, without any force perpendicular to it. Inside the specimen, whose thickness cannot change, plane strain exists and also stress parallel to the crack front. We can see that the plasticised region on the sample sides is larger (thanks to more favourable conditions for plastic flow) than inside, at places more distant from the edges. The energy consumption at the edges will be higher. Therefore, in a thin specimen, whose prevailing part is in the state of plane stress, more energy is consumed than in a thick specimen, where plane strain prevails, with smaller size of plastic zone. A thin specimen starts breaking at higher stress than a thick one. The specimen for the measurement of fracture toughness should therefore have at least certain minimum thickness ensuring that plain strain will exist in the crack region, and giving the lower (i.e. conservative) value of fracture toughness. The corresponding



**Fig. 8.7.** Plastic zone in front of the crack tip. Plane stress is on side surfaces; the smaller zone in the interior corresponds to the plane strain [11].

thicknesses are given, for example, in the standards for metal constructions [7]. If a component with larger thickness were dimensioned using the (higher) value of fracture toughness obtained on thin specimens, such component could break unexpectedly earlier. The critical value of stress intensity factor for thin-walled components could be found by a suitable test, or from a finite element model based on elastic-plastic material model.

Let us look at an interesting feature of stress distribution in front of the crack. The attention is usually oriented at the stress acting perpendicularly to the crack plane. This stress increases strongly with decreasing distance from the tip, and material flow in plastic manner if the stress attains (or exceeds) the yield strength (Fig. 8.2, 8.7). This limits further increase of stresses, which should grow to infinity at the tip according to the elastic theory and Hooke's law. (In reality, they would be limited by plastic flow or another process.) However, the distribution of elastic stresses in front of the crack is more complicated. In addition to the stress perpendicular to the crack plane, also tensile stress acts here in the direction of its propagation in a small region (Fig. 8.8). Cook and Gordon [8, 9] have shown that this stress can be used for the stopping of the principal crack, horizontal in the figure. The sufficient condition is lower strength of material in the direction of crack propagation. This Cook-Gordon mechanism is sometimes used for increasing the resistance against crack propagation in composite materials. A growing crack is deflected as soon as it arrives at the weak interface with another phase. In this way, a crack propagating in polymeric matrix perpendicularly to the fibres can turn and branch many times. Sometimes it can be observed also on a broken branch of a tree or a bush. The crack deflecting and branching increases significantly the consumption of energy



**Fig. 8.8.** Stress field in front of elliptic crack [8, 9]. **a** – stresses perpendicular to the crack plane, **b** – stresses in the crack direction. In case **b** note the region with relatively high tensile stress at small distance ahead of the crack tip.

during the fracture. Similarly, deflection at the interface can prevent the penetration of the crack from the coating into a massive body (see also Chapter 11). The price for this can be the gradual delamination of this protective layer and the deterioration of the surface exposed to the harmful environment.

## 8.2 Growth of fatigue cracks

Nucleation of fatigue cracks was described in the previous chapter. Now we shall look at their growth. The velocity of slow propagation of fatigue cracks under cyclical or periodical loading depends on the range of stress intensity factor

$$\Delta K = K_{\max} - K_{\min} , \quad (8.8)$$

where  $K_{\max}$  and  $K_{\min}$  are maximum and minimum value of  $K$ -factor in a loading cycle. Also the mean stress plays a role. The velocity as a function of  $\Delta K$  is depicted schematically in Fig. 8.9a. The crack starts growing if the range  $\Delta K$  exceeds certain threshold value  $\Delta K_{th}$  of the material (part I). Its velocity increases with increasing stress range, and finally it passes into the fast stage (region III). The region II is most important for the prediction of the time to failure of a

component with a crack. Here, the velocity of crack propagation is often approximated as

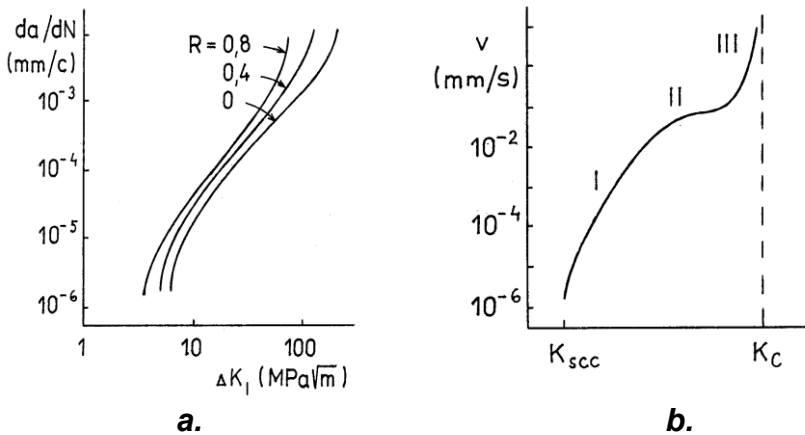
$$v = da/dN = A\Delta K_I^n; \quad (8.9)$$

$da/dN$  is the increment of crack length per loading cycle, and  $A, n$  are constants for the material. (The power-law function (8.9) looks as a straight line in logarithmic coordinates.) With respect to the definition of stress intensity factor, it follows from Eq. (8.9) after rearrangement that the number of cycles  $N$  for increase of the crack from initial length  $a_i$  to length  $a$  under loading by cyclical stress of range  $\Delta\sigma$  is:

$$N = \int_{a_i}^a \frac{da}{A\Delta K_I^n} = \int_{a_i}^a \frac{da}{A(\Delta\sigma)^n Y^n a^{n/2}} \quad (8.10)$$

If the upper limit  $a$  equals the critical length  $a_{cr}$  (or  $l_{cr}$  in Eq. 8.5) corresponding to the instant when the maximum value of stress intensity factor in a loading cycle attains the critical value  $K_{IC}$ , the number of cycles to failure is obtained.

The fact that fatigue crack does not grow if the range of stress intensity factor is smaller than the threshold value, has important practical consequence: the growth of an existing crack can be stopped by reducing load so that  $\Delta K$  drops below  $\Delta K_{th}$ .



**Fig. 8.9.** Velocity of growth of fatigue cracks as functions of stress intensity factor: *a* – in ductile materials, *b* – in brittle materials (*a* schematic).

Cracks in ceramic materials grow sometimes very slowly even under constant stress, due to the corrosion of the stressed material at the crack root by the action of

the environment (so-called stress corrosion cracking); one speaks of static fatigue. The crack velocity  $v = da/dt$  depends on the stress intensity factor. The course  $v(K)$  is depicted schematically in Fig. 8.9b. The crack starts growing if the stress intensity factor is higher than a threshold value  $K_{\text{sc}}c$ . The growth becomes faster with increasing  $K_I$ , and for  $K_I \geq K_{\text{IC}}$  it goes into a very fast stage.

The part I (with the exception of vicinity to  $K_{\text{sc}}c$ ) is often approximated by a power-law function

$$v = da/dt = A' K_I^{n'} ; \quad (8.11)$$

the constants  $A'$  and  $n'$  (different from  $A, n$  in Eq. 8.9) are obtained experimentally for the given material and environment. Similarly to the previous case, it is possible to determine the time for crack growth from the initial length  $a_i$  to  $a$ :

$$t = \int_{a_i}^a \frac{da}{A' K_I^{n'}} = \int_{a_i}^a \frac{da}{A' \sigma^{n'} Y^{n'} a^{n'/2}} \quad (8.12)$$

and the time corresponding to attaining the critical crack length  $a_{\text{cr}}$ .

### 8.3 Increasing the resistance to crack propagation

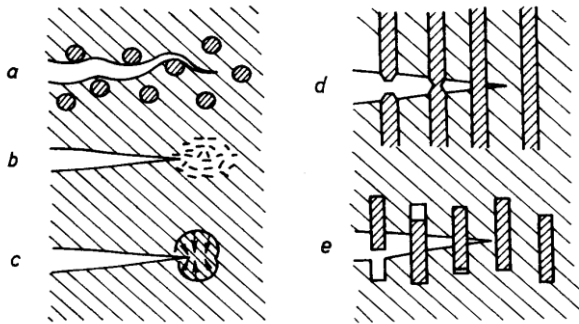
General ways for increasing the material resistance to crack growth are shown in Fig. 8.10. An efficient way is increasing the energy consumption in the crack region. The absorbed energy is proportional to the product of specific fracture energy  $\Gamma$  ( $\text{J/m}^2$ ) and fracture area  $S$ ,

$$W = \Gamma \times S. \quad (8.13)$$

The increase of energy absorption in brittle materials can be achieved (for example) by making longer the actual crack way (and fracture surface) by dispersing hard particles in the matrix of a composite material (Fig. 8.10a). The crack must circumvent them, which makes the way and area of fracture larger. In special kinds of ceramics the material in front of the crack gets multiply cracked (Fig. 8.10b). Numerous fracture surfaces arise here, which absorb energy. An interesting way is used in partially stabilised zirconia ceramics  $\text{ZrO}_2$ . Very high stress in front of the crack induces phase transforms here. Monoclinic phase is created here, whose volume is larger than that of the original tetragonal phase. In this way regions with compressive stresses are continuously formed in front of the propagating crack, which hinder its growth (Fig. 8.10c). Long strong fibres in

fibrous composites (Fig. 8.10d) increase the strength. On the other hand, short fibres used for strengthening are pulled out of the matrix during the fracture (Fig. 8.10a). For this process, friction forces between the fibres and matrix must be overcome, and also the corresponding work must be expended.

The main mechanism of energy consumption in ductile metallic materials is plastic deforming in the crack region. Tensile stress at a distance  $r$  in front of the crack in elastic material (Fig. 8.2) is given by Eq. (8.1). At the distance  $r_{pl}$  this stress attains



**Fig. 8.10.** Increasing of the resistance to crack propagation.

the yield strength  $\sigma_Y$  and the material flows plastically there. This distance can be assessed as that corresponding to the stress  $\sigma_Y$  in (8.1). A rearrangement gives the radius of plastic zone

$$r_{pl} = \left( \frac{\sigma_{nom}}{\sigma_Y} \right)^2 a. \quad (8.14)$$

The plastic zone will be larger for lower yield strength of the material. If more energy should be absorbed in a fracture, lower yield strength would be better.

The resistance against propagation of fatigue cracks in metallic materials can be increased also by creating compressive prestress in the surface layer by local plastic forming, for example by shot peening or rolling described in Chapter 4.8.



### References to Chapter 8.

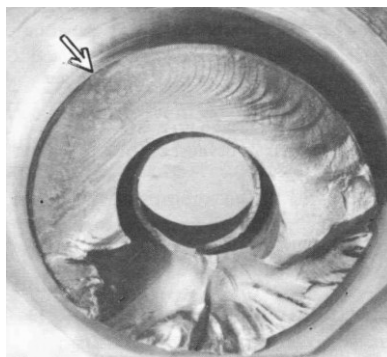
1. Broek, J. D.: *Elementary Engineering Fracture Mechanics*. 4th Ed. Kluwer Academic Publishers, Dordrecht, 1991.
2. Fuchs, H. O., Stephens, R. I.: *Metal Fatigue in Engineering*. J. Wiley and Sons, New York, 1980.
3. Menčík, J.: *Strength and fracture of glass and ceramics*. Elsevier, Amsterdam, 1992, 357 p. (Pevnost a lom skla a keramiky. SNTL, Praha, 1990. 392 p.)
4. Menčík, J.: *Mechanics of Components with Treated or Coated Surfaces*. Kluwer Academic Publishers, Dordrecht, 1996.
5. Murakami, Y. (editor): *Stress Intensity Factors Handbook 1, 2, 3*. Pergamon Press, Oxford - New York, 1978 - 1992.
6. Rooke, D. P., Cartwright, D. J.: *Compendium of Stress Intensity Factors*. HM Stationery Office, London, 1976.
7. ČSN 73 1401. *Design of steel structures*. (In Czech: Navrhování ocelových konstrukcí.) Český normalizační institut, 1998. 134 p.
8. Gordon, J. E.: *The New Science of Strong Materials*. Penguin Books Ltd., Harmondsworth, England, 1968. 269 p.
9. Gordon, J. E.: *The Science of Structures and Materials*. Times Books, New York, 1988. 217 p. (Strukturen unter Stress. Spektrum der Wissenschaft, Heidelberg, 1989. 216 p.)
10. Klesnil, M., Lukáš, P.: *Fatigue of Metallic Materials*. Academia, Praha, 1992.
11. Veles, P.: *Mechanické vlastnosti a skúšanie kovov*. ALFA, Bratislava, 1985. 408 p.

## 9. Fracture analysis

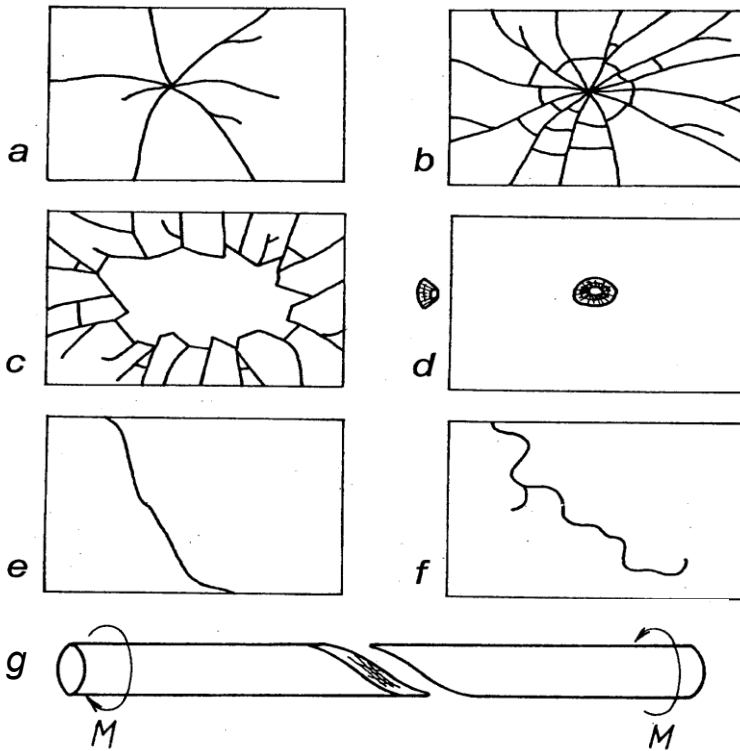
General knowledge on the state of stress and behaviour of cracks is very useful in the analysis of failures. This analysis has three sources: appearance of the damaged body, history of the failure, and the information on the loads, material properties and conditions of operation. Analysis of fractures is treated in more detail in [1], the analysis of failures in [2 – 6]. Here some notes will be given.

Observation of the failed body can show the starting point of the fracture (Fig. 9.1, 9.2), and to reveal its internal cause, for example a material defect. Fracture mechanics then helps in the determination of magnitude of stresses and forces acting in the critical point at the instant of failure. The appearance of the fracture surface and trajectory of the crack inform on the course of fracture process, characteristic fracture mode (e.g. brittle fracture, fatigue fracture) and on the kinds of acting stresses (e.g. shear stresses leading to torsional fracture, Fig. 9.2g). Some details are visible by the naked eye, while some other need an electron microscope. Always it is useful to create photographic documentation, or, at least, the detailed description of the damaged object

On macroscale, the crack has a tendency to propagate perpendicularly to the highest tensile stress. The final failure of the individual grains in polycrystalline ductile materials occurs by shear. Therefore, the fracture surface on microscopic scale is



**Fig. 9.1.** Fatigue fracture of a shaft. The arrow shows the failure origin. The fatigue crack propagated slowly from here (smooth lines) to the rough part of the cross section, typical of the final fast period of fracture.



**Fig. 9.2.** Examples of crack trajectories. *a - f: cracks in glass panes (after [1]): a - force acting perpendicularly to the pane, b - as a, but more intensive load, c - explosion in the room, d - shot through, e - fracture caused by twisting, f - thermal stress, g - fracture of a rod from brittle material by twisting.*

formed by a large amount of various oblique areas, corresponding to the directions of shear stresses in the individual grains. Certain role is also played by the different ability of the material to resist normal and shear stresses. Figure 9.3 shows a specimen of a relatively brittle Al alloy destroyed in tensile test. The fracture surface in one direction is perpendicular to the rod axis, i.e. perpendicular to the maximum normal stress, while in the other direction it is inclined by  $45^\circ$ , which corresponds to the direction of maximum shear stress.

Another example of the effect of thermal stresses was shown in Fig. 8.1. The cracks in the pavement at the edges of a metal hatch arose due to restraining free asphalt dilatations during daily temperature changes.



**Fig. 9.3.** Specimen of an Al alloy after tensile test. Width 11 mm, thickness 3 mm.

Fracture analysis starts with the observation of the general appearance of fractured body. The analysis is facilitated by the following rules:

1) Usually only one fracture focus exists. The fracture of a body with crack-like defects goes out from the place where the stress intensity factor has first reached the critical value. The formula  $K_I = \sigma Y \sqrt{a}$ , together with the knowledge of the defect size, can be used for the determination of stress (and load) at the instant of fracture,

$$\sigma = \frac{K_{IC}}{Y\sqrt{a}}, \quad (9.1)$$

or for the determination of the size  $a$  of the critical flaw for the known stress magnitude  $\sigma$ .

$$a = \left( \frac{K_{IC}}{\sigma Y} \right)^2. \quad (9.2)$$

This approach is used in search for critical defects in ceramic or metal materials [1] and elsewhere.

2) The failure nearly always starts on the surface. An exception is a material defect inside the body, or crack nucleation below the surface under contact load.

3) The crack has tendency to propagate perpendicularly to the maximum tensile stress. An exception is the initial short part of a fatigue crack in components in ductile materials under cyclical load, where the direction of propagation coincides with the direction of maximum shear stress. Later it turns to the direction perpendicular to the maximum tensile stress (Fig. 7.4).

4) Crack branching occurs in brittle materials, such as glass, if the stress intensity factor has attained certain critical value for branching [7]. Generally, a relation exists between the energy release rate and the area of the fracture surface. For example, tempered glass disintegrates into many small pieces during fracture (Fig. 5.5), smaller for higher internal stress and thus also higher accumulated energy. High number of small pieces corresponds to the larger fracture surface, and, therefore, to higher total consumed energy. With fatigue cracks in metals, the transition to fast stage of fracture is accompanied by significant roughening of the fracture surface, which has larger surface area.

An interesting case is a glass plate that was shot through (Fig. 9.2d). At the first contact of the bullet with the glass a small circular ring arises at the edge of contact area. As compressive force acts on the central part of the loaded area, and the region out of it resists to this force, shear stresses appear at the crack tip. Their effect is similar to the effect of tensile stress in the direction inclined by  $45^\circ$  (Fig. 9.2d). The crack therefore starts growing in the directions perpendicular to this tensile stress, which everywhere contain  $45^\circ$  with the direction of the bullet movement. A conical crack thus arises here, diverging from the point of first contact (see also Fig. 6.9). Finally, a small piece of glass flies out together with the bullet.

Figure 9.4 shows a cracked wall. The oblique direction of the crack indicates the presence of shear stresses. The most probable reason was insufficient bearing capacity of foundations below the left part of the wall.



**Fig. 9.4.** Crack in the wall of an old building

The analysis of a particular failure is based on its time course and the situation before it, and on the information about the history of operation and conditions of use. This part of analysis is based on the records from the operation (time course of temperatures, pressures, further loads acting on the object, information about the environment and personnel). Useful are the records of measuring devices and in logbooks, and the reports from inspections.

Often analysis of the stresses acting in the component is done, and also analysis of mechanical properties, including mechanical tests of specimens taken out from the critical parts (tensile or fatigue tests, tests of notch or fracture toughness, etc.).

Failure analysis can lead to the measures for avoiding similar failures in similar components. Well known are detailed analyses done after aircraft accidents, but also after every accident with fatal consequences. Some rules are summarised in [2]. Examples of many failures can be found in the literature, for example [3 – 6]. Very interesting are also the TV series „Seconds from disaster“ or „Air crash investigations“, available on YouTube.

### **References to Chapter 9.**

1. Menčík, J.: Strength and fracture of glass and ceramics. Elsevier, Amsterdam, 1992, 357 p. (Pevnost a lom skla a keramiky. SNTL, Praha, 1990. 392 p.)
2. Menčík, J.: Concise Reliability for Engineers. Intech, Rijeka, 2016, An open access publication: <http://www.intechopen.com/books/concise-reliability-for-engineers>, ISBN 978-3540629375. 204 p.
3. Neale, B. S., editor: Forensic engineering. The investigation of failures. Thomas Telford Publishing, London, 2001. 219 p.
4. Ratay, R. T., editor: Forensic Structural Engineering Handbook. McGraw-Hill, New York, 2009. 688 p.
5. Wearne, P.: Collapse. When Buildings Fall Down. TV books, New York, 2000. 255 p.
6. Lancaster, J.: Engineering catastrophes. 3rd ed. CRC Press, Woodhead Publishing Ltd., Abington, 2005. 269 p.
7. Kerkhof, K.: Bruchvorgänge in Gläsern. Verlag der DGG, Frankfurt am Main, 1970.

## 10. Mechanics of viscoelastic materials

Deformations of many materials depend not only on the load magnitude, but also on its duration and time course. Examples are plastics and other polymeric materials, biological materials, but also metals and ceramics at high temperatures. We speak in these cases of viscoelastic materials. Their response to load can be represented by combination of basic elastic and viscous elements. The elastic elements characterise the instantaneous elastic response, the viscous elements characterise the time dependent components of deformation. As we shall see, viscoelastic models can also be used for the description of delayed elastic deforming, relaxation of forces and stresses, and of creep. So-called linear viscoelasticity pertains to the cases where the instantaneous effect is directly proportional to the stress. Hooke's law is valid for elastic elements, and Newton's law for viscous elements. The following text will show the most important material models; more can be found in literature [1 – 4].

### 10.1 Ideally elastic material

It is depicted by a spring (Fig. 10.1a). The deformations obey Hooke's law, which has the following form for the strain  $\varepsilon$  in the direction of normal stress  $\sigma$ :

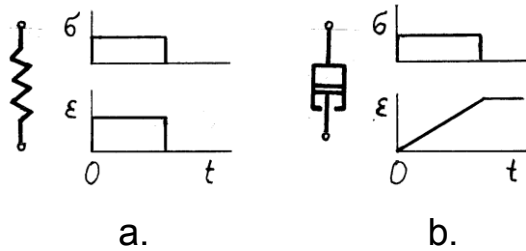
$$\varepsilon = \sigma/E; \quad \sigma = E\varepsilon. \quad (10.1a)$$

$E$  is the tensile modulus of elasticity. Similar relations hold for shear deformation:

$$\gamma = \tau/G; \quad \tau = G\gamma; \quad (10.1b)$$

$G$  is the shear modulus of elasticity, which is related to the Young (tensile) modulus as  $G = E/[2(1 + \mu)]$ . The constant  $\mu$  is the coefficient of lateral contraction (Poisson's number). Its value can vary in the range 0 – 0,5. Usually it is between 0,15 for brittle and 0,35 soft ductile metallic materials; for steel,  $\mu = 0,3$ . For incompressible materials,  $\mu = 0,5$ ; the same value is used for liquids.

These materials are called Hookean, and their response to load is instantaneous. Figure 10.1a shows the time course of deformation corresponding to the sudden (step) increase of stress to the value  $\sigma$  at time 0, and step decrease to 0 at time  $t_1$ .



**Fig. 10.1.** (a) Ideally elastic element, (b) Ideally viscous element.

## 10.2 Ideally viscous material

This material can be depicted schematically as a dashpot, where a fluid flows between the piston and cylinder (Fig. 10.1b). Newton's law is valid:

$$\dot{\gamma} = \tau / \eta, \quad \tau = \eta \dot{\gamma}, \quad \text{or} \quad \dot{\epsilon} = \sigma / \lambda, \quad \sigma = \lambda \dot{\epsilon}; \quad (10.2a,b)$$

$\eta$  is dynamic viscosity (dimension Pa.s),  $\dot{\gamma}$  is the shear strain rate, and  $\tau$  is the shear stress,  $\lambda$  is dynamic viscosity in tension (Pa.s), and  $\dot{\epsilon} = d\epsilon/dt$  is the rate of relative elongation. These materials are called Newtonian.

Remark. This chapter deals with viscoelastic behaviour of more or less solid objects. Therefore the term “tensile viscosity” will be used here. The dynamic viscosity in tension  $\lambda$  and in shear  $\eta$  of an incompressible material are related as  $\lambda = 3\eta$ . Here, the symbol  $\eta$  will be used everywhere.

Figure 10.1b also shows the time course of stress (sudden increase to  $\sigma$  in time  $t_0$ , dwell at this value till the time  $t_1$ , followed by sudden drop to zero) and the corresponding course of deformation of a viscous material.

The following part of this chapter, devoted to the individual models, will show relationships between stresses, strains, and strain rates. Similar relationships exist between forces, total deformations, and their velocities; the differences exist only in the constants characterising the geometry of the body. For example, the total elongation of an elastic rod loaded by axial tensile force is  $\delta = [FL/S]/E = \sigma l/E$ , and the relative elongation is  $\epsilon = \sigma/E$ .

More complicated responses can be modelled by combination of several elements. The typical models were named after their authors.

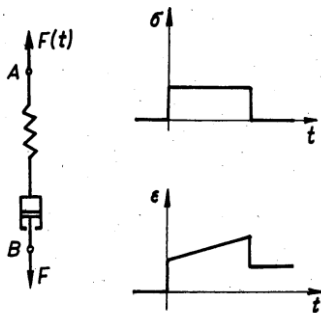


### 10.3 Maxwell model

It is a spring and a dashpot in series (Fig. 10.2). The same force acts in both elements, but their deformations are added together. The stresses and strains are:

$$\sigma = \sigma_H = \sigma_N, \quad \varepsilon = \varepsilon_H + \varepsilon_N; \quad (10.3a, b)$$

subscript H means Hookean, N means Newtonian. The resultant strain in this case, however, cannot be calculated directly, as the stress in a viscous element is



*Fig. 10.2. Maxwell model. Creep under constant load and after unloading.*

directly proportional not to the strain, but to the strain rate. The base for the solution is the expression for this strain,

$$\frac{d\varepsilon}{dt} = \dot{\varepsilon} = \dot{\varepsilon}_H + \dot{\varepsilon}_N = \frac{1}{E} \frac{d\sigma}{dt} + \frac{\sigma}{\eta} \quad (10.4)$$

The response of Maxwell's body for two important cases will be shown here.

#### 1) Creep under $\sigma = \sigma_0 = \text{const}$

The basic case of creep under constant stress is shown in Fig. 10.2 at right. At time  $t = 0$  a mass point is hanged on the Maxwell's body. It acts on it by a force  $F$  and generates the stress  $\sigma_0$  in it. The spring is elongated immediately to the length corresponding to the stress  $\sigma_0$ , and the piston in the cylinder starts moving. At time  $t$  the action of force is suddenly terminated. The time course of force, or stress, is depicted in the top of the figure, and the course of deforming is below. The increase of force or stress is immediate, and also its drop on unloading. The deformation following the instantaneous elastic elongation grows proportionally with time, faster for higher force. The maximum deformation remains without change after the load has passed. In this case,  $d\sigma/dt = 0$ , so that the strain is

$$\varepsilon(t) = \int_{\varepsilon_0}^{\varepsilon(t)} d\varepsilon = \int_{t_0}^t \left( 0 + \frac{\sigma_0}{\eta} \right) dt = \varepsilon_0 + \frac{1}{\eta} \sigma_0 (t - t_0) . \quad (10.5)$$

This can be written also as

$$\varepsilon(t) = \sigma_0 \left[ \frac{1}{E} + \frac{1}{\eta} (t - t_0) \right] . \quad (10.6)$$

This increase of length with time can be written generally as:

$$\varepsilon(t) = \sigma_0 J(t) . \quad (10.7)$$

$J(t)$  is so-called **creep function**, expressing the time course of response to unit load;  $J(t) = \varepsilon(t)/\sigma_0$ . In this case, it is defined by the expression in square brackets in Eq. (9.6). Its usefulness will be obvious better at more complex models.

## 2) Relaxation of forces and stresses at $\varepsilon = \varepsilon_0 = \text{const}$

The situation is depicted in Fig. 10.3. At time  $t = 0$  the free end of the spring is moved by  $\delta_0$  and fixed. At the first instant only the spring reacts, so that force  $F_0$  and stress  $\sigma_0$  appear. The dashpot has not reacted to the sudden increase of deformation, but the fluid in it started flowing due to the acting force, and the piston gradually starts moving. This gradually reduces the spring extension and also the force. As the total deformation remains constant, it holds  $d\varepsilon/dt = 0$ . The insertion into Eq. (10.4) gives the equation

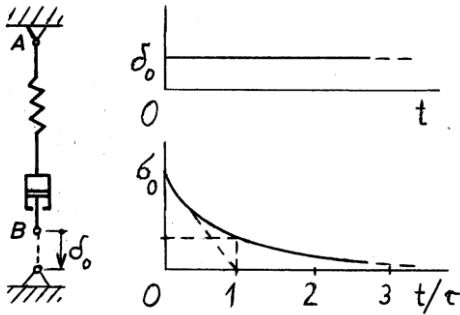
$$\frac{1}{E} \frac{d\sigma}{dt} + \frac{1}{\eta} \sigma = 0 , \quad (10.8)$$

which, after the separation of variables, can be rewritten to the form

$$\frac{d\sigma}{\sigma} = - \frac{E}{\eta} dt . \quad (10.9)$$

Integration of this expression in the limits 0,  $t$ , and  $\sigma_0$ ,  $\sigma(t)$  gives

$$\ln \frac{\sigma}{\sigma_0} = - \frac{E}{\eta} (t - t_0) . \quad (10.10)$$



**Fig. 10.3.** Maxwell model, with the time course of the relaxation of forces and stresses under constant (enforced) deformation.

The operation inverse to taking logarithms gives

$$\sigma = \sigma_0 \exp\left(-\frac{E}{\eta} t\right). \tag{10.11}$$

Let us look at this expression in detail. The argument at exponential function must be nondimensional. And really, the dimension of the ratio  $E/\eta$  je  $\text{Nm}^{-2}/\text{Pas} = \text{Pa}/\text{Pas} = 1/\text{s}$ , so that the product  $t \times E/\eta$  is nondimensional. The reciprocal expression  $\eta/E$  has the dimension of time, and it is sometimes called **relaxation time  $\tau$** . Equation (10.11) can therefore be written also in the form

$$\sigma = \sigma_0 \exp(-t/\tau) = \varepsilon_0 E \exp(-t/\tau). \tag{10.12}$$

The forces and stresses in Maxwell body under enforced deformation thus relax according to exponential function (Fig. 10.3 at right down). The following table shows their relative diminishing with time.

**Table 10.1.** Stress relaxation in Maxwell element under constant deformation.

$t/\tau$	$\sigma/\sigma_0$	$1 - \sigma/\sigma_0$
0	1	0
1	0,3685	0,6315
2	0,1353	0,8647
3	0,0499	0,9501
4	0,0183	0,9817
5	0,0067	0,9933
6	0,0025	0,9975

After the time, corresponding to the relaxation time  $\tau$  (i.e.  $t = \tau$ ), the force and stress drop to about 37% of its initial value, at time  $2\tau$  they drop to less than 14%,

at time  $4\tau$  they are lower than 2%, etc. For practical reasons, sometimes it is assumed that after time longer than 4 to  $5\tau$  the viscoelastic effects have diminished.

Relaxation time  $\tau$  can be measured easily, for example from the rate of force decrease. It is therefore useful for practical characterising of viscoelastic materials, especially with more complex models, where the terms like modulus of elasticity and viscosity lose any sense (as it will be demonstrated later).

The stress decrease in time, equation (10.11), can be expressed generally as

$$\sigma(t) = \varepsilon_0 Y(t), \quad (10.13)$$

where  $Y(t)$  is the **relaxation function**, which expresses the time course of stress decrease corresponding to the unit strain;  $Y(t) = \sigma(t)/\varepsilon_0$ .

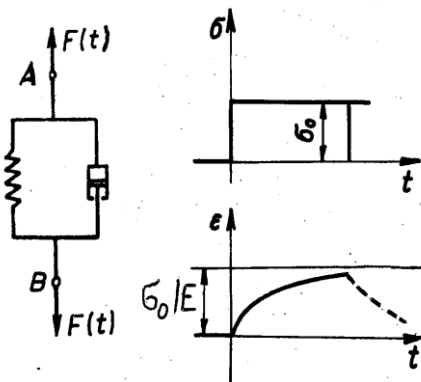
#### 10.4 Kelvin – Voigt model

It consists of a spring and a dashpot connected in parallel (Fig. 9.4). The deformation of both elements is the same, and the forces are added. The strain and stress are:

$$\varepsilon = \varepsilon_H = \varepsilon_N, \quad \sigma = \sigma_H + \sigma_N, \quad (10.14)$$

Expressing the stress in the individual elements by means of Eqs. (10.1) and (10.2) gives the total stress

$$\sigma = E\varepsilon + \eta \frac{d\varepsilon}{dt}. \quad (10.15)$$



*Fig. 10.4. Kelvin-Voigt model. At right down the time course of deformation under constant load and after unloading are shown.*

Now we shall look at the reaction of this body to the instantaneous load  $\sigma_0$  at time  $t = 0$ , which then remains constant till the time  $t_1$ . Division of Eq. (10.15) by dynamic viscosity  $\eta$  and rearrangement gives differential equation of the first order with constant coefficient and nonzero right side:

$$\frac{d\varepsilon}{dt} + \frac{E}{\eta} \varepsilon = \frac{1}{\eta} \sigma_0 . \quad (10.16)$$

Its complete solution is obtained as the sum of the solution of homogeneous equation (with zero at the right side) and particular integral,

$$\varepsilon(t) = \varepsilon_{\text{hom}} + \varepsilon_{\text{part}} . \quad (10.17)$$

The solution of homogeneous equation is  $\varepsilon_{\text{hom}} = C \exp(-t/\tau)$ , and the particular integral is  $\varepsilon_{\text{part}} = \sigma_0/E$ . The resultant solution has general form

$$\varepsilon(t) = C \exp(-t/\tau) + \frac{\sigma_0}{E} . \quad (10.18)$$

The constant  $C$  is obtained from the initial condition. For  $\varepsilon(t = 0) = 0$ ,  $C = -\sigma_0/E$ , so that the final expression for the gradual growth of deformation (or strain) is

$$\varepsilon(t) = \sigma_0 \frac{1}{E} \left( 1 - e^{-t/\tau} \right) , \quad (10.19)$$

which can be written simply as

$$\varepsilon(t) = \sigma_0 J(t) , \quad (10.20)$$

where

$$J(t) = \frac{1}{E} \left( 1 - e^{-t/\tau} \right) \quad (10.21)$$

is a creep function for Kelvin-Voigt body. The constant  $\tau (= \eta/E)$  denotes now the **retardation time**.

The situation is depicted in Fig. 10.4 at right. After the application of load the deformation starts growing and approaches gradually to the limit value  $\varepsilon_{\text{elim}} = \sigma_0/E$ , as if here only the spring were present. The deformation at time  $t = \tau$  makes about 63% of the maximum possible deformation (see Table 10.1;  $0,6315 = 1 - 0,3685$ ).

If the force ceases at time  $\tau_1$ , the stretched spring starts shrinking, so that the deformation decreases (as depicted by a dashed curve in Fig. 10.4). With linear viscoelasticity, the principle of superposition may be used, so that the resultant deformation is obtained as the sum of the permanent increase of the initial deformation and the deforming by the force acting in the opposite direction from the time  $t_1$ :

$$\varepsilon(t \geq t_1) = \sigma_0 \frac{1}{E} \left( e^{-(t-t_1)/\tau} - e^{-t/\tau} \right). \quad (10.22)$$

### 10.5 Standard linear solid

It is a spring in series with Kelvin-Voigt body (Fig. 10.5). The resultant deformation equals the sum of deformations of both bodies:

$$\varepsilon(t) = \frac{\sigma_0}{E_0} + \sigma_0 \frac{1}{E_1} \left( 1 - e^{-t/\tau_1} \right) = \sigma_0 \left[ \frac{1}{E_0} + \frac{1}{E_1} \left( 1 - e^{-t/\tau_1} \right) \right], \quad (10.23)$$

where  $\tau_1 = \eta_1/E_1$ .

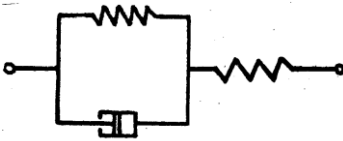


Fig. 10.5. Standard linear solid.

At the instant of load application the deformation of elastic body of magnitude  $\varepsilon_0 = \sigma_0/E_0$  appears immediately, and gradually grows with decreasing rate, as it corresponds to the viscous element. After long time, the deformation approaches to the final (limit) value  $\varepsilon_\infty = \sigma_0(1/E_0 + 1/E_1)$ . The dashpot in this case is no more active, and the situation is the same as with two springs  $E_0, E_1$  in series.

The time course of deformation can be expressed as  $\varepsilon(t) = \sigma_0 J(t)$ , where the creep function  $J(t)$  corresponds to the expression in square brackets. The meaning of  $E$  as the modulus of elasticity has been lost here.

If unloading occurs at time  $t^*$ , the elastic deformation  $\varepsilon_0 = \sigma_0/E_0$  disappears immediately, and the displacement decreases slowly. The resultant deformation in times  $t \geq t^*$  could be obtained again using the superposition principle, similarly to Kelvin-Voigt body.

### General standard linear solid

This body is obtained by adding one or more Kelvin-Voigt bodies in series to a standard linear solid. Also the formula for total deformation under constant load is obtained by adding further expressions corresponding to these bodies:

$$\varepsilon(t) = \sigma_0 \left[ \frac{1}{E_0} + \frac{1}{E_1} \left(1 - e^{-t/\tau_1}\right) + \frac{1}{E_2} \left(1 - e^{-t/\tau_2}\right) + \dots \right]. \quad (10.24)$$

The individual retardation times are  $\tau_j = \eta_j/E_j$ . We can see that the original meaning of the terms such as modulus of elasticity or viscosity is getting lost. Equation (9.24) can thus be rewritten generally as

$$\varepsilon(t) = \sigma_0 \left[ C_0 + C_1 \left(1 - e^{-t/\tau_1}\right) + C_2 \left(1 - e^{-t/\tau_2}\right) + \dots \right] = \sigma_0 J(t), \quad (10.25)$$

where the constants  $C_j$  correspond to compliances, and  $J$  is the creep function. Equation (9.25) can be further simplified, if all constant terms are put together:

$$\varepsilon(t) = \sigma_0 \left[ \sum_{j=0}^n C_j + \sum_{j=1}^n C_j e^{-t/\tau_j} \right] = \sigma_0 J(t). \quad (10.26)$$

The expression in square brackets represents so-called Prony series, defined as

$$y = a_0 + a_1 \exp(-t/\tau_1) + a_2 \exp(-t/\tau_2) + a_3 \exp(-t/\tau_3) \dots \quad (10.27)$$

**Remark.** The commercial programs for the analysis of structures by the finite element method enable the work with Prony series.

### 10.6 Burgers model

This model arises by extending the standard linear solid by a viscous term, or by series connection of Maxwell and Kelvin-Voigt body (Fig. 10.6). The time course of deforming under constant load is obtained by extending Eq. (10.18) by the increase of deformation corresponding to the viscous term. After a rearrangement it gives

$$\varepsilon(t) = \sigma_0 \frac{t}{\eta} + \sigma_0 \left[ \frac{1}{E_0} + \frac{1}{E_1} \left(1 - e^{-t/\tau_1}\right) \right]. \quad (10.28)$$

Similar time course of deforming is shown in Fig. 10.8. According to this model, the deformations could grow without limits. However, this is a hypothetical case.

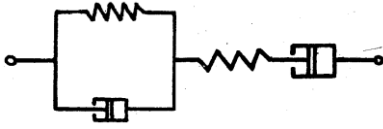


Fig. 10.6. Burgers model.

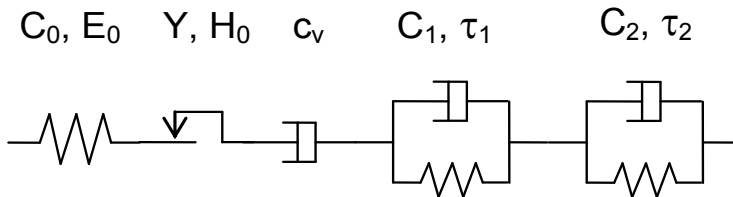
The constants in viscoelastic models can be obtained from experimentally found time course of deforming, as it will be shown in the following example.

**Example. Load response of viscoelastic material**

Viscoelastic properties of polymethylmetacrylate (PMMA) were determined by instrumented indentation [5]. The indenter was loaded and the force held constant for long time. The time course of its penetration into the material was measured and then fitted by the regression function

$$y(t) = F K [A_0 + c_v t - \sum B_j \exp(-t/\tau_j)] , \quad (10.29)$$

which represents a generalised standard linear solid connected in series with a viscous element and one element characterising irreversible plastic deformations, which could arise due to very high stresses under load (Fig. 10.7).  $F$  is the load,  $K$  is the constant characterising the indenter geometry, and  $A_0$ ,  $c_v$ ,  $B_j$  a  $\tau_j$  are regression constants, found by the least squares method.



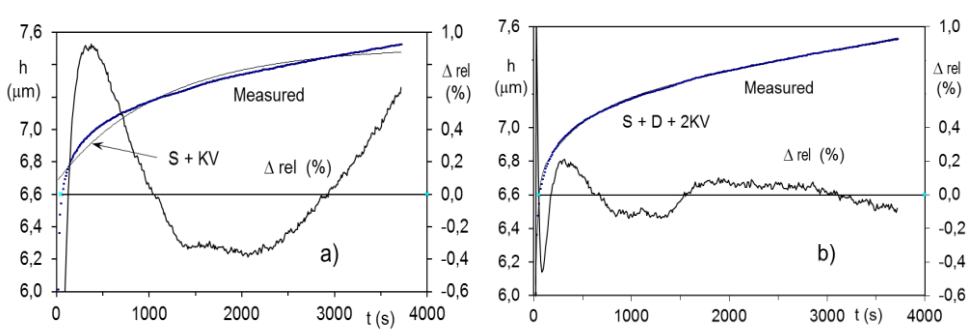
**Fig. 10.7.** Viscoelastic-plastic model „spring + plastic element + dashpot + 2 Kelvin-Voigt bodies“.  $C_0$ ,  $C_1$ ,  $C_2$ ,  $c_v$  – compliances,  $E_0$  and  $H_0$  – instantaneous elastic modulus and hardness,  $Y$  – yield strength,  $\tau_1$ ,  $\tau_2$  – retardation times.

Figure 10.8 shows two approximations, with three and six regression constants. For better check of the suitability of regression function, and for comparison of both approximations, also **relative (standardised) residuals** are plotted, defined as

$$\Delta_{j,\text{rel}} = (y_{j,\text{meas}} - y_{j,\text{calc}}) / y_{j,\text{calc}} . \quad (10.30)$$



The subscripts meas and calc mean measured and calculated values. The advantage of relative residuals is their independence on the scale of  $y$ . The residuals can help in distinguishing various approximations, especially if the curves in the original coordinate system  $y(t)$  look very similarly (Fig. 10.8b). We can see that the approximation with six constants is significantly better.

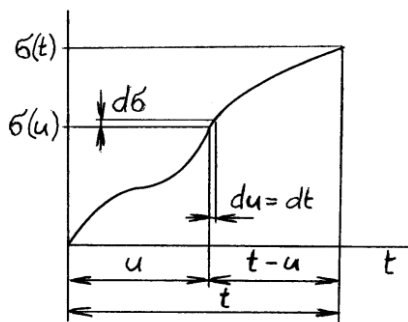


**Fig. 10.8.** Indenter penetration into PMMA under constant load [5]: measured values (thick lines) and two approximations (thin lines). a) model  $S+KV$  (3 constants), b) model  $S+D+2KV$  (6 constants);  $S$  - spring,  $D$  - dashpot,  $KV$  - Kelvin-Voigt body. Model  $S+D+2KV$  approximated the measured values very well, the differences were visible only via the relative residuals  $\Delta_{rel}$  (zig-zag lines, right scale).  $h$  - depth,  $t$  - time.

### 10.7 Determination of deformations under varying load

Until now, we showed how deformations under constant load grow with time according to various models. However, the load often varies. Here, a procedure will be explained for the case with force increasing in general way (Fig. 10.9).

The increase of force (or stress) can be interpreted as composed from a series of minute increments. Linearly viscoelastic material will be assumed, where the resultant effect of several loads equals the sum of the effects of individual loads.



**Fig. 10.9.** General course of load growth.

If the stress  $\sigma$  increases at time  $u$  by  $d\sigma$ , its influence exists only since this instant. As this force  $d\sigma$  will act till the time  $t$  only during the time  $t - u$ , the increment of deformation  $d\varepsilon$ , caused by the load  $d\sigma$  (applied at time  $u$ ), equals  $J(t - u)d\sigma$ , where  $J$  is the creep function for the considered material model. At time  $u + du$  a further increment  $d\sigma$  is added to the present load, etc. If the time course of load increase  $\sigma(t)$  is known  $\sigma(t)$ , the increment  $d\sigma$  can be expressed as

$$d\sigma(t) = \frac{d\sigma}{dt} dt, \quad \text{resp.} \quad d\sigma(u) = \frac{d\sigma}{du} du. \quad (10.31)$$

The total deformation is then obtained as a sum of infinitesimal increments during the time from 0 to  $t$  (so-called convolutory integral):

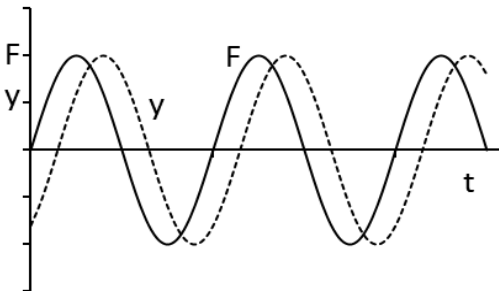
$$\varepsilon(t) = \int_0^t J(t - u) \frac{d\sigma}{du} du. \quad (10.32)$$

### 10.8 Response of viscoelastic materials to alternating load

An important case is harmonic load, defined as

$$\sigma(t) = A \sin(\omega t); \quad (10.33)$$

$A$  is the amplitude and  $\omega$  circular frequency of harmonic motion, related with the frequency  $f$  as  $\omega = 2\pi f$ . The course is depicted in Fig. 10.10 by a solid line. If such force acts on a body of viscoelastic material, the deformation (after the transitional phenomena have faded away) will change also in harmonic way, with the same frequency, but delayed behind the force by  $\delta$  (see dashed curve in Fig. 10.10; the **phase shift**  $\delta$  is obvious at the time axis at left). This shift depends on the type of the body and the frequency. For example, for Maxwell body (Fig.10.5) it holds  $\text{tg } \delta = 1/(\omega\tau)$ , and for Kelvin-Voigt body (Fig. 10.9) the shift is  $\text{tg } \delta = \omega\tau$ , where  $\tau$  is retardation (or relaxation) time.



**Fig. 10.10.** Forced vibration of a viscoelastic body.

The tensile stiffness of elastic materials is characterised by Young's modulus, defined as the ratio of stress and strain,  $E = \sigma / \varepsilon$ . In viscoelastic materials both quantities,  $\sigma$  and  $\varepsilon$ , have harmonic course with certain amplitude, but they are shifted by angle  $\delta$  (Fig. 10.10). In this case, several moduli can be defined. **Complex modulus of elasticity** equals the ratio of the stress and strain amplitudes,

$$E^* = \frac{\sigma_a}{\varepsilon_a} . \quad (10.34)$$

This modulus has two components. **Storage modulus**,

$$E' = \frac{\sigma(\varepsilon_{\max})}{\varepsilon_{\max}} = E^* \cos \delta , \quad (10.35)$$

expresses such part of the complex modulus, which is in phase with the strain, and characterises the reversible part of deformation. **Loss modulus**,

$$E'' = \frac{\sigma(t=0)}{\varepsilon_{\max}} = E^* \sin \delta , \quad (10.36)$$

expresses the part shifted to strain by  $90^\circ$ . The relationship is shown in Fig. 10.11.

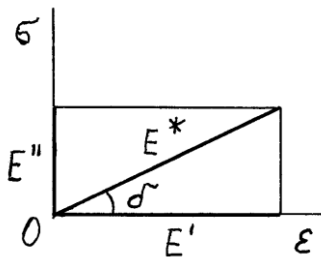


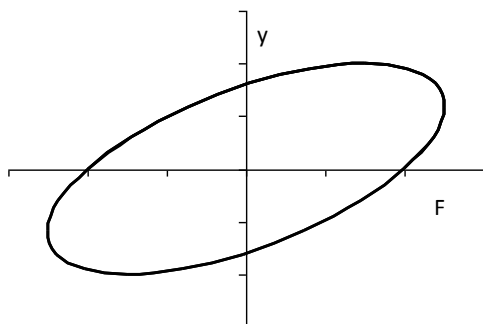
Fig. 10.11. Moduli of viscoelastic material.

Recording all pairs of stress and strain values in one cycle in the plane  $\sigma - \varepsilon$  gives an ellipse with the main axis inclined to the strain axis by angle  $\delta$  (Fig. 10.12). Area of this hysteresis loop in the coordinates force – displacement is proportional to the work dissipated during one loading cycle, and to the energy density in coordinates stress – strain. The density of energy accumulated during one quarter of the loading cycle is

$$W_s = 1/2 E' \varepsilon_0^2 , \quad (10.37)$$

and the density of energy dissipated in one quarter of the loading cycle is

$$W_d = 1/4 E'' \varepsilon_0^2 . \quad (10.38)$$



**Fig. 10.12.** *Hysteresis loop.*

The work dissipated in a loading cycle changes into heat. This must be considered in long-time loaded components, and its conduction away must be ensured, so that the increase of temperature will not change the properties nor it damages the component.

### **References to Chapter 10.**

1. Tschoegl, N. W.: The Phenomenological Theory of Linear Viscoelastic Behavior: An Introduction. Springer Verlag, Berlin, 1989. 769 p.
2. Haddad, Y.M.: Viscoelasticity of Engineering Materials. Chapman & Hall, London, 1995. 378 p.
3. Höschl, C.: Pružnost a pevnost ve strojnictví. SNTL, Praha, 1971. 375 p.
4. Roylance, D.: Mechanics of materials. John Wiley & Sons, Inc., New York, 1996. 315 p. Available on web (Google). (27.1.2019)
5. Menčík, J., He, L.H., Němeček, J.: Characterization of viscoelastic-plastic properties of solid polymers by instrumented indentation. Polymer Testing, 30, 2010, p. 101-109.

# 11. Mechanics of components with treated surfaces

## 11.1 Introduction

A weak part of every component is the surface. It is exposed to the harmful action of the environment, usually highest stresses act here, and the most favourable conditions for nucleation and growth of cracks are also here. The external load is usually transmitted on the component by the surface. If it is concentrated, it can generate local plastic deformations in a ductile material, or a crack in a brittle material. Plane stress exists always on the unloaded surface, and this is favourable for plastic deforming. Also under cyclical loading of metal components extrusions and intrusions and nuclei of fatigue cracks arise usually on the surface (Fig. 7.9) rather than in the interior, where the crystalline grains of different orientation hamper mutually their slips. A fatigue crack in a notch arises on its surface.

The conditions for growth of cracks are also better on the surface. The situation in bodies with cracks was described in Chapter 7; therefore here only the principal terms will be reminded. Most important is the stress field in front of the crack, which can be characterised by the stress intensity factor

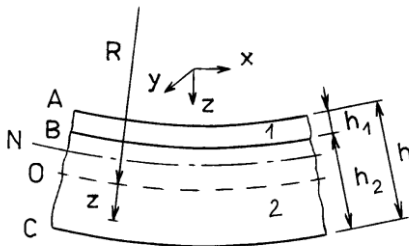
$$K_i = \sigma_n Y \sqrt{a} ; \quad (11.1)$$

$\sigma_n$  is the nominal stress here,  $a$  is the length or another characteristic dimension of the crack, and  $Y$  is the form factor that depends on the shape and size of the crack and the body, and on the stress distribution. The subscript  $i$  expresses the mode of crack opening. A crack grows quickly if the stress intensity factor exceeds the critical value  $K_C$ . But the crack can grow slowly even under lower load, in fatigue processes, if the stress intensity factor has exceeded the threshold  $K_{sc}$  or  $\Delta K_{th}$ . The velocity of crack propagation also depends on the stress intensity factor. For common crack shapes, the stress intensity factor for a surface crack is about 60% higher than for the crack of the same length, but under surface [1, 2]. This also means that certain stress can cause growth of significantly smaller surface crack than of an internal one.

The other approach for the assessment of the behaviour of bodies with cracks is based on energy balance: the crack grows if more energy is released by this growth than consumed for the creation of new fracture surfaces. The characteristic quantity is the energy release rate  $G$  ( $\text{J}\cdot\text{m}^{-2}$ ) and specific fracture energy  $\Gamma$  ( $\text{J}\cdot\text{m}^{-2}$ ), and the condition for crack growth is  $G \geq \Gamma$ . Both approaches (with stress intensity factor or energy release rate) are equivalent.

An efficient means for increasing the resistance to failure or fatigue are various kinds of surface treatment. In Chapter 4.8 strengthening of metal components by creation of compressive prestress in the surface layer by local plastic deforming was explained. Here, we shall look at the situation in bodies with solid coatings. Examples of coatings from material different than the substrate are enamels, thin layers created by electroplating, sputtering (PVD or CVD processes) or plasma spraying, or a thicker metallic layer connected with the metallic substrate by cladding, rolling or welding on. In all these cases a difference exists between the properties of the coating and the substrate, and relatively sharp interface with sudden change of properties.

At first, characteristic features will be shown of stress distribution in components with surface layer of another material (Fig. 11.1). Formulae will be given here for stresses caused by the temperature change, by tension or in contact. Only the principal features will be mentioned; for details, the reader is referred to [1, 2].



**Fig. 11.1.** Bi-layer plate – geometry.  
*N* – neutral axis.

## 11.2 Stresses due to the difference of thermal expansions

These stresses arise when the operation temperature of the component differs from the temperature for creation of the surface layer. Examples are enameled items. During cooling after firing the layer with higher coefficient of thermal expansion tries to shrink more, and the layer with lower expansion prevents it. This generates stresses. At sufficiently high temperatures these stresses relax, but from certain

temperature  $T_0$  they remain in the body permanently. At places distant from edges state of biaxial isotropic stresses exists, where  $\sigma_x(z) = \sigma_y(z)$ ,  $\varepsilon_x(z) = \varepsilon_y(z)$ . If we denote the quantities corresponding to the surface layer by subscript 1, and substrate by subscript 2, then (provided that the properties are constant in the volume of the pertinent layer) we can write the following general expressions for the stresses:

$$\sigma_1(z) = E_1' \{ \varepsilon(y) + \alpha_1 [T_0 - T(z)] \} , \quad (11.2a)$$

$$\sigma_2(z) = E_2' \{ \varepsilon(y) + \alpha_2 [T_0 - T(z)] \} , \quad (11.2b)$$

where

$$E_1' = E_1 / (1 - \mu_1) , \quad E_2' = E_2 / (1 - \mu_2) \quad (11.3)$$

are effective moduli of elasticity for biaxial stress state;  $\mu$  is Poisson's number.

Two cases can occur, depending on whether the plate can deflect due to internal stresses or not.

### Free deflection is not possible

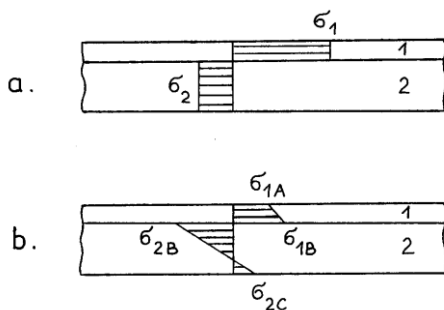
Strain and stress have the same value everywhere, and the stress in the coating is

$$\sigma_1 = \frac{(\alpha_1 - \alpha_2)(T_0 - T)}{\frac{1}{E_1'} + \frac{1}{E_2'} \frac{h_1}{h_2}} , \quad (11.4)$$

$h_1$ ,  $h_2$  is the thickness of the coating and substrate. The stress in the substrate follows from the condition that the resultant force in the cross section equals zero:

$$\sigma_2 = -\sigma_1 \frac{h_1}{h_2} . \quad (11.5)$$

The stress distribution is shown in Fig. 11.2a.



**Fig. 11.2.** Stresses in bilayer plate due to the differences of temperature and thermal expansions of the layers [1, 2]. **a** – plate without deflection, **b** – plate with free deflection.

Equations (11.4) and (11.5) hold also for plates with surface layers on both sides. In such case, the sum of the thicknesses of both layers must be inserted.

### Free deflection is possible

The internal stresses cause the deflection of the plate into a part of spherical surface. This significantly changes the distribution and magnitude of the individual stresses (Fig. 11.2b). These stresses vary linearly across the thickness, and their magnitudes at the surfaces of individual layers (points A, C on the plate surface and point B at the interface of both layers ) are

$$\sigma_{1,A,B} = \sigma_{1\max} \frac{[1+1/(e'h^3)] \mp 3(1+1/h')}{(1+1/h')^2 \left\{ 3+(1+e'h^3)[1+1/(e'h^3)]/(1+h')^2 \right\}}, \quad (11.6a)$$

$$\sigma_{2,B,C} = \sigma_{1\max} \frac{-h'[1+1/(e'h^3)] \mp 3(1+1/h')/(e'h')}{(1+1/h')^2 \left\{ 3+(1+e'h^3)[1+1/(e'h^3)]/(1+h')^2 \right\}}, \quad (11.6b)$$

where  $\varepsilon' = E_1'/E_2'$  and  $h' = h_1/h_2$  [1, 2]. The upper sign (–) in the numerator of (11.6a) corresponds to the surface A in Fig. 11.1, and lower sign (+) corresponds to the contact surface B. The upper sign (–) in the numerator of (11.6b) pertains to the contact surface B, and the lower sign (+) corresponds to the surface C. The influence of the layer thickness is negligible till the thickness ratio  $h_1/h_2 = 0,01$ ; then it grows more significantly [1, 2]. The influence of free deflection will be shown on an example after [2].

**Example 1.** Calculate stresses in a plate  $100 \times 100$  mm and thickness  $h_2 = 4,0$  mm, with a layer of thickness  $h_1 = 1,0$  mm. Material constants are:  $E_1 = E_2 = 75$  GPa,  $\mu_1 = \mu_2 = 0,25$ ,  $\alpha_1 = 6 \times 10^{-6} \text{ K}^{-1}$ ,  $\alpha_2 = 8 \times 10^{-6} \text{ K}^{-1}$ ,  $T_0 - T = 500$  K.

If the plate cannot deflect, the stress in the coating, given by Eq. (11.4) is  $\sigma_1 = -80$  MPa; in the plate  $\sigma_2 = 20$  MPa. If the plate can deflect, the stress on the coating surface is  $\sigma_{1A} = -32$  MPa, in the contact surface it is  $\sigma_{1B} = -51$  MPa,  $\sigma_{2B} = 49$  MPa, and on the surface of plate 2 it is  $\sigma_{2C} = -28$  MPa. The differences are significant. The maximum free deflection in the centre of the plate is  $y_{\max} = 0,24$  mm, which is hardly observable by the naked eye.

**Remark.** For negligible coating thickness ( $h_1 \ll h_2$ ) Equation (11.4) changes to

$$\sigma_1 = E'(\alpha_1 - \alpha_2)(T_0 - T). \quad (11.4a)$$



The corresponding stress in the coating is  $\sigma_{1\max} = -100$  MPa. The stress  $\sigma_2$  in massive would approximately equal zero.

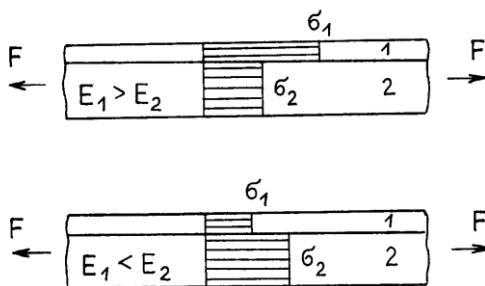
The above theory is valid also if the **internal stress** was caused by **another mechanism**, for example by phase transform in the surface layer, accompanied by volume change. It is sufficient to replace the expression  $(\alpha_1 - \alpha_2)(T_0 - T)$  by the term  $(\Delta V/V)/3$ , where  $\Delta V/V$  is the relative volume change corresponding to the phase transformation.

### 11.3 Stresses caused by membrane forces

The principal features will be shown on a bilayer plate loaded by forces acting in the plate in direction  $x$  (Fig. 11.3). The stresses in the individual layers are determined from the force equilibrium and from the condition that both layers deform as a whole. Subscript 1 denotes the coating, subscript 2 denotes the substrate. The situation is simple if Poisson's ratio (for transverse contraction) is the same for the coating and substrate,  $\mu_1 = \mu_2 = \mu$ . No stress appears in the direction  $y$ , and those in direction  $x$  are

$$\sigma_{1x} = F'_x \frac{E_1}{E_1 h_1 + E_2 h_2}, \quad \sigma_{2x} = \sigma_{1x} \frac{E_2}{E_1} = F'_x \frac{E_2}{E_1 h_1 + E_2 h_2}; \quad (11.7a, b)$$

$F'_x$  is the force per unit of plate width. If the **Poisson's numbers are different**,



**Fig. 11.3.** Stress in a bilayer plate caused by a membrane force [1, 2].

the situation is more complicated. Free transverse deformations of each layer were different. Since the resultant deformation must be the same, stress at direction  $y$  appears far from the edges. The stresses in a relatively thin coating in the direction of force ( $x$ ) and in the unloaded direction ( $y$ ) are approximately [1, 2]:

$$\sigma_{1x} = F_x \frac{E_1}{E_1 h_1 + \frac{1-\nu_1^2}{1-\nu_1\nu_2} E_2 h_2} ; \quad \sigma_{1y} = \sigma_{1x} \frac{\nu_1 - \nu_2}{1 - \nu_1\nu_2} . \quad (11.8)$$

The stresses  $\sigma_{2x}$ ,  $\sigma_{2y}$  in the substrate are obtained by interchanging the subscripts 1 and 2 in Equations (11.8) and (11.9).

The stresses  $\sigma_{1x}$  and  $\sigma_{2x}$  from the force  $F_x$  have always the same sign, and are in the same ratio as their moduli of elasticity  $E_1$  a  $E_2$ . The stresses in transverse direction have the opposite signs and are in reciprocal ration than the thicknesses of the layers. The highest stress in the surface layer acts if this layer is much thinner than the substrate.

Let us look now at the stresses in a rod with circular cross section, loaded by axial force. The situation is similar to the previous case. The axial force causes axial stress both in the rod and the coating, and also the reduction of their transverse dimensions. With different Poisson's numbers circumferential stress appears in the coating and also the stress perpendicular to the interface. The corresponding stress appears in the rod, as well. We shall show here the formulae for the rod of diameter  $D = 2R$ , with a relatively thin coating. The rod has modulus of elasticity  $E_2$  and Poisson's number  $\mu_2$ ; the corresponding constants of the coating are  $E_1$  and  $\mu_1$ .

The axial force  $F$  causes the axial stress in the rod (subscript 2) and coating (subscript 1):

$$\sigma_{2a} = \frac{F}{\pi R^2} , \quad \sigma_{1a} = \sigma_{2a} \frac{E_1}{E_2} \frac{1 - \mu_1\mu_2}{1 - \mu_1^2} . \quad (11.10a,b)$$

In the coating circumferential stress will act

$$\sigma_{1\varphi} = \frac{E_1}{E_2} \frac{\mu_1 - \mu_2}{1 - \mu_1^2} \sigma_{2a} . \quad (11.11)$$

Remark. Expressing the axial stress in the rod by means of axial stress in the coating gives, after a rearrangement, Eq. (11.11) for hoop stress in the coating.

Example 2. Compare circumferential stress  $\sigma_{1\varphi}$  and the axial stress  $\sigma_{1x}$  in glass enamel on a steel rod loaded by axial force. Poisson's numbers of glass and steel are  $\mu_1 = 0,2$  a  $\mu_2 = 0,3$ .

For a relatively thin coating Eq. (11.9) gives

$$\sigma_{1\varphi} = \frac{0,2 - 0,3}{1 - 0,2 \cdot 0,03} \sigma_{1x} = -0,106 \sigma_{1x} \cdot$$

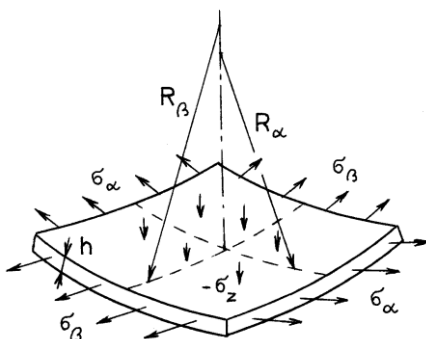
The minus sign is because the lateral deformation of steel is larger than that of glass. This means that loading of the rod by axial compressive force causes (unexpected) tensile stress in the coating, which can lead even to its fracture!

#### 10.4 Stresses in coatings on curved surfaces

In coatings on curved surfaces of loaded components radial stress perpendicular to the interface with the substrate appears (Fig. 11.4). If the coating is thin, the radial stress between it and the substrate can be determined via the equation [1, 2]

$$\sigma_r = -h \left( \frac{\sigma_\alpha}{R_\alpha} + \frac{\sigma_\beta}{R_\beta} \right); \quad (11.12)$$

$h$  is the coating thickness,  $\sigma_\alpha$ ,  $\sigma_\beta$  are membrane stresses in the coating in two mutually perpendicular directions ( $\alpha$ ,  $\beta$ ), and  $R_\alpha$ ,  $R_\beta$  are the radii of curvature of the surface. The radius is positive if the coating is convex in the pertinent direction, and negative for concave shape. If compressive stress acts in the coating in the tangential direction, tensile radial stress appears at the interface, which will try to tear the coating away from the substrate. Equation (11.12) also says that if radial stress appears between the coating and substrate (if, e.g., the substrate hampers the coating in free shrinking), membrane tangential stress appears in the coating.



**Fig. 11.4.** Stress in a thin coating on a curved surface.  $\sigma_z$  – radial stress.

The Laplace equation (11.12) assumes that the stresses are distributed uniformly in the coating; if they vary with depth, e.g. in nonuniform temperature distribution,

the mean values are used. Radial stresses will be higher in coatings thicker compared to the radius of curvature. These stresses act not only in the interface, but also in the coating and substrate, so that they can influence the propagation of cracks in the vicinity of the interface.

### 11.5 Situation at the coating edge

The stresses distribution at places, where the coating suddenly ends, is more complex. A simplified analysis will be shown for a flat bar loaded by tensile force. At the free end of the coating no stress acts and all load is carried by the substrate. At some distance from here the axial force is carried by both the substrate and coating. The load carried by the coating must be transmitted into it from the substrate by shear stresses. The following relationships hold between the shear stress  $\tau$  at the interface and the mean stress  $\sigma_1$  in the coating and  $\sigma_2$  in the substrate

$$d\sigma_1(x)h_1 = \tau(x) dx, \quad d\sigma_2(x) h_2 = -\tau(x) dx; \quad (11.13)$$

$x$  is the distance from the free end of the coating;  $h_1$  or  $h_2$  is the thickness of the coating and substrate (Fig. 11.5 at the left). The stresses move the points of the mean plane of the coating and substrate of coordinate  $x$  by  $u_1(x)$  and  $u_2(x)$ . The corresponding mean strains are

$$\varepsilon_1(x) = du_1/dx, \quad \varepsilon_2(x) = du_2/dx. \quad (11.14)$$

Under the assumption of equal Poisson's numbers and validity of Hooke's law the mean stresses will be

$$\sigma_1(x) = E_1 \varepsilon_1(x) = E_1 du_1/dx, \quad \sigma_2(x) = E_2 du_2/dx. \quad (11.15)$$

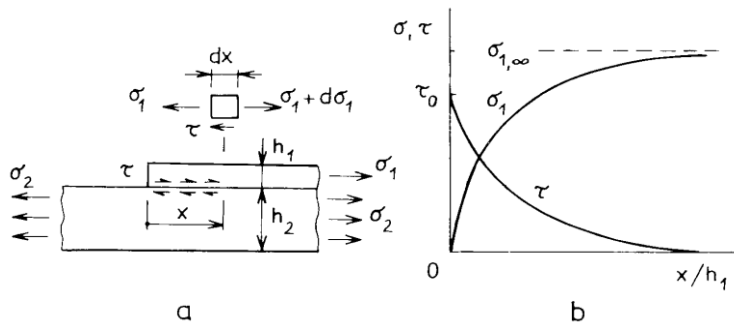


Fig. 11.5. Stress distribution in the coating and interface [2].

The shear stress at the interface will be assumed directly proportional to the mutual shift of both layers,

$$\tau = k_{\tau} (u_1 - u_2) ; \quad (11.16)$$

$k_{\tau}$  is a constant characterising the shear stiffness of the joining. Expressing the stress in (11.13) by means of displacements (11.14) and (11.16) gives the system of two differential equations of second order. Its solution gives the stress in the coating:

$$\sigma_1(x) = \sigma_{1,\infty} (1 - e^{-\lambda x}), \quad \tau(x) = \sigma_{1,\infty} h_1 \lambda e^{-\lambda x} = \tau_0 e^{-\lambda x}, \quad (11.17)$$

where

$$\lambda = \sqrt{k_{\tau} [(E_1 h_1)^{-1} + (E_2 h_2)^{-1}]} ; \quad (11.18)$$

$\sigma_{1,\infty}$  is the stress in the coating far from the edge, and  $\tau_0$  is the shear stress at the coating edge ( $x = 0$ ). Equations (11.17) and (11.18) are also valid for stresses caused by the differences of thermal expansion.

The stress distribution is shown in Fig. 11.5. The membrane stress in the coating increases continuously from zero at the free edge to the asymptotic value  $\sigma_{1,\infty}$ , while the shear stress decreases from the value  $\tau_0$  to zero. These changes are faster for higher  $\lambda$ , i.e. for higher shear stiffness and lower tensile stiffness of both layers. If the coating is directly on the substrate, approximate expression may be used [2]

$$\lambda = 1 / (h_1 \sqrt{1 + (E_1 / E_2)}) , \quad (11.19)$$

from which it follows that the influence of free edge for common material combinations is limited to three- five times the coating thickness.

This solution corresponded to purely elastic deformations. If the substrate material is elastic-plastic with low yield strength and without strain hardening, the shear stress between it and the coating constant, equal the yield strength in shear. The situation is similar to pulling out a fibre from a matrix in a fibrous composite.

More detailed solutions exist also; some of the can be found in [2], where further works are mentioned.

## 11.6 Elastic-plastic deforming

As soon as the stress in a body from ductile material attains the yield strength, plastic flow occurs here. If the load grows further, the stress distribution changes. The stress in the plasticised region is either constant or increases slowly. The total

deformations increase faster. After unloading, the components remain deformed and residual stresses act in them, which sum up with the stresses from new load.

A first idea on the stresses in elastic plastic state can be obtained from the bilayer plate without possibility of free deflection. Each layer is from ideal elastic-plastic material without strain hardening and with the same yield strength in tension and compression (Fig. 11.6a). The tensile load in x direction will be considered.

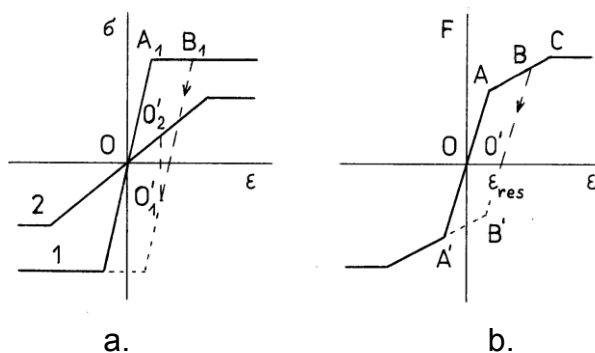
At the beginning, both layers deform elastically. The line OA in Fig. 11.6b is valid for the force  $F$ , and lines  $OA_1$  and  $OO_2'$  and Eqs. (10.7a,b) for the stresses  $\sigma_1$ ,  $\sigma_2$ . Higher stress acts in the layer with higher modulus of elasticity. With increasing load the stresses in both layers grows until the stress in one layer attains the yield strength. It is not necessarily in the layer with lower yield strength, but, generally in the layer with lower strain  $\varepsilon_Y$  at yield. Further we assume that plastic flow occurs earlier in the layer 1; other relationships would be obtained by interchanging the subscripts 1, 2. The yield strength in layer 1 is attained at the strain

$$\varepsilon = \varepsilon_{1Y} = \sigma_{1Y} / E, \quad (11.20)$$

with the corresponding force

$$F' = \sigma_{1Y} h_1 \left( 1 + \frac{E_2' h_2}{E_1' h_1} \right). \quad (11.21)$$

If the load grows further, the stress in layer 1 remains constant (material without strain hardening is assumed),  $\sigma_1 = \sigma_{1Y}$ . The second layer is still deformed



**Fig. 11.6.** Elastic-plastic deforming of a bilayer plate. **a** – stress strain diagrams for layers 1 and 2, **b** – total membrane force.

elastically, and the stresses in it are  $\sigma_2 = E_2 \varepsilon$ . The relationship  $F(\varepsilon)$  is represented by segment AC in Fig. 10.6b. The deformation grows faster. The stress in layer 2 is

$$\sigma_2 = (F - \sigma_{1Y} h_1) / h_2 . \quad (11.22)$$

The body is deformed in this way till the yield strength is reached in layer 2 (point C in Fig. 11.6b). The corresponding load is

$$F'' = \sigma_{1Y} h_1 + \sigma_{2Y} h_2 . \quad (11.23)$$

From this instant, the deformations could grow without limits even under constant load (horizontal line in Fig. 11.6b). However, the material usually strain hardens.

Let us look at **unloading**. If, during loading,  $F < F'$  (that is the point A was not exceeded), both layers deformed only elastically, the body returns into the initial condition. If, however, plastic deforming in one or both layers, the plate remains somewhat longer and residual stresses will act in it. The situation is depicted in Fig. 11.6. The broken line OAB holds for the force  $F$ , and lines  $OA_1B_1$  and  $OA_2B_2$  for stresses in layers 1 and 2. The unloading proceeds in elastic manner along the line  $BO'$  parallel with the initial part of the diagram  $F(\varepsilon)$ , or  $\sigma(\varepsilon)$ . The point  $O'$  corresponds to the situation when no load acts. The residual stresses can be determined as the difference of the actual elastic-plastic stresses under load and the stresses which would be caused by the same load, but if the body deformed only elastically (as if it had, for example, much higher yield strength).

The residual stress in layer 1 thus will with respect to Eq. (11.21) be

$$\sigma_{1,res} = \sigma_{1,Y} - \frac{F}{h_1} \left/ \left( 1 + \frac{E_2' h_2}{E_1' h_1} \right) \right. . \quad (11.24)$$

As  $\varepsilon > \varepsilon_Y$ , it is obvious that the residual stress will have the opposite sign than under load.

The residual stress in layer 2 could be determined in the same manner. However, it can be obtained more easily from the equation of force equilibrium, and it is

$$\sigma_{2,res} = -\sigma_{1,res} \frac{h_1}{h_2} . \quad (11.25)$$

The sense of this stress is the same as under load. The residual stress in the investigated case is distributed uniformly in both layers, with higher magnitude in

the thinner layer. If the plate can deflect due to the residual stresses, their magnitude and character will change similarly as it was described earlier.

The permanent elongation of the plate after unloading from point B is depicted in Fig. 11.6b as O'.

The residual stresses attain the maximum values if the previous load attained the limit value C in Fig. 11.6b. In such case

$$\sigma_{1,res,max} = \sigma_{1,Y} - \left(1 - \frac{\varepsilon_{2Y}}{\varepsilon_{1Y}}\right) / (1 + \varepsilon'h') \cdot \quad (11.26)$$

The response of the bilayer plate with residual stress under new load is obvious from Fig. 11.6b. The unloaded situation is marked by point O'. If the plate is loaded by tension, it deforms elastically along the line O'B. The total stress in layer 1 is lower by  $\sigma_{1,res}$ , and higher by  $\sigma_{2,res}$  in layer 2 than in a plate without residual stress. After unloading the plate returns back to the point O'. This holds as long as the loading force does not exceed the value  $F(B)$ . After its exceeding the extent of plastic deformations becomes larger, and also the residual stresses after unloading.

If the plate is loaded by compression, stress in layer 1 attains the yield value at lower total load than in the plate without residual stress (point B' in Fig. 11.6b). If plastic flow occurred, the original residual stresses will be lower after unloading. The previous load with plastic flow thus has the resistance of the component to the load of the same sense, but decreased the resistance to the opposite load.

Many components are loaded by alternating tension and compression. If the bilayer plate is without residual stress, and the load varies not more than from  $F(A)$  to  $F(A')$ , the deforming is elastic. If the plate was prestressed to the point B, it will deform elastically only if the load varies within the interval  $\langle F(B'); F(B) \rangle$ . If the maximum or minimum force will be out of this interval, but the total range will be not larger than  $2F(A)$ , the one-way plastic deformation occurs, but after it the component will again deform elastically. (This is called shake-down.) If the force range will be larger than  $2F(A)$ , for example the maximum tensile force will be  $F(B)$ , and maximum compressive force will be  $F(A')$ , the layer 1 will be deformed permanently in alternating way. The pertinent loading cycle is depicted by line BB'A'AB in Fig. 11.6b. The area below this curve is proportional to the work dissipated in one loading cycle by plastic deforming. After the fatigue resistance of the material has been exhausted by repeated deforming, a fatigue crack can appear



### 11.7 Fracture mechanics of interfaces

The stress field in front of a crack in a bimaterial near the interface is more complex. The general expression for the stress ahead the crack tip (Fig. 11.7) is

$$\sigma_{ij}(r, \varphi) \sim \sigma_n(L/r)^s f_{ij}(\varphi); \quad (11.27)$$

$\sigma_{ij}(r, \varphi)$  denotes the stress component at distance  $r$  in front of the crack ( $\varphi$  is the angle between the crack plane and the investigated point),  $\sigma_n$  is the nominal stress in the crack region,  $L$  is the length or another characteristic dimension of the crack,  $s$  is a constant, and  $f_{ij}$  is a function of angle  $\varphi$ . The exponent of stress singularity in homogeneous material  $s = 0,5$ , but  $s$  in bimaterials with different elastic properties and sudden change at the interface has different values. Nevertheless, reasonable conclusions can be made even if the different value of exponent  $s$  is neglected.

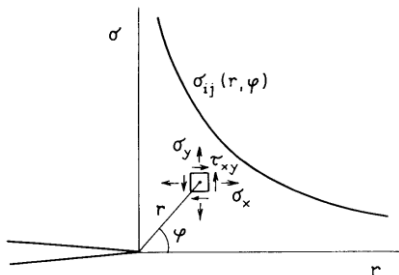


Fig. 11.7. Stresses in front of the crack.

For the description of elastic properties of isotropic material two constants are necessary: modulus of elasticity and Poisson's number  $\mu$ . Two materials thus need generally four constants. However, if both materials are strongly connected so that they form a bimaterial, only two constants are sufficient for the description of properties near the interface, so-called Dundurs' parameters  $\alpha$  and  $\beta$ :

$$\alpha = \frac{k(\kappa_1 + 1) - (\kappa_1 + 1)}{k(\kappa_1 + 1) + (\kappa_1 + 1)}, \quad \beta = \frac{k(\kappa_1 - 1) - (\kappa_1 - 1)}{k(\kappa_1 + 1) + (\kappa_1 + 1)}, \quad (11.28)$$

where  $k = G_2/G_1$  is the ratio of shear moduli of elasticity of both materials, and  $\kappa_1 = 3 - 4\mu_1$  for plane strain, and  $(3 - \mu_1)/(1 + \mu_1)$  for plane stress; subscript 1 or 2 pertains to the material 1 or 2. Parameter  $\alpha$  characterises the difference between elastic moduli of both materials; parameter  $\beta$  reflects more the difference of Poisson's numbers [2, 3].

The further parameter is the effective elastic modulus of the bimaterial, defined similarly as in the contact problem:

$$\frac{1}{E_e} = \frac{1}{2} \left( \frac{1}{E_1} + \frac{1}{E_2} \right). \quad (11.29)$$

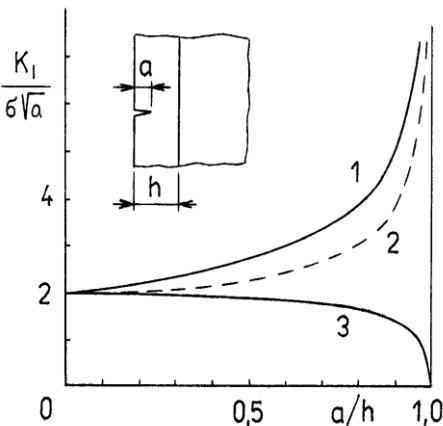
The following table presents Dundurs' parameters for various materials.

**Table 11.1.** Dundurs' parameters and effective modulus of elasticity for some material combinations [2, 3].

Combination	$\alpha$	$\beta$	$E_{ef}$
steel – ZrO <sub>2</sub>	0,632	0,123	86,2
steel – Ni	0,004	0,013	233,2
steel – Ti	0,257	0,024	173,8
steel – glass	0,517	0,186	113,1
steel – epoxy	0,963	0,232	8,7
glass – epoxy	0,888	0,210	8,3

### Crack approaching to interface

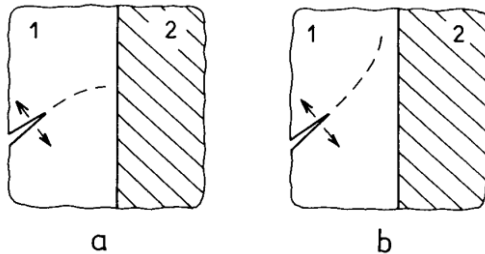
The situation for a crack in a coating, approaching to a surface in a body loaded by tension in the direction of the interface is shown in Fig. 11.8. The vicinity of another material of different stiffness influences the stress intensity factor. This factor increases if the crack approaches to the material of lower elastic modulus, and decreases if it approaches to a stiffer material. In the former case the crack tip easily arrives at the interface. In the latter case, the crack should stop before touching the interface. With respect to various inhomogenities and material defects the crack also here sometimes touches the interface. If the crack is not perpendicular to the interface, it will turn in the vicinity according to Figure 11.9.



**Fig. 11.8.** Stress intensity factor for a crack in the coating, approaching to the interface with substrate [4].

1. combination Al-epoxy ( $E_{Al} > E_{epoxy}$ ),
2. steel-Al ( $E_{steel} > E_{Al}$ ),
3. Al – steel ( $E_{Al} < E_{steel}$ ).

A crack in the stiffer coating on more compliant substrate turns into the direction perpendicular to the interface (Fig. 11.9a). A crack in more compliant coating has the tendency to turn into the direction parallel with the interface (Fig. 11.9b). This influences its behaviour in the interface.



**Fig. 11.9.** Oblique crack approaching the interface.  
*a:*  $E_1 > E_2$ , *b:*  $E_1 < E_2$ .

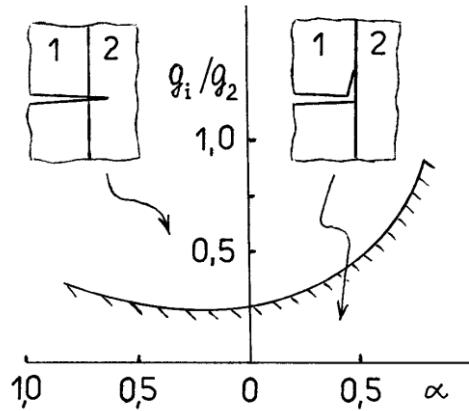
### Behaviour of a crack at the interface

An important question for a crack, whose tip is at the interface of two materials, is whether it will stop here, or if it will continue into the substrate in its initial direction, or if it turns along the interface (Fig. 11.10). The solution of this problem was complicated by the fact that the stress singularity exponent at the crack tip changes at the contact of two layers with sudden change of properties. Fortunately, with some simplification it can be said that the crack will have a tendency to grow in the original direction or deflect according to whether the ratio of energy release rate for the growth in the initial direction and in the deflecting direction will be higher or lower than the ratio of specific fracture energies in the corresponding directions. Simply said: the crack will propagate in the direction of higher surplus of the released energy above the consumed one.

If the crack is perpendicular to the interface, and opened by tensile stress parallel to the interface, the condition of its deflection is formulated in the following way:

$$\frac{G_i}{G_2} > \frac{\Gamma_i}{\Gamma_2} . \quad (11.30)$$

If this condition is not fulfilled, the crack will not deflect, but penetrates into material 2.  $G$  expresses the energy release rate,  $\Gamma$  is the specific fracture energy, and subscript 1 or 2 says whether the crack will propagate along the interface or penetrate into material 2. If the elastic constants are the same for both materials, it comes to the crack deflection and separation of both layers for  $\Gamma_i/\Gamma_2 < 1/4$ , that is if the specific fracture energy of interface is lower than 25% of the specific fracture



**Fig. 11.10.** Ratio of the energy release rate of deflecting crack ( $G_1$ ) and penetrating into the substrate ( $G_2$ ) for various values of Dundurs' parameter  $\alpha$  [2 – 4].

energy of layer 2 (= substrate). It also means that if the specific fracture energy of the interface  $\Gamma_i$  is not smaller than 25% of the material 2, the crack cannot deflect.

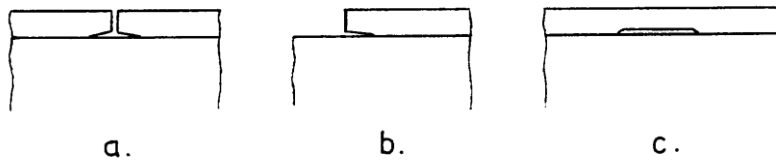
The solution for different elastic properties of materials 1 and 2 is more complex, as the character of stress field for the crack at the interface and in homogeneous material. He and Hutchinson have solved the problem [3]. Figure 11.10 shows the ratio  $G_1/G_2$  as a function of Dundurs' parameter  $\alpha$  for  $\beta = 0$ . The influence of  $\beta$  is relatively small. The figure gives a general idea on the behaviour of a crack touching the interface. If the ratio of specific fracture energies  $\Gamma_1/\Gamma_2$  for a bimaterial with Dundurs' parameter  $\alpha$  lies above the curve  $G_1/G_2$ , the crack can penetrate into the material 2. If it will lie below the curve, the crack will deflect. It is obvious that for  $\Gamma_1/\Gamma_2 < 1/4$  the crack deflects for any material combination, and that the conditions for delamination are better in general, if the crack is in the more compliant material, i.e. for  $E_1 < E_2$ .

The necessary condition for crack deflection is that the energy release rate  $G_1$  must be higher than the specific fracture energy  $\Gamma_i$  of the interface. Vice versa, the condition for the crack penetration into material 2 is  $G_2 > \Gamma_2$ .

#### Crack in the interface; delamination

At an interface crack (Fig. 11.11) usually normal and shear stress act simultaneously. Let us consider a case when compressive (normal) stress from the

manufacture acts in the undamaged coating in the direction parallel with the interface. If a part of the coating breaks away at some place, its edge will be free here, without stress (Fig. 11.11b). If tensile stress acted in the coating, it will be released even due to simple cracking of the coating. The relatively fast decrease of the force at the edge causes shear stresses in the interface. The stress state at the crack tip will thus be characterised by two components of stress intensity factor,  $K_I$  and  $K_{II}$ . The consequence of shear stresses is that a crack here would like to turn here into material 1 or 2, with respect to the orientation of these stresses. Whether it turns depends on the stress intensity for the pertinent directions, and also on the energy consumption needed for the crack propagation in the interface or material 2.



**Fig. 11.11.** Crack in the interface between coating and substrate.

If both materials have the same elastic constants, one can work with the modulus (amplitude) of stress intensity factor  $|K|$  and phase angle  $\psi$ :

$$|K| = \sqrt{K_I^2 + K_{II}^2} \quad , \quad \psi = \arctan(K_{II} / K_I) \quad . \quad (11.31)$$

The crack behaviour can also be assessed via the energy release rate  $G$ , which is scalar. The specific fracture energy  $\Gamma$  is also scalar. The values of these quantities, however, depend on the phase angle  $\psi$ . The crack will propagate in the direction with the highest surplus of the released energy  $G(\psi)$  compared to the consumed energy  $\Gamma(\psi)$ .

With different materials 1 and 2, the exponent  $s$  in Eq. (11.27) is a complex number. According to the solution based on linear fracture mechanics, the individual stress components (normal and shear) should oscillate in the vicinity of the crack tip, as if the resultant stress vector rotated by higher and higher velocity. Similarly also theoretical displacements oscillate. They should even interpenetrate near the tip, which is impossible. The pertinent region, however, is extremely small, comparable with the interatomic distances, where the theoretical models developed for the continuum lose their validity. In reality, always a very thin

transitional layer exists at the interface, where the properties change more or less continuously. Moreover, if the stress attains a certain critical value, irreversible deforming occurs here, and Hooke's law loses its validity. For practical assessment of behaviour of cracks at the interface, general conclusions following from the linear fracture mechanics (including factors  $K_I$ ,  $K_{II}$ ) may be applied with some caution. For more, see [2, 3].

### Crack propagation in the interface from the coating edge

Here we shall look at the delamination starting at the long crack below the coating, in which tensile stress  $\sigma_0$  acts (Fig. 11.12). The stress intensity factor for a surface crack of depth  $h$  is

$$K_I = 1,12 \sigma_0 \sqrt{(\pi h)} = 1,99 \sigma_0 \sqrt{h} , \quad (11.32)$$

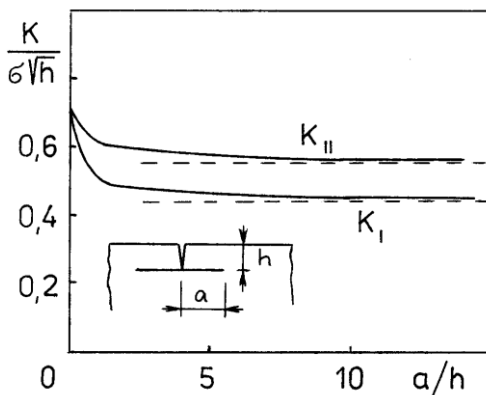
with corresponding stress intensity factors in the interface [2, 3]:

$$K_{I,0} = K_{II,0} = 0,702 \sigma_0 \sqrt{h} \quad (11.33)$$

The corresponding energy release rate is

$$G_0' = 0,99 \frac{1 - \mu^2}{E} \sigma_0^2 h . \quad (11.34)$$

If  $G_0'$  is higher than the specific fracture energy  $\Gamma_i$  of the interface for the phase angle  $\psi$  ( $= \arctg (K_{II}/K_I) = 40^\circ$ ), a crack able of growth arises in the interface. (Subscript 0 at  $K$  and  $G$  means that still the crack length is zero.)



**Fig. 11.12.** Stress intensity factors for the propagation of a crack from the coating edge [10].

The stress intensity factors for a delamination crack decrease with its increasing length (Fig. 11.13) and approach to the asymptotic value (for a very long crack):

$$K_{I,\infty}' = 0,434 \sigma_0 \sqrt{h} \quad , \quad K_{II,\infty}' = 0,558 \sigma_0 \sqrt{h} \quad , \quad (11.35)$$

The corresponding energy release rate is

$$G_\infty = \frac{1-\mu^2}{E} (K_{I,\infty}'^2 + K_{II,\infty}'^2) = 0,5 \frac{1-\mu^2}{E} \sigma_0^2 h \quad . \quad (11.36)$$

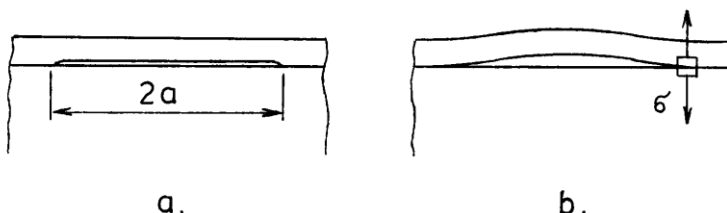
If the specific fracture energy  $\Gamma_i$  of the interface is between  $\Gamma_0'$  and  $\Gamma_\infty'$ , the crack starts growing, but stops soon. However, if  $\Gamma_i < \Gamma_\infty'$ , it can grow without limits, and significant spalling of the coating will occur.

Propagation of delamination far from edges – a hot spot

Let us look at the case if the coating does not hold firmly on the substrate. For simplicity we can assume that the unbonded region has the shape of a circle of diameter  $2a$ . In the coating, often a biaxial compressive stress  $\sigma_0$  acts. It can be a residual stress or stress caused by higher coating temperature when the component is heated. As long as this stress is low, the coating above the delamination is straight and nothing happens. As soon as  $\sigma_0$  exceeds certain critical limit, a free part of the coating buckles (Fig. 11.13). Bending stresses appear in addition to the uniformly distributed stress, and high stress peak appears at the delamination edge. The critical stress for the coating buckling is [8, 9]

$$\sigma_C = k \frac{E}{12(1-\mu^2)} \left(\frac{h}{a}\right)^2 \quad . \quad (11.37)$$

Under certain conditions, the delaminated area begins to grow. This causes the release of energy from the compressed coating, and this will cover its consumption



**Fig. 11.13.** Delamination at places distant from edges.  
*a – geometry, b – situation after the coating has buckled.*

for the creation of new fracture area. If this happens at the heated place, the heat transfer into the body is worse at the delamination, so that the coating temperature and compressive stress in it increase. This promotes coating spalling and cracking.

More about buckling of coatings above a delamination, and about fracture mechanics for these cases can be found, e.g., in [1, 2, 8, 9]. Here, only one formula will be given. During the growth of circular delamination the energy release rate grows with increasing radius  $a$  and approaches the asymptotic value:

$$G_{\infty} = (1 - \beta) h \sigma_0^2 (1 - \mu) / E . \quad (11.38)$$

If this value is lower than the specific fracture energy of the interface, no delamination can propagate due to the stress  $\sigma_0$ , regardless its dimensions. If a coating is to be designed, the  $h$ ,  $\sigma_0$  and  $E$  values should always be so that  $\Gamma_i > G_{\infty}$ .

#### Growth of a crack in surface layer into width

As soon as the surface crack in a coating has reached the interface with substrate, it can turn here along it (delamination), stop or penetrate into the substrate. If the substrate is tough, the crack tip stops here and becomes blunt (Fig. 11.14b). Further crack propagation occurs sideways (Fig. 11.14c). If tensile stress  $\sigma_0$  in the coating is the crack driving force, the energy release rate for the crack growth to depth at reaching the substrate equals [3]

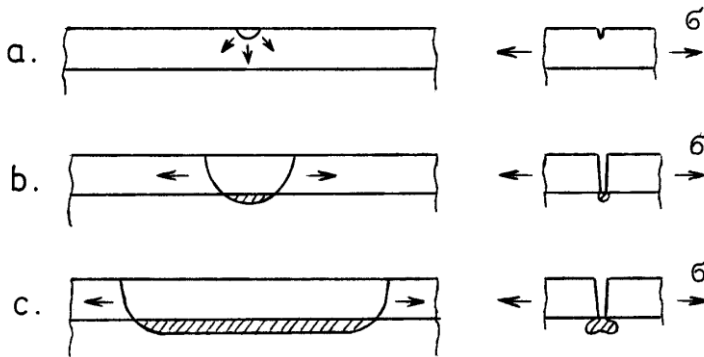
$$G(h) = 3,94 \frac{1 - \nu^2}{E} \sigma_0^2 h . \quad (11.39)$$

The energy release rate for the growth of this crack sideways is

$$G_1 = 1,97 \frac{1 - \nu^2}{E} \sigma_0^2 h . \quad (11.40)$$

This is half of the value of energy release rate (10.39) for crack growth perpendicularly to the surface. This means that a crack, which has penetrated through the coating to the interface, but cannot penetrate into the substrate, will always propagate sideways. Equation (11.40) also indicates that certain critical coating thickness exists for the cracks caused in the coating by local damage, from which they will spontaneously propagate sideways. This thickness is smaller for higher stress acting in the coating and for its smaller specific fracture energy  $\Gamma_i$ .





**Fig. 11.14.** Propagation of surface crack in the coating on a tough substrate. *a* – onset of growth, *b* – the crack has grown to the substrate, *c* – crack propagates sideways. After [2].

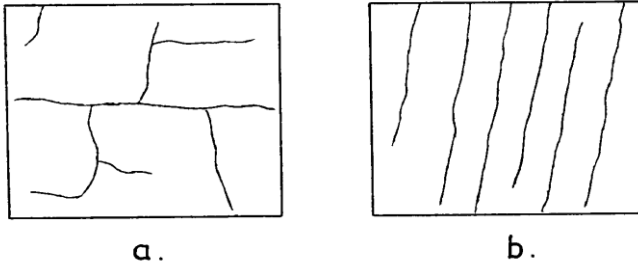
Sometimes a crack network is formed in a brittle coating on ductile substrate. This is because the individual cracks stop at the substrate, so that further cracks can be created under increasing load. The system of cracks corresponds to the character of acting stresses. Under biaxial isotropic state of stress, which arises, for example, at sudden change of temperature, the crack network is irregular and the cracks have various directions (Fig. 11.15a). Under uniaxial stress, e.g. in a body loaded by tension, a row of cracks perpendicular to the direction of maximal tensile stress is created (Fig. 11.15b). The density of cracks is related to the stress magnitude. As the forces are transmitted from the substrate to the coating by shear stresses, an important role is also played by the strength of adhesion of the coating on the substrate, and, sometimes, by the substrate yield strength, similarly to the transfer of forces between the fibre and matrix in composite materials, see Chapter 12.

### 11.8 Determination of mechanical properties of coatings

For coatings and various surface layers, the following properties are determined most often: modulus of elasticity, strength, hardness and wear resistance, internal stresses and fracture mechanics parameters, including adhesive strength. Here only several notes will be presented; more information can be found, for example, in [3].

#### Young modulus

Usually is determined from the deflection of a specimen or by indentation.



**Fig. 11.15.** Network of cracks in a coating due to:  
*a* – thermal stress, *b* – uniaxial tension.

Bending tests are often done with a coated specimen of rectangular cross section, whose one end is clamped and the other is loaded by transverse force, and the deflection of the loaded end here is measured. The specimen can also lie on two supports and loaded in its centre. If the coating is on both surfaces, the following formula can be used [2]:

$$E_1 = \left( S_b - \frac{E_2 b h_2^3}{12} \right) \frac{12}{b(h^3 - h_2^3)} ; \quad S_b = \frac{Pl^3}{48w} ; \quad (11.41a,b)$$

$S_b$  is bending stiffness of the coated specimen,  $b$  is its width, and  $h = 2h_1 + h_2$  is the total thickness ( $h_1$  is the thickness of one coating,  $h_2$  is the substrate thickness),  $P$  is the load;  $l$  is the distance of the supports,  $w$  is the deflection in the center. (If the specimen is wide, the stiffness  $S_b$  must be multiplied by the term  $(1 - \mu^2)$ ). The solution for specimens with only one surface coated is more complicated, as the neutral axis is not in the half of the height.

Young modulus of coatings is also determined by nanoindenters, which measure simultaneously the indenter load and displacement. In this case the indenter displacement is influenced by the stiffness of both the coating and substrate. The response is measured for various depths (or continuously), and the measured values are fitted by a suitable function. The true modulus of elasticity of the coating corresponds to zero depth of indenter penetration. For more, see [3, 7].

### Hardness

If hardness of a coating is measured by impressing an indenter into the specimen, the properties of the substrate must be considered. When evaluating the data,

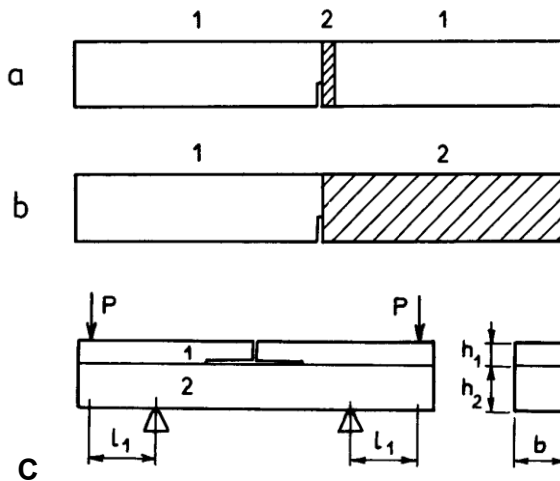
various models are used, depending on whether hard coating is on a hard substrate, or hard coating on a ductile substrate, or compliant coating on a hard substrate. More can be found in [3] and the sources quoted there.

### Residual stresses

Residual stresses in surface layers are determined by various methods [3]. Destructive methods gradually remove thin layers from the specimen by grinding off or by etching, and its deflection is measured. Semidestructive methods measure the length of cracks created by an indenter. Nondestructive methods working with X-Ray diffraction utilise the fact that mechanical stress changes the distances of atoms in the crystal lattice. Also methods based on photoelasticimetry can be used.

### Fracture toughness

The knowledge of fracture toughness or specific fracture energy of the coating and interface, as well as of the substrate is important. These quantities are determined on sandwich or bimaterial specimens loaded by bending (Fig. 11.16a, b), on DBCB specimens (double cantilever beam), or on a bilayer bend specimens UCSB (University of California Santa Barbara, Fig. 10.16c).



**Fig. 11.16.** Specimens for determination of fracture mechanics parameters of coatings and interfaces. a – sandwich, b – bimaterial, c – specimen UCSB.

Adhesive strength of coatings is determined by various tests of adhesion. For more, see [2].

### References to Chapter 11.

1. Menčík, J.: Výpočty strojních součástí s povrchovými úpravami na pevnost a životnost. (Cyklus Stavba strojů, č. DT01-211-91) DT ČSVTS, Praha, 1991. 120 p.
2. Menčík, J.: *Mechanics of Components with Treated or Coated Surfaces*. Kluwer Academic Publishers, Dordrecht, 1996. 360 p.
3. Hutchinson, J. W., Suo, Z.: Mixed mode cracking in layered materials. In: *Advances in Applied Mechanics*, 29, Academic Press, New York, 1991. pp. 63 – 191.
4. Beuth, J.: Cracking of thin bonded films in residual tension. *Int. J. Solids Structures*, **29** (1992) No. 13, pp. 1657 – 1675.
5. He, M. Y., Hutchinson, J. W.: Crack deflection at an interface between dissimilar elastic materials. *Int. J. Solids Structures*, **25** (1989) No. 9, 1053 – 1076.
6. Dundurs, J.: Discussion to the paper: Edge-bonded dissimilar orthogonal elastic wedges under normal and shear loading. *J. Appl. Mech. (Trans ASME, Ser. E)* **36**, No. 3, pp. 650 – 652.
7. Menčík, J. et al.: Determination of elastic modulus of thin layers using nanoindentation. *J. Mater. Res.*, **12** (1997) No. 9, pp. 2475 – 2484.
8. Evans, A. G., Hutchinson, J. W.: On the mechanics of delamination and spalling in compressed films. *Int. J. Solids Structures*, **20** (1984) No. 5, pp. 455 – 466.
9. Menčík, J.: Mechanics of delamination of thin films under thermal and residual compressive stresses. *Ceramics - Silikáty*, **36** (1992) No. 2, pp. 93 - 100.
10. Thouless, M. D., Cao, H. C., Mataga, P. A.: Delamination from surface cracks in composite materials. *J. Mater. Sci.*, **24** (1989) No. 4, pp. 1406 - 1412.

## 12. Mechanics of composite materials

### 12.1 Introduction

Composite materials consist of two or more components with different properties. The resultant property differs significantly from them, and is not their simple sum. Usually the resultant properties are significantly better. As examples, fiberglass laminates, fishing rods or parts of aircrafts stiffened by carbon fibers, concrete reinforced by steel bars or wires, and also common concrete, which is a composite with particles of sand and gravel in the cement or polymer matrix. In fact, also wood is a natural composite. More on composite materials in general can be found in [1 – 5].

The basic type is composites with two components. One component is **matrix**, in which suitable **particles** or **fibers** are dispersed. The matrix material is, for example, a polymeric resin, but also metal, glass, ceramic material, gypsum or concrete. **Particulate composites** contain particles, where no dimension prevails. They are usually added to the composite for other reasons than increasing its strength, which sometimes even get worse. They are used for reduction of costs, for improvement of thermal or electric properties or wear resistance. They can also increase the stiffness.

**Fiber composites** contain glass fibers, polymeric (e.g. kevlar), carbon or metal fibers, and sometimes natural fibers. The usual aim is improvement of mechanical properties, especially strength or stiffness, and the weight reduction. Sometimes we strive for higher toughness and non-catastrophic (i.e. slow) fracture, and ability to absorb energy.

In this chapter we shall treat fiber composites. Their properties depend on the properties of matrix and fibers and their proportions, and also on their geometry, mutual arrangement, and the properties of their bonding. Here, the basic formulae will be given. More details can be found in literature, for example [6 – 11].

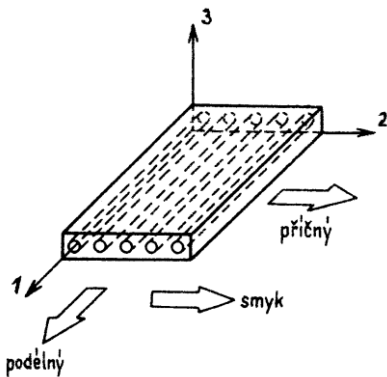
**Fiber composites** can be with **long** or **short fibers**. Long fibers are such, whose length is many times larger than the diameter, and „do not end inside the component“. Their properties are anisotropic. The length of short fibers is only several times the diameter and is much smaller than the size of the component in

their direction. Short fibers are often oriented randomly in the body, and the resultant properties of the composite are rather isotropic.

## 12.2 Composites with long fibers

The basic mechanical properties, such as strength and stiffness, will be shown on an example of a composite with fibers parallel to the direction of acting load (Fig. 12.1). Strong bonding of fibers with matrix is assumed. At lower loads both components deform elastically. The characterisation of the resultant response needs the knowledge of elastic moduli ( $E_f$ ,  $E_m$ ) and relative fraction of each component ( $V_f$ ,  $V_m$ ). Subscripts f and m pertain to the fibers and matrix. The resultant property of the composite is denoted by subscript c. The volumen fractions  $V_f$  and  $V_m$  are the same as the fractions of cross section areas  $S_f$  and  $S_m$ . It holds

$$V_f + V_m = 1, \quad V_m = 1 - V_f. \quad (12.1a, b)$$



**Fig. 12.1.** Composite with long parallel fibers. Longitudinal (*podélný*) and transverse (*příčný*) directions [6]. *smyk* = shear

### Longitudinal strength and stiffness of the composite

If the force acts in the direction of fibers, its part  $F_f$  is transferred by the fibers and the part  $F_m$  by the matrix, and it holds

$$F_f = \sigma_f S_f = E_f \varepsilon S_f, \quad F_m = \sigma_m S_m = E_m \varepsilon S_m; \quad (12.2)$$

$E_f$  or  $E_m$  denote the elastic (Young) modulus of the pertinent component, and  $\varepsilon$  is the strain (relative elongation). The total force is

$$F_c = F_f + F_m. \quad (12.3)$$

This can be written by means of stresses as

$$F_c = \sigma_c S_c = \sigma_f S_f + \sigma_m S_m . \quad (12.4)$$

Dividing this by the total area of the cross section and considering that  $S_f = V_f$  and  $S_m = V_m$ , gives the average stress in the composite:

$$\sigma_c = \sigma_f V_f + \sigma_m V_m . \quad (12.5)$$

The strain of both, strongly bonded components, is the same,

$$\varepsilon_c = \varepsilon_f = \varepsilon_m = \varepsilon . \quad (12.6)$$

The subscript is thus not necessary, and the stresses can be expressed as

$$\sigma_f = E_f \varepsilon , \quad \sigma_m = E_m \varepsilon , \quad (12.7)$$

These stresses are in the same proportion as their moduli of elasticity,

$$\sigma_f / \sigma_m = E_f / E_m , \quad \text{or} \quad \sigma_f / \sigma_c = E_f / E_c ; \quad (12.8)$$

The higher stress acts in the component with higher modulus. Division of Eq. (12.5) by the strain gives the elastic modulus of the composite:

$$E_c = E_f V_f + E_m V_m = E_f V_f + E_m (1 - V_f) . \quad (12.9)$$

The properties of the composite are usually expressed as a function of the fiber proportion. This is shown in the right-side part of Equation (12.9).

If the composite consists of more ( $n$ ) components, the resultant stress and modulus of elasticity are

$$\sigma_c = \sum_{i=1}^n \sigma_i V_i , \quad E_c = \sum_{i=1}^n E_i V_i . \quad (12.10 \text{ a,b})$$

Two examples adapted from [6] will be given here for illustration.

**Example 1.** Calculate the fraction of the load transferred by fibers in two composites with glass fibers in epoxy matrix. One composite contains 10% volume fraction of fibers, and the other 50%. Elastic modulus of the fibers is  $E_f = 72$  GPa, the matrix modulus is  $E_m = 3,6$  GPa (i.e.  $E_f/E_m = 72/3,6 = 20$ ).

The ratio of the force transferred by the fibers to the total force in the composite is

$$\frac{F_f}{F_c} = \frac{\sigma_f V_f}{\sigma_f V_f + \sigma_m V_m} = \frac{1}{1 + \frac{E_m V_m}{E_f V_f}} . \quad (12.11)$$

With 10% of fibers,  $V_m/V_f = 0,9/0,1 = 9$ , so that  $F_f/F_c = 0,690 = 69\%$ . With 50% of fibers,  $V_m/V_f = 1$ , and  $F_f/F_c = 0,95$ ; fibers thus transfer 95% of all load.

Example 2. How the forces will be changed for carbon fibers with  $E_f = 432$  GPa?

$E_f/E_m = 432/3,6 = 120$ , so that  $F_f/F_c$  for 10% of fibers is 0,930, i.e. 93%. For 50% of fibers,  $F_f/F_c = 0,992 = 99\%$ .

We can see that fibers with high modulus of elasticity transfer substantial part of the load, even if their proportion is relatively low.

Now we shall show how the longitudinal strength of a composite varies with increasing proportion of fibers.

a) Fibers and matrix have the same strength and strain at failure,  $\sigma_{f,u} = \sigma_{m,u}$ . (“u” means ultimate.) For simplicity, no dispersion of properties is assumed.

The composite fractures at critical stress:

$$\sigma_{c,u} = \sigma_{f,u} V_f + \sigma_{m,u} V_u = \sigma_{f,u} V_f + \sigma_{m,u} (1 - V_f) . \quad (12.12)$$

b) Fibers have higher strength, but the matrix is more ductile and fails at higher strain. An example is a composite with carbon fibers in polymeric matrix. As long as the fibers do not break, the mean stress in the composite is

$$\sigma_c = \sigma_f V_f + \sigma_m (1 - V_f) . \quad (12.13)$$

The fibers break at strain  $\varepsilon_{f,u}$ . If the strain of the composite attains this value, the fibers break. (Again no dispersion of properties is assumed.) Then the load can be transferred only by the matrix, which fails at the stress  $\sigma_{m,u}$ . As “holes” after the fractured fibers remained in the matrix, the load carrying cross section is smaller than the total cross section, so that the ultimate strength of the composite is lower:

$$\sigma_{c,u} = \sigma_{m,u} (1 - V_f) . \quad (12.14)$$

The load carrying capacity thus decreases with the increasing proportion of fibers! Fortunately, this relation holds only for very low fractions of fibers; for  $V_f$  higher than several percent the resultant strength is higher (Fig. 12.2). The volume fraction of fibers, corresponding to the minimum strength, is

$$V_{f,\min} = \frac{\sigma_{m,u} - \sigma_{m,ef,cr}}{\sigma_{f,u} + \sigma_{m,u} - \sigma_{m,ef,cr}} ; \quad (12.15)$$



$\sigma_m(\varepsilon_{f,cr})$  is the stress in the matrix, corresponding to the critical deformation of fibers. For epoxy resin stiffened by carbon fibers ( $\sigma_{m,u} = 0,07$  GPa,  $\sigma_{f,u} = 3.2$  GPa,  $E_m = 3,1$  GPa,  $\varepsilon_{f,u} = 0,014$ ), the critical stress  $\sigma_m(\varepsilon_{f,cr}) = 0,0434$  GPa. Insertion of these values into Eq. (12.15) gives  $V_{f,min} = 0,0088 \approx 0,9\%$ . This means that more than 1% of fibers will have strengthening effect. The situation is depicted in Fig. 12.2. However, the resultant strength with  $V_{f,min}$  is lower than the strength of the matrix alone (without fibers)! If the addition of fibers should increase the composite strength, the resultant strength must be higher than  $\sigma_{m,u}$ , and the fiber proportion must be higher than the critical value ( $V_{krit}$  in Fig. 12.2).

$$V_{f,cr} = \frac{\sigma_{m,u} - \sigma_{m,ef,cr}}{\sigma_{f,u} - \sigma_{m,ef,cr}} \quad (12.16)$$

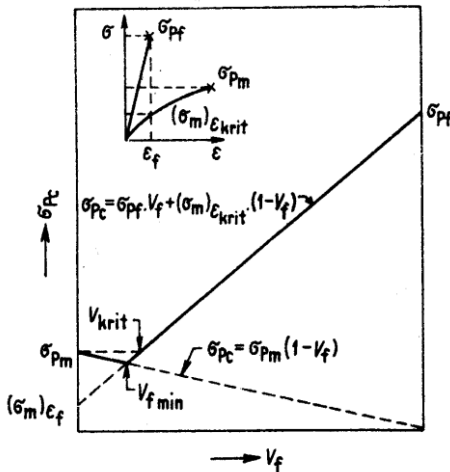


Fig. 12.2. Strength of fiber composites as a function of fiber fraction  $V_f$  [6].

### Transverse stiffness and strength of the composite

In the above model, the fibers were arranged parallel in the matrix. The deformation of all components was the same, and the forces were summed up. If the load acts perpendicularly to the fibers (Fig. 12.1), which is a series arrangement, with the same force acting in each component, and the deformations are summed (and also the compliances). The approximate value of elastic modulus is obtained as

$$\frac{1}{E_{c,T}} = \frac{V_f}{E_{f,T}} + \frac{V_m}{E_m} = \frac{V_f}{E_{f,T}} + \frac{(1-V_f)}{E_m} \quad (12.17)$$

subscript T means transverse direction. With more components,

$$\frac{1}{E_{c,T}} = \sum_{i=1}^n \frac{V_i}{E_{i,T}} . \quad (12.18)$$

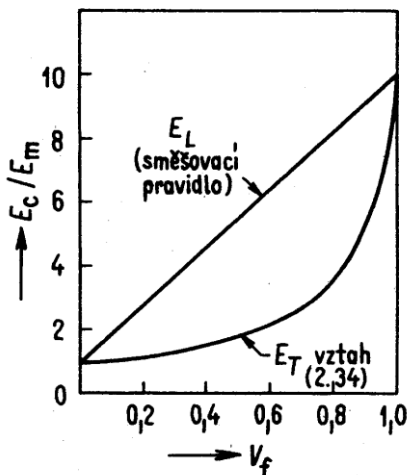
The reality is more complex, as the formula corresponds to the case of series arrangement of flat rectangular layers, while the fibers have circular cross section and are not arranged regularly. Certain role can be played by different values of Poisson's numbers of the individual components; here their equality was assumed for simplicity,  $\mu_f = \mu_m$ .

Figure 12.3 shows the ratio of the longitudinal (L) and transverse (T) modulus of elasticity of the composite and the matrix as a function of the volume proportion of fibers  $V_f$ . The figure corresponds to the case  $E_f/E_m = 10$  [6].

A composite loaded perpendicularly to the fibers fails if the stress exceeds the transverse strength of any component ( $\sigma_{f,u,T}$ ;  $\sigma_{m,u,T}$ ). The transverse strength is

$$\sigma_{c,u,T} = \min(\sigma_{f,u,T}; \sigma_{m,u,T}) . \quad (12.19)$$

Long ordered fibers are suitable everywhere the directions of stresses in the component are known and do not vary, or change only slowly, so that their laying during creation of the composite body is simple. If these directions are not known, or vary quickly from a place to place, isotropic properties are better, and thus the composites with short fibres (see later). A layer with parallel fibers is orthotropic. Anisotropy can be eliminated by suitable arrangement of several orthotropic layers.



*Fig. 12.3. Ratio of elastic modulus of the composite ( $E_c$ ) and matrix ( $E_m$ ) in the longitudinal ( $E_L$ ) and transverse ( $E_T$ ) direction.  $V_f$  - fibers volume fraction [6].*

If the direction of forces and stresses acting in the composite body, it is possible to optimise the orientation of fibers, and create a more weight-efficient structure. As an example, a laminated cylindrical pressure vessel will be analysed here [7, 8].

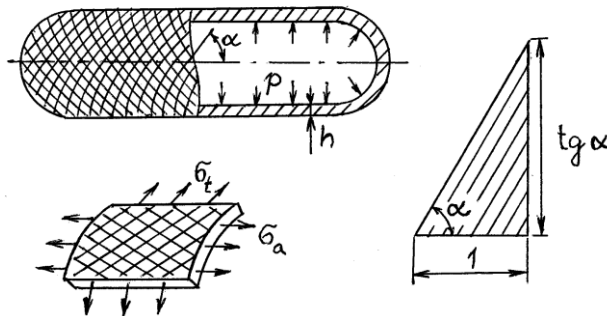
Example 3.

Determine the optimum directions for fibers in a cylindrical pressure vessel made by filament winding.

Solution. If the pressure  $p$  acts in the vessel, it causes circumferential stress  $\sigma_t$  and axial stress  $\sigma_a$  in the wall:

$$\sigma_t = p \frac{R}{h}, \quad \sigma_a = p \frac{R}{2h}, \quad (12.20)$$

$R$  is the radius of the vessel and  $h$  is the wall thickness. Circumferential stress is thus twice higher than the axial stress. If the vessel would be made of isotropic material, it must be dimensioned with respect to the maximum, i.e. circumferential stress. However, if it is made by filament winding, it can be lighter thanks to suitable orientation of fibers. The situation is shown in Fig. 12.4. The fibers are inclined to the axis by angle  $\alpha$ . In the direction  $\alpha$  the force  $nF_f$  acts in the fibers, where  $F_f$  is the force in one fiber and  $n$  is the number of fibers in the investigated (triangular) part of the shell [7, 8].



**Fig. 12.4.** Cylindrical pressure vessel made from fiber composite by filament winding.  $\sigma_t$ ,  $\sigma_a$  – circumferential and axial stress,  $\alpha$  – optimum angle of fibers.

In the circumferential direction (vertical direction at right side of Fig. 11.4) the following component of this force acts, which is in equilibrium with the circumferential force caused by the internal pressure:

$$nF_f \sin \alpha = \frac{pR}{h} \times 1 \times h \quad (12.21)$$

The force component in axial direction (horizontal direction in Fig. 12.4) is in equilibrium with the resultant of axial stress,

$$nF_f \cos \alpha = \frac{pR}{2h} \times \operatorname{tg} \alpha \times h \quad (12.22)$$

The expression  $1 \times h$  at right part of Eq. (12.21) is the area of that part of the wall, which corresponds to the horizontal cathetus of the triangle (Fig. 12.4), in which circumferential stress acts. Similarly  $\operatorname{tg} \alpha \times h$  in (12.22) represents the area corresponding to the vertical cathetus, where axial stress acts.

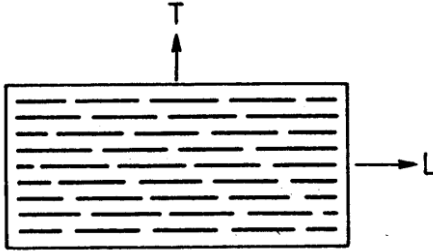
Division of Equation (12.21) by Eq. (12.22) and a rearrangement gives

$$\operatorname{tg}^2 \alpha = 2, \text{ odkud vyplývá } \alpha = 54,7^\circ \quad (12.23)$$

This is the basic angle of the slope of fibers in a wound pressure vessel, which ensures that the strength in circumferential direction is twice as high as in the axial direction. If more layers will be used, the fibers in the next layer will have the opposite slope ( $\alpha = -54,7^\circ$ ), etc.

### 12.3 Composites with short fibers

If the directions of stresses in the component vary relatively quickly (or if they are different in various loading cases, or are unknown), short fiber composites are better. In such case, with random orientation of fibers, the resultant properties are isotropic. With some technologies, such as injection, the fibers arrange themselves during the flow through the mould, and this can be advantageous with respect to the stresses in the finished component. A part of the component with ordered fibers is shown in Fig. 12.5. While in composites with long fibers these fibers are along the whole body, and the force  $F_f$  acts in them everywhere, in composites with short fibers places exist, where the force in the fiber direction is transferred only by the matrix. Therefore the question of force transfer from the matrix into the fibers or vice versa is very important. The situation for one fiber is depicted in Fig. 12.6. Shear stress  $\tau$  acts between the fiber and matrix. If the load is low, the deformations are elastic, Hooke's law holds, and the shear stress along the interface is distributed nonuniformly, with the highest value at the ends of fibers [6 – 9]. This character of stress distribution lasts till the instant when the maximum value



**Fig. 12.5.** Composite with short ordered fibers (a schematic).  
*L* – longitudinal direction,  
*T* – transversal direction.

of stress attains either the adhesive strength or the yield strength of the matrix from elastic-plastic material, depending on which value is lower. According to the simplified model we shall assume that the shear stress during movement of the fiber in the matrix is constant, equal adhesive strength  $\tau_a$ . The equation of equilibrium of forces acting on the segment of the fiber of infinitesimal length  $dx$  is

$$(\pi r^2)\sigma_f + (2\pi r dx)\tau_a = (\pi r^2)(\sigma_f + d\sigma_f), \quad (12.24)$$

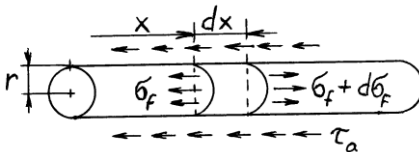
from where it follows

$$\frac{d\sigma_f}{dx} = \frac{2\tau_a}{r}. \quad (12.25)$$

Integration of this expression from the fiber end ( $x = 0$ ), where stress  $\sigma_{f,0}$  is transferred to its face, to the place  $x$ , where the stress  $\sigma_f(x)$  acts, gives

$$\sigma_f(x) = \sigma_{f,0} + 2\tau_a(x/r). \quad (12.26)$$

We see that the stress in the fiber grows linearly with the distance from the face. The force transferred by the face is small compared to the force transferred by the long cylindrical surface, and is usually neglected.



**Fig. 12.6.** Forces acting on the fiber in the matrix

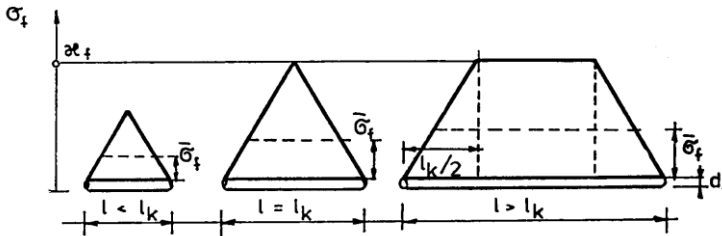
In the case shown in Fig. 12.6 the matrix tries to extend the fiber, and the forces transmitted to it from the left and from the right, have the opposite sign in each half. The stress in the fiber increases from each end, and is highest in the centre. If stress  $\sigma_c$  is acting in the composite, the stress in the fiber can have the maximum value at least equal to that in a composite with long fibers, that is

$$\sigma_{f,\max} = \sigma_c (E_f/E_c); \quad (12.27)$$

see Eq. (12.8). This stress is attained at so-called **load transfer length**

$$l_t = \frac{d}{2} \frac{\sigma_{f,\max}}{\tau_a} = \frac{d}{2} \frac{\sigma_c}{\tau_a} \frac{E_f}{E_c}, \quad (12.28)$$

where  $d (= 2r)$  is the fiber diameter. If the fiber is longer than  $l_t$ , the stress in it does not increase (Fig. 12.7), and remains equal to the value (12.27).



**Fig. 12.7.** Transfer of force between fiber and matrix under constant shear stress at the interface.  $d_f$  – fiber diameter,  $\sigma_f$  – stress in the fiber,  $l_k$  – critical length [6].

The fiber length near the ends, where the stress is lower, is **ineffective length**. The load transfer is more efficient if this length is short.

Let us look at the case when one end of the fiber is in the matrix and the other protrudes out. If relatively short part is in the matrix, the fiber can be pulled out as soon as the adhesive strength  $\tau_a$  was overcome. If the length of the fiber in the matrix is very long, the fiber can be broken. The **critical length**  $l_{cr}$  is such, for which the same probability exists that the fiber will be broken or pulled out of the matrix. The equilibrium of the shear force  $\pi d l_k \tau_a$  at the interface and the tensile force in the fiber on attaining its strength,  $S_f \sigma_{f,U}$ , gives to the critical length,

$$l_{cr} = \frac{d}{4} \frac{\sigma_{f,U}}{\tau_a}. \quad (12.29)$$

**Remark.** One reason for the use of short fibers is the effort to increase the consumption of energy during fracture by pulling the fibers out of the matrix, when the work is done by the friction forces between the fiber and matrix.

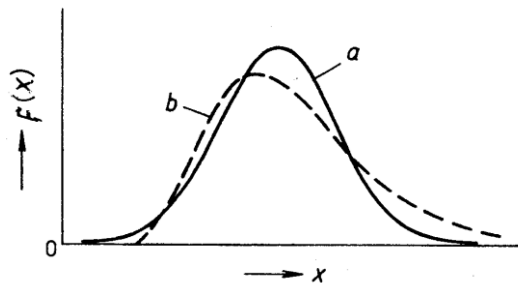
## 12.4 Dispersion of fiber properties

In the previous considerations it was assumed that all fibers in the composite have the same strength  $\sigma_{f,U}$ . In reality the strengths of individual fibers vary in a wide range. The distribution of these strengths can be described reasonably well by Weibull distribution function (Fig. 12.8)

$$F(\sigma_{f,U}) = 1 - \exp \left[ - \left( \frac{\sigma_{f,U} - c}{a} \right)^b \right]. \quad (12.30)$$

Here,  $a$  is the scale parameter,  $b$  is the shape parameter, and  $c$  is the threshold value, which is the lowest value that could appear. As strength cannot be negative, it is sometimes assumed  $c = 0$ , which simplifies the distribution. (The determination of parameters of Weibull distribution is described, e.g., in [13].)

The fibers in a composite are surrounded by the matrix, and – if some fiber breaks, the load can be transferred from the region of its end into the matrix, and behind the damaged place back into another fiber. This means that even a broken fiber can transfer the full load – with the exception of its ends, where the stress increases from 0 to the maximum value  $\sigma_{f,max}$ . Therefore, the fibers in a composite carry more and are utilised better than a bundle of free individual fibers. More to these issues can be found in [6, 9].



**Fig. 12.8.** Probability distributions of random quantity  $x$  (e.g. strength): a) normal, b) Weibull.

### Consequences of dispersion of strength properties

It is suitable to bring here several comments to the dispersion of strength of not only the fibers, but of any material. Every design engineer should be aware of two things. Quantities like strength, yield stress and fatigue strength vary. Material data

sheets usually give the range and minimum value of the pertinent quantity. However, it is principally impossible to determine accurately the minimum strength of a certain material. We can determine the strength of a particular specimen by breaking it. Unfortunately, we cannot use it, as it was broken. Therefore, usually several specimens are tested, and the measured values are statistically processed. As the minimum, such value is given, for which 5% probability exists of occurrence of a weaker piece. The uncertainty in dimensioning is mitigated by means of allowable stress, which is obtained by dividing the strength or yield stress by a (chosen) factor of safety. This is the higher the lower is the knowledge about material, component, load and conditions of operation.

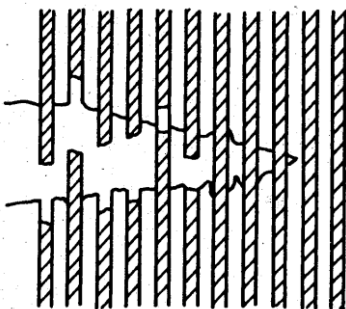
The second consequence of the dispersion of strength properties is the influence of the loaded area on strength. Failure always starts at the weakest point (broken crystalline grain, inclusion...). And, the larger the loaded area, the higher probability of occurrence of a larger defect. In many cases, the following relationship exists between the strength and volume of the body:

$$\sigma_p = C V^{-m} . \quad (12.31)$$

where  $C$  and  $m$  are constants. If the strength can be described by Weibull distribution (12.30), the constant  $m$  is related to the shape parameter  $b$  as  $m = 1/b$ . More about these questions can be found, for example, in [14], where also other works are quoted.

## 12.5 Failure of composites

Fiber composites with ordered fibers can fail in various ways. If tensile load acts in the direction of fibers, the crack will propagate through the matrix perpendicularly to this direction (Fig. 12.9). Short fibers, whose length is shorter than  $l_{cr}$ , will be gradually pulled out of the matrix. Long fibers will break.

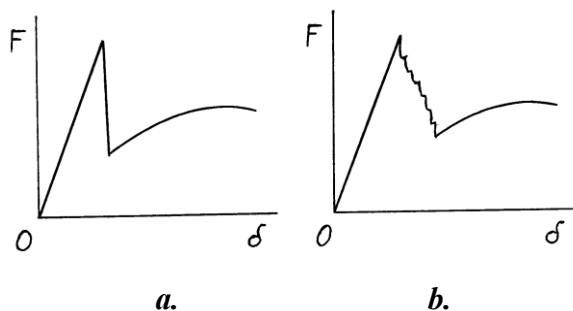


*Fig. 12.9. Characteristic failure modes of a fibrous composite: breaking of fibers and pulling out of the matrix, and matrix fracture.*



A role is played not only by the strength and ductility of fibers, but also by the properties of the matrix, whether it is brittle or ductile, and by the properties of fibers. The behaviour is influenced also by the adhesion between the fibers and matrix, and the ratio of elastic moduli of both components and the ratio of thermal expansions. In the simplest case the fibers break gradually if the crack arrives at them or if it goes behind the fiber. Sometimes the crack at the interface with a fiber has tendency to turn aside or around the fiber. It is especially if the fiber has higher modulus than the matrix and the interface strength is low

Gradual breaking of fibers is visible in load-displacement diagram of tensile test of a composite (Fig. 12.10). A brittle matrix can sometimes break into more parts.

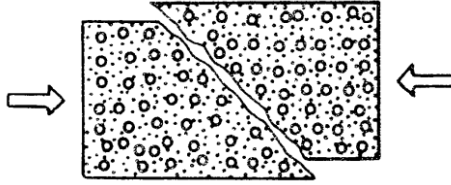


**Fig. 12.10.** Tensile test of a composite (a schematic):  
a) with one fiber in the matrix, b) with many fibers.

Failure is influenced by the differences of thermal expansions and by residual stresses arising due to temperature changes in the preparation. If the fibers have higher thermal expansion than the matrix, they contract more during cooling after the resin curing. Radial tensile stress acts between the fiber and matrix, so that the fibers can tear away from the matrix. On the other hand, if they have lower thermal expansion than the matrix, they are compressed during cooling, and tensile stress appears around them in the matrix, which can lead to its cracking.

Failure can occur also under compression. If this load acts perpendicularly to the fibers, the matrix can fail due to shear stresses (Fig. 12.11). The fracture surface is inclined, because the maximum shear stress contains angle  $45^\circ$  with the direction of compressive stress. If the compressive load acts in the direction of fibers, these can microbuckle. In this process the neighbouring fibers can be “in phase” or in “antiphase”. A long thin compressed component can buckle as a whole.

More about failure of composite materials can be found, e.g., in [6, 9].



*Fig. 12.11. Loading of a composite perpendicularly to the fibers (failure of matrix due to shear stresses).*

## 12.6 Elastic response of orthotropic materials under multiaxial stresses

Elastic deformations of isotropic bodies with stresses acting in planes  $x, y$  are described by Hooke's law

$$\varepsilon_x = E^{-1}(\sigma_x - \mu\sigma_y), \quad \varepsilon_y = E^{-1}(\sigma_y - \mu\sigma_x), \quad \varepsilon_z = -E^{-1}(\sigma_y + \mu\sigma_x); \quad (12.31)$$

$\varepsilon$  is strain and  $\sigma$  is stress (in the individual directions. In  $z$  direction, perpendicular to the plane  $x, y$ , no stress acts; the layer thickness, however, will be changed due to stresses  $\sigma_x$  a  $\sigma_y$ .) Elastic constants are three: modulus of elasticity in tension  $E$ , shear modulus  $G$ , and the coefficient of lateral contraction  $\mu$  (Poisson's number). These constants are mutually related as

$$E = 2(1 + \mu) G, \quad (12.32)$$

so that the knowledge of any two constants is sufficient for the stress analysis.

More complex calculations with multiaxial stress are done better with matrix notation. Hooke's law (12.31) in this case has the following form:

$$\begin{Bmatrix} \varepsilon_1 \\ \varepsilon_2 \\ \gamma \end{Bmatrix} = \begin{bmatrix} 1/E & -\mu/E & 0 \\ -\mu/E & 1/E & 0 \\ 0 & 0 & 1/G \end{bmatrix} \begin{Bmatrix} \sigma_1 \\ \sigma_2 \\ \tau \end{Bmatrix}, \quad \text{resp. } [\varepsilon] = [S][\sigma]; \quad (12.33)$$

$[\varepsilon]$  is the strain matrix (vector),  $[S]$  is square matrix of compliances, and  $[\sigma]$  is the stress matrix.

**Long-fiber composites** are **orthotropic**, and five constants are needed for the description of their elastic response: modulus of elasticity  $E_1$  in the fiber direction and  $E_2$  in the direction perpendicular to the fibers, shear modulus of elasticity  $G_{12}$ ,

and two Poisson's numbers,  $\mu_{12}$  a  $\mu_{21}$ . The first,  $\mu_{12}$ , is the principal Poisson's number, which expresses the ratio of relative shortening in direction 2 caused by relative elongation in direction 1. On the contrary,  $\mu_{21}$  gives the relative shortening in direction 1 caused by relative elongation in direction 2.

The relation between strain and stress for this composite is [7, 8]

$$\begin{Bmatrix} \varepsilon_1 \\ \varepsilon_2 \\ \gamma_{12} \end{Bmatrix} = \begin{bmatrix} 1/E_1 & -\mu_{21}/E_2 & 0 \\ -\mu_{12}/E_1 & 1/E_2 & 0 \\ 0 & 0 & 1/G_{12} \end{bmatrix} \begin{Bmatrix} \sigma_1 \\ \sigma_2 \\ \tau_{12} \end{Bmatrix}. \quad (12.34)$$

As the direction 2, perpendicular to the fibers, has usually much lower stiffness than direction 1, it is obvious that certain strain in direction 1 causes much larger strain in direction 2, than the same strain in direction 2 would cause in direction 1. Usually therefore  $\mu_{12} > \mu_{21}$ . In Equation (12.34) only four of the constants are independent ( $E_1$ ,  $E_2$ ,  $G_{12}$ ,  $\mu_{12}$  a  $\mu_{21}$ ), and the compliance matrix is symmetrical and it holds  $\mu_{21}/E_2 = \mu_{12}/E_1$ .

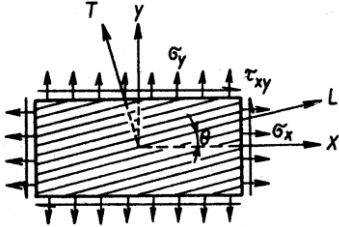
The individual elements in the compliance matrix characterise the relationships between stresses and strains in the individual directions. The zeros in Eq. (12.34) correspond to the case without any relations among normal and shear components. This is if the coordinate axes coincide with the principal directions of the material, which are here the direction of fibers and the perpendicular one. If they are oriented in other directions (Fig. 12.12), the compliance matrix is changed. If, for example, the tensile load contains some angle with the fibers, shear stresses appear also between the fibers, because the fibers would like to orientate themselves into the load direction. A bonding thus arises between the normal stress and shear strain – something which does not exist in isotropic materials.

The relationships for transformation of elastic constants into other directions can be found, for example, in [6].

## 12.7 Multilayer composites, laminates

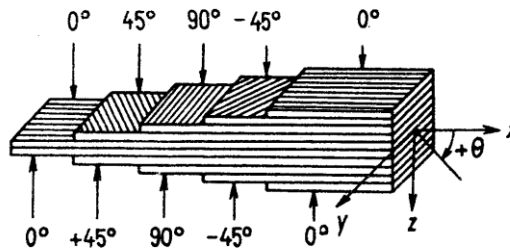
The formulae for the calculation of stiffness and strength of a composite with aligned fibers, given earlier, were valid for one layer, called **lamina** (Fig. 12.12). Suitable properties are often obtained by combining several layers, which are then denoted as laminate. Simple creation of multilayer composites is facilitated by the use of prepregs. A **prepreg** is a single layer, where uniaxially oriented fibers lay in

a matrix of partially polymerised resin. Several suitably oriented prepregs are then laid one on the other and pressed down at high temperature, so that final polymerisation occurs.



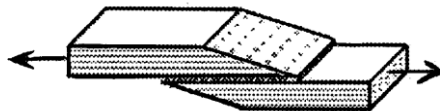
**Fig. 12.12.** Orthotropic lamina. Principal axes are inclined by angle  $\Theta$  to the coordinate system  $x - y$

Various orientations of the laminae exist. The simplest arrangement with mutually perpendicular fibers is denoted  $[0^\circ/90^\circ]$ . Lower degree of anisotropy is achieved if the fibers are laid in angles  $45^\circ$ , for example  $[0/45/90/-45/0]$ ; the numbers denote the orientation of the layers (Fig. 12.13). Also the angle  $60^\circ$  is used and other.



**Fig. 12.13.** Multiulayer laminate – layer arrangement  $[0/45/90/-45/0]$ .

A weak point of laminates are their edges, where high stress concentration arises at sudden change of properties at the transition from one layer to another. This sometimes leads to delamination, which is failure of layer bonding. Weak also are the places of joining of various components. Any sudden change of the cross section means higher stress. Better joints are those with smooth transition of shape (Fig. 12.14), and also with increased compliance, for example by using a resin with lower modulus of elasticity. For more, see for example [11].



**Fig. 12.14.** Reduction of stress concentration by suitable shape design.

## References to Chapter 12.

1. Bareš, R. A.: Kompozitní materiály. SNTL, Praha, 1988. 328 p.
2. Daďourek, K.: Kompozitní materiály – druhy a jejich užití. Technická univerzita v Liberci, Fakulta strojní, Liberec, 2007, 55 s. ISBN 978-80-7372-279-1.
3. Bodnárová, L.: Kompozitní materiály ve stavebnictví. VUT v Brně, Akademické nakladatelství CERM, Brno, 2002. 122 p. ISBN 80-214-2266-1.
4. Táborský, L., Šebo, P.: Konštrukčné materiály spevnené vláknami. ALFA Bratislava + SNTL Praha, 1982. 208 p.
5. Mráz, P., Talácko, J.: Konstrukce strojů s kompozitními materiály. Nakladatelství ČVUT, Praha, 2006. 226 p.
6. Agarwal, B. D., Broutman, L. J.: Analysis and Performance of Fiber Composites. John Wiley & Sons, 1980.
7. Roylance, D.: Mechanics of materials. John Wiley & Sons, Inc., 1996. 315 p. Available on Google via the book title.
8. Roylance, D.: Introduction to Elasticity. MIT, Cambridge, MA 02139, Dept. of Materials Sciences and Engineering. January, 21, 2000. Available on Google via the book title.
9. Daďourek, K.: Kompozitní materiály – modely a vlastnosti. Technická univerzita v Liberci, Fakulta strojní, Liberec, 2005, 113 s. ISBN 80-7083-972-4.
10. Laš, V.: Mechanika kompozitních materiálů. Západočeská univerzita, Fakulta aplikovaných věd, Plzeň, 2004. 156 s., ISBN 80-7043-273-X
11. Kokcharov, I.: Structural Integrity Analysis, Chapter 9: Composites. 29 p. Dostupné (3.12.2018) na: [http://www.kokch.kts.ru/me/t9/SIA\\_9\\_Composites.pdf](http://www.kokch.kts.ru/me/t9/SIA_9_Composites.pdf)
12. Kokcharov, I., Burov, A.: Structural Integrity Analysis. Amazon Digital Services LLC, 2013. 438 p.
13. Menčík, J.: Introduction to experimental analysis. University of Pardubice, Pardubice, 2017. 142 p. Available on Google via the book title, or via <http://hdl.handle.net/10195/66961>.

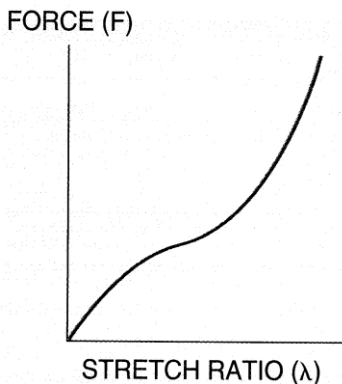
# 13. Mechanics of elastomers and very compliant bodies

This chapter will show some features typical for deforming of elastomeric materials, such as rubber and some polymers. Also deforming of textile materials and membranes will be mentioned briefly. All these cases are typical of large deformations and strains, nonlinear relationships between stress and strain, and often also the time dependence of response.

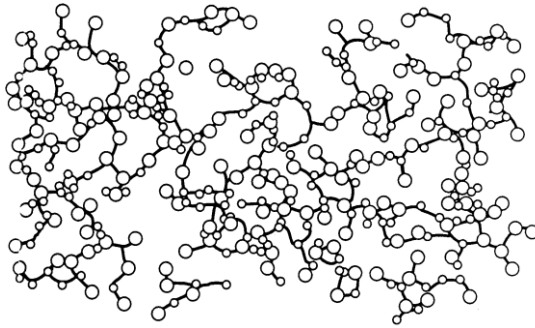
## 13.1 Elastomeric (hyperelastic) materials

Elastomeric, or hyperelastic materials have the following properties: low tensile modulus of elasticity ( $E = 1 - 10$  MPa) and nonlinear stress – strain diagram (Fig. 13.1), high coefficient of lateral contraction ( $\mu > 0,49$ ), large strain at fracture (sometimes up to several hundred percent), ability to absorb (temporarily) high amount of energy, viscoelastic behaviour (delayed elastic deforming, stress relaxation, energy dissipation at cyclical loading) and fatigue under static and dynamic loading.

The ability of large deformations of elastomeric materials is explained by their microstructure. It is three-dimensional network of very long meandering molecular chains, which resemble a tangle of spaghetti and are interconnected at many places by transverse bonds (Fig. 13.2). The bonds in the chains are relatively strong, but the transverse bonds are weak (like with spaghetti). The load thus causes straightening of the chains and their sliding rather than their stretching.



**Fig. 13.1.** Nonlinear diagram of rubber  
„Force  $F$  – Stretch ratio  $\lambda$ “ [1].



**Fig. 13.2.** Typical appearance of polymeric chains [1].

### Characterisation of large strains and stresses

Large strains arise at deforming rubber and other compliant materials. In such cases the conventional strain, defined as  $\varepsilon = \Delta l / l_0$ , is not sufficiently realistic. More suitable is the so-called **stretch ratio** (or, shortly, **stretch**):

$$\lambda = l/l_0 = (1 + \Delta l/l_0) = 1 + \varepsilon. \quad (13.1)$$

Remark. The stretch ratio is related to the true strain  $\varphi$  as

$$\varphi = \ln(l/l_0). \quad (13.2)$$

Here we shall use the stretch  $\lambda$  [1, 2]. It can be defined in three mutually perpendicular directions. The values in a particular case depend on the orientation of the coordinate system. The **principal stretches**  $\lambda_1, \lambda_2, \lambda_3$ , correspond to the three principal directions. Also certain functions of stretch ratios exist, which do not depend on the orientation of coordinate system. These so-called **stretch invariants** are:

$$I_1 = \lambda_1^2 + \lambda_2^2 + \lambda_3^2, \quad (13.3a)$$

$$I_2 = \lambda_1^2 \lambda_2^2 + \lambda_2^2 \lambda_3^2 + \lambda_3^2 \lambda_1^2, \quad (13.3b)$$

$$I_3 = \lambda_1^2 \lambda_2^2 \lambda_3^2. \quad (13.3c)$$

For incompressible material,  $I_3 = 1$ .

Since large relative elongation is related with large relative contraction, it is better to use **true stress**, defined as

$$\sigma_{\text{true}} = F / S_{\text{true}}, \quad (13.4)$$

instead of conventional stress  $\sigma = F/S_0$ , usual in the mechanics of solids. Similarly it is reasonable to replace the conventional stress-strain diagram  $\sigma - \varepsilon$  by the diagram  $\sigma_{\text{true}} - \lambda$ , or  $F - \lambda$  (Fig. 13.1).

One more quantity is also suitable for characterising the stress state. It is **strain energy density**  $A$ ; the pertinent formulae will be shown further. Among other properties it holds that stress can be obtained by differentiating the energy density with respect to strain.

### 13.2 Models for response of elastomeric materials

Hooke's law (and sometimes certain viscoelastic model) is sufficient for small strains. Other functions have been proposed for the load response of elastomeric (hyperelastic) materials at larger strains. They are usually based on the strain energy density defined by means of stretch invariants. Two simplest models will be shown here [1, 2]:

Neo-Hookean model:

$$A = C_{10}(I_1 - 3) , \quad (13.5)$$

where  $C_{10}$  is a constant. This model agrees well with experimental data for stretch up to 40% in uniaxial tension, and to 90% under simple shear.

Mooney-Rivlin model:

$$A = C_{10}(I_1 - 3) + C_{01}(I_2 - 3) . \quad (13.6)$$

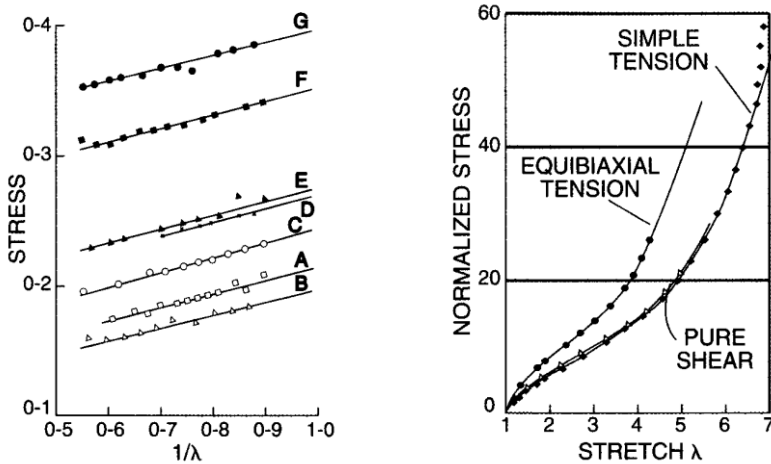
This model agrees well with tensile tests up to stretch 100%. However, it is not very suitable for the description of compression or stiffening under high stretches.

In addition to the above models also other exist (Ogden, Yeoh and other), which are described in [1, 2]. Some models were implemented into FEM programs.

The constants in the models are obtained by testing special specimens loaded by uniaxial tension, biaxial tension and shear (Fig.13.3).

Rubber and other elastomers are nearly incompressible. In analytical solution, perfect incompressibility is sometimes assumed, with the Poisson's ratio  $\mu = 0,5$ . If numerical solution is used, for example with the finite element method, a perfect





**Fig. 13.3.** Diagrams of tensile tests for the determination of Mooney – Rivlin constants of vulcanised rubber [1, 7].

incompressibility would cause numerical instability, and a little lower value of  $\mu$  is used instead, for example  $\mu = 0,49$ .

One theory of elastomer deforming is based on the **entropy** as a measure for arrangement and probability of attaining certain state. A straight polymeric chain is very improbable, while various unarranged states are much more probable. If one end of an imaginary segment of an elastomer is fixed, and the probability of the occurrence of its other end at certain distance from it is expressed, for example, by means of three-dimensional Gauss distribution, and if the increment of the internal energy in the second thermodynamic law is expressed, then a series of transformations [1, 2] gives the following formula for the strain energy density in an ideal elastomer, corresponding to stretch ratios  $\lambda_x, \lambda_y, \lambda_z$ :

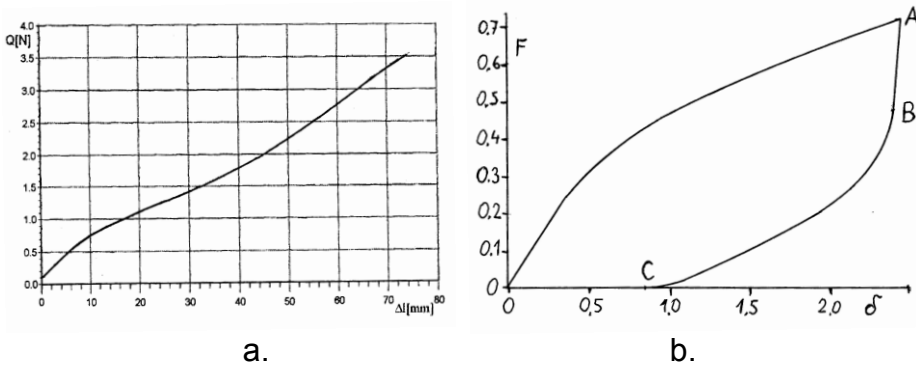
$$A = -T \Delta S = \frac{1}{2} NkT (\lambda_x^2 + \lambda_y^2 + \lambda_z^2 - 3) ; \quad (13.7)$$

$T$  is the absolute temperature,  $N$  is the number of chain segments per unit volume,  $k$  is the Boltzmann's constant ( $k = 1,38 \times 10^{-23}$  J/K), and  $\Delta S$  is the entropy change of one segment. The form of equation (13.7) is identical with Eq. (13.5) for the strain energy density of Neo-Hookean model.

### 13.3 Textile fibers and structures

The behaviour of fibers, threads and ropes and the structures made of them is influenced by their stiffness in tension and bending. In textile materials, certain role is also played by mutual arrangement and interlocking of threads, their mutual friction, and density per area unit of the textile material.

The mechanical properties of fibers and textile products are determined by tensile tests. Figure 13.4 shows a test diagram of yarn; Fig. 13.4b shows a diagram of a knitted fabric, in both cases in coordinates force – elongation. The diagrams can be approximated by suitable functions and rheological models, whose parameters characterise elastic and viscoelastic properties. Various viscoelastic models were described in Chapter 10.



**Fig. 13.4.** Test diagrams: a – tensile test of yarn, b – „load - unload“ cycle of a knitted fabric [3].

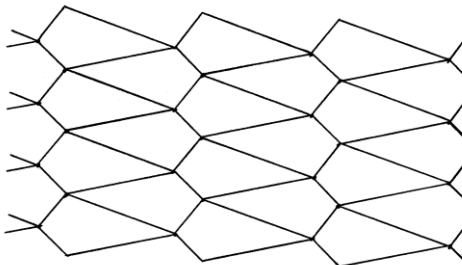
Hooke's law and moduli of elasticity for tension and shear are usually determined for onedimensional fabric. Bending properties are expressed by means of bending stiffness  $EJ$ , where  $E$  is the Young modulus of elasticity ( $\text{N/m}^2$ ) and  $J$  is the quadratic moment of the cross section in bending ( $\text{m}^4$ ). The dimension of bending stiffness is  $\text{Nm}^2$ . If it is determined from the deflection of a textile specimen by its own weight, the deflections are large. Similar situation exists in the use of textile materials. Instead of simple differential equation  $w'' = -M/EJ$ , suitable for small deflections of beams from relatively stiff materials, its original form must be used for large deflections [4]:

$$\frac{w''}{[1 + (w')^2]^{3/2}} = -\frac{M(x)}{EJ}. \quad (13.8)$$

For fibers and threads tensile strength  $P$  is measured. In fibers that are significantly bent, additional stress from bending acts, which causes breakage at lower load. Therefore also the strength of the loop,  $P_s$ , is measured so that a loop is created on one fiber, another fiber is pulled through it, and both fibers are broken using a dynamometer. Similarly, the knot strength  $P_u$  is measured. Both procedures are standardised. Besides them, also the relative loop strength  $P_{r,s}$  and relative knot strength  $P_{r,u}$  are measured, in both cases in percent:

$$P_{r,s} = \frac{P_r}{P} \times 100; \quad P_{r,u} = \frac{P_u}{P} \times 100 . \quad (13.9)$$

If the response of a fabric for technical application should be modelled, it is useful to replace it by a continuous thin body with the same mechanical properties. Figure 13.5 shows a part of a regular thread net. It is possible to create equations of equilibrium of forces in the knots, and, with the use of the force-deformation diagram, to find the deformations and stiffness of this configuration. Another approach is based on the deformation properties of a small specimen of the investigated fabric. If an equivalent homogeneous body should be modelled, it is necessary to account for the anisotropy. For further study it is possible to recommend the textbook [3] that also contains the transformation equations and the necessary tensor calculus and list of references.



**Fig. 13.5.** *Model of a knitted fabric [3].*

### 13.4 Membrane structures

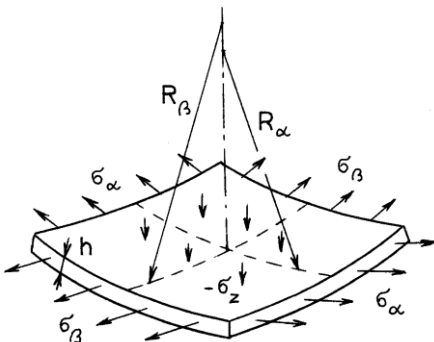
A membrane is such thin-walled body of curved surface, whose dimensions in two directions are much larger than its thickness, and which is able to transfer only the forces acting in the directions tangential to the surface. A membrane has negligible bending stiffness, so that it is unable to transfer bending moments. An example is an inflated hall or a balloon.

Remark. Membrane stress is distributed uniformly across the wall thickness, so that it fully utilises the material ability to transfer forces. In this way it is possible to cut down the material consumption, so that various containers or tanks (from metals, for example) have such shape that membrane stresses will prevail in them [4 – 6]. If the structure also has nonnegligible bending stiffness, so that besides membrane stresses also bending stresses act in the wall, bending theory of shells must be used in the analysis; see [4 – 6].

A membrane structure is often loaded by pressure of liquid or gaseous medium. This pressure  $p$  causes forces in the membrane in two mutually perpendicular directions, which are tangent to the investigated surface at the pertinent point. If the equation of equilibrium of forces acting on an infinitesimal element of the membrane is written for the direction perpendicular to the tangent plane (Fig. 13.6), so-called Laplace equation of membrane can be obtained[5, 6]:

$$p = \frac{N_{1\alpha}}{R_\alpha} + \frac{N_{1\beta}}{R_\beta} . \quad (13.10)$$

$N_{1\alpha}$  or  $N_{1\beta}$  is the force in the direction  $\alpha$  or  $\beta$  per unit of width of the membrane (dimension N/m) and  $R_\alpha$  and  $R_\beta$  are radii of curvature of the membrane in the pertinent directions.  $\alpha, \beta$  are two (any) mutually perpendicular directions. The radii  $R_\alpha, R_\beta$  can vary depending on the orientation of these cuts. Two **principal directions** exist, for which these radii are extreme (one is minimum, the other maximum); they are then denoted  $R_1, R_2$ . Division of the forces  $N_{1\alpha}, N_{1\beta}$  by the membrane thickness gives the normal membrane stresses.



*Fig. 13.6. A membrane - geometry and stresses.*

Remark. Laplace equation (13.10) holds also for liquids. In this case the forces  $N_{1\alpha}$ ,  $N_{1\beta}$  must be replaced by surface stress  $\gamma$ , with the same value in all tangential directions. This equation is decisive, for example, for the shape of water drops, or even for small glass beads rounded at high temperatures in an oven.

### References to Chapter 13.

1. MARC. Nonlinear Finite Element Analysis of Elastomers. MARC Analysis Research Corporation. Palo Alto, CA, 1996. 48 p.
2. Roylance, D.: Mechanics of materials. John Wiley & Sons, Inc., 1996. 315 p. Available via web after inserting the title into Google.
3. Stříž, B.: Mechanika textilií. Část 2. Aplikace mechaniky kontinua. Technická univerzita v Liberci, Fakulta textilní. Liberec, 2003. 83 p.
4. Höschl, C.: Pružnost a pevnost ve strojnictví. SNTL, Praha, 1971. 375 p.
5. Timoshenko, S. P.: Strength of materials, Part II. D. van Nostrand Company, inc., Princeton, New Jersey, 1956.
6. Placák, V., Kunc, J.: Výpočet napjatosti skořepin. SNTL, Praha, 1966.
7. Ogden, R. W.: Large deformation isotropic elasticity: On the correlation of theory and experiment for incompressible rubberlike solids. Proc. Roy. Soc. A, 326, 1972. pp. 565 – 584.

## 14. Optimisation of shape and dimensions of components and constructions

Components and constructions must be safe and reliable. Their manufacture or building should also be economical. In this chapter several approaches and rules will be shown for improvement thanks to shape optimisation.

### 14.1 Components and structures of constant stress

In the classic approach to dimensioning the stress in the most stressed section is calculated and compared with the allowable value. The stresses in other places are usually lower, and the ability of material to transfer forces and stresses is not fully utilised there and the design is less economical. In **constant stress constructions** one strives that the stress everywhere equals the allowable value. This approach will be illustrated here on several problems. For easier understanding, simple shapes will be considered, whose solution leads to simple analytical expressions.

#### Dimensioning and optimisation of cross section along a beam

Figure 14.1 shows a beam with one end fixed and the other loaded by a transverse force  $F$ . The geometry and distribution of bending moment along the length are shown. The maximum moment acts at the fixed end. If the cross section is constant, it must be so large that the stress here does not exceed the allowable value

$$\sigma_{\max} = F l / W \leq \sigma_{\text{dov}}; \quad (14.1)$$

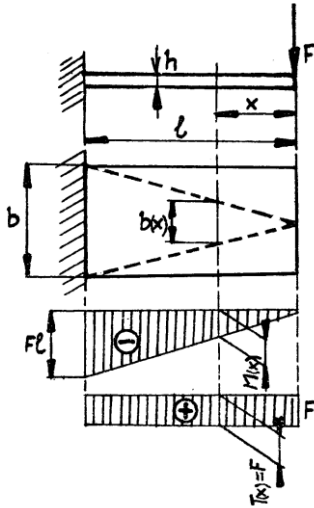
$W$  is the section modulus in bending. The maximum stress at distance  $x$  is

$$\sigma_{\max}(x) = M(x) / W = F x / W. \quad (14.2)$$

With the exception of the place of fixing the stresses are lower everywhere. Such design is less economical. Maximal utilisation of the material is achieved in the **components of constant stress**. Their cross section is not constant, but varies along the length so that the stress everywhere equals the allowable stress. The section modulus is determined according to the general formula

$$W(x) \geq M(x) / \sigma_{\text{dov}}. \quad (14.3)$$

The symbol „higher or equal“ is used because due to various constraints it can be



*Fig. 14.1. Constant stress beam (dashed lines). Geometry and distribution of bending moment and transverse force.*

impossible to use everywhere the accurate value of the section modulus as obtained by the calculation. For example, bending moment acting in a beam loaded at the end by force  $F$  is

$$M(x) = F x \quad , \quad (14.4)$$

The section modulus of a constant stress beam should therefore vary as:

$$W(x) \geq F x / \sigma_{dov} \quad , \quad (14.5)$$

The dimensions of cross section can vary in various ways, depending on its shape. If the beam has rectangular cross section  $b \times h$ , where  $b$  is the width and  $h$  is the height in the direction of loading, the section modulus is  $W = bh^2/6$ .

The simplest case is with constant thickness and variable width. With constant width and prescribed thickness  $h$  the necessary width would be

$$b_0 = \frac{6Pl}{\sigma_{dov} h^2} \quad . \quad (14.6)$$

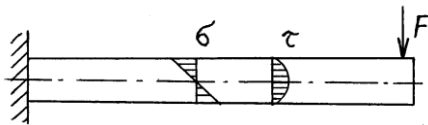
The width  $b(x)$ , optimised for constant bending stress, is in the ideal case

$$b(x) = \frac{6Fx}{\sigma_{dov} h^2} \quad . \quad (14.7)$$

The width thus increases with the distance from the loaded end linearly; from above it looks as a triangle (dashed oblique lines in figure 14.1). We can see that

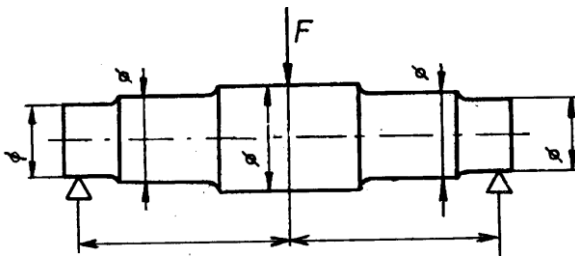
the same service as by the beam of constant cross section can be given by the beam of constant stresses at half of its weight!

The situation is, however, more complicated. In addition to the bending stresses also shear stresses act in the beam loaded by transverse force, and these stresses have the same value along the whole length, also near the point of the load application, where the bending moment is very low. The cross section here had to be dimensioned also with respect to the shear stresses. A more appropriate criterion would be constant equivalent stress, considering simultaneous action of normal and shear stresses. One should also consider that bending stress is maximal on the surface, while the maximum shear stress acts on the neutral axis (Fig. 14.2). Moreover, stiffness of the tapered beam is lower than with the beam of constant width  $b$ , so that the deformations would be larger. Sometimes, the decisive criterion for dimensioning is the allowable maximum deformation rather than maximum stress. Also the actual situation at the place of force application had to be solved in detail. The actual optimum shape will therefore be more complex.



**Fig. 14.2.** Distribution of bending ( $\sigma$ ) and shear ( $\tau$ ) stress.

Instead of width, the height could be variable. Similar optimisation could be done for a shaft supported by two bearings (Fig. 14.3), bogie of an opened freight wagon or the shape of main beams of a bridge. The formulae for continuous optimisation along the component can be more complex, but the way of derivation is the same. With respect to the necessity of fulfilling several demands simultaneously (and not only from the strength point of view) continuous optimisation is often not possible, similarly to the shaft shown in Fig. 14.3. Sometimes components with standardised (graded) dimensions are used, as it is cheaper. Generally, however, the section modulus at any place must fulfil Equation (14.3).



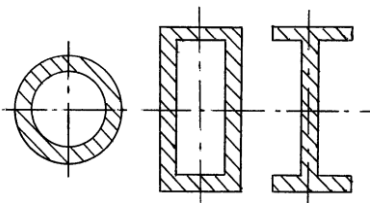
**Fig. 14.3.** A massive shaft.



Remark. A danger is hidden in constructions of constant stress. In a common construction only several places exist, where the stress (and thus the danger of failure initiation) is the highest. The stress in a component of constant stress has the same value everywhere, so that the failure could start anywhere. The check for fatigue cracks must therefore be done in detail over the whole surface.

### Dimensioning and optimisation of size and shape of cross section of a beam

Until now, we talked about the optimisation of the beam cross section „along the length“. Also the shape of the cross section can be optimised. The bending stress is distributed across the height so that the highest values are at places most distant from the neutral axis; on this axis it equals zero (Fig. 14.2). Therefore effort exists that only little amount of material is used at the neutral axis, because here it nearly does not contribute to the transfer of bending moment, and, on the contrary, most material should be at larger distances from the neutral axis. Examples are hollow profiles or I-profiles (Fig. 14.4). However, limitations exist. If, for example, the dimensions of simple solid rectangular cross section should be optimised so that its section modulus is largest at the lowest weight (or area), the solution would be the cross section with the largest height possible and thickness approaching to zero. However, such beam would lose its stability and collapse at the lowest load. Therefore, beams for carrying transverse loads (in the web direction) have usually profile I, where the transverse stiffness of both flanges prevents easy buckling. Similarly the tubes for carrying transverse load cannot have very thin wall, despite the theoretical advantage of the largest diameter together with the thinnest wall. Here again the danger would exist of loss of stability by local buckling.



*Fig. 14.4. Weight efficient profiles.*

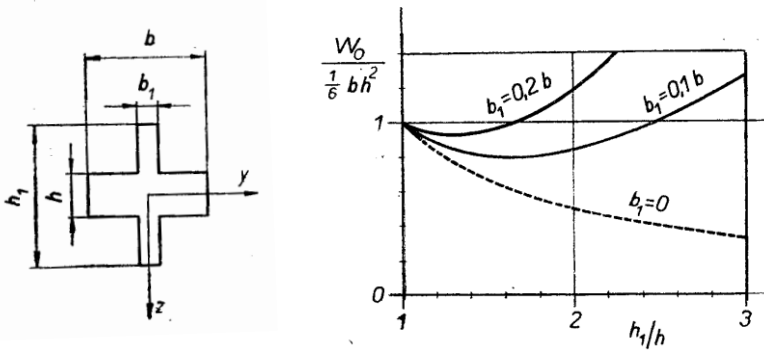
The load carrying capacity of a component can be increased by adding stiffening ribs. Caution is necessary also here. Addition of material at an unsuitable place and in unsuitable amount can – on the contrary – increase the stress and reduce the safety. This can be illustrated on an example of a beam with rectangular cross

section, which is stiffened by a rib according to Fig. 14.5. The moment of inertia and section modulus in bending around the horizontal axis are [1]:

$$J_o = \frac{1}{12}(b-b_1)h^3 + \frac{1}{12}b_1h_1^3, \quad (14.8)$$

$$W_o = \frac{J_o}{h_1/2} = \frac{1}{6h_1} \left[ (b-b_1)h^3 + b_1h_1^3 \right]. \quad (14.9)$$

For a beam without a rib,  $h_1 = h$  and  $W_o = bh^2/6$ . The ratio of section moduli in bending of a beam with a rib and without it is depicted for various ratios of rib height and thickness in Fig. 14.5 at right. We can see that the resultant section modulus for small rib thicknesses and heights can be even smaller than for the unstiffened beam. Despite of addition of material, the section modulus became smaller! On the other hand, the bending stiffness, characterised by the moment of inertia, is increased by any rib.



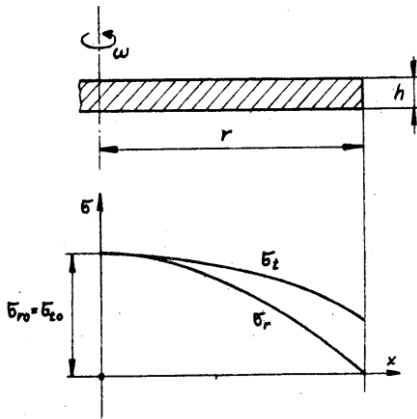
**Fig. 14.5.** Influence of the rib geometry on the stiffening [1].

### Optimisation of cross section of a rotating part

Another case showing the possibility of analytical finding the cross section of a component with constant stress is a thin rotating disc (Fig. 14.6). In this disc, circumferential stress ( $\sigma_t$ ) and radial stress ( $\sigma_r$ ) act. If the disc has constant thickness, the stresses are as follows [1, 2]:

$$\sigma_t(r) = \rho \omega^2 \left( \frac{3+\mu}{8} R^2 - \frac{1+3\mu}{8} r^2 \right), \quad (14.10)$$

$$\sigma_r(r) = \frac{3+\mu}{8} \rho \omega^2 (R^2 - r^2), \quad (14.11)$$



**Fig. 14.6.** Rotating disc.  $\sigma_r$  – radial stress,  $\sigma_t$  – circumferential stress,  $\sigma_{r0}$ ,  $\sigma_{t0}$  – stresses at the axis

where  $\rho$  is the density and  $\mu$  Poisson's number of the disc material,  $\omega = 2\pi f$  is the angular velocity,  $f = n/60$  is the frequency and  $n$  is the number of revolutions per minute,  $R$  is the outer radius of the disc, and  $r$  is the radius of the investigated point. The distribution of stresses is depicted in Fig. 14.6. The highest values are at the disc axis, where

$$\sigma_r(0) = \sigma_t(0) = \frac{3+\mu}{8} \rho \omega^2 R^2 . \quad (14.12)$$

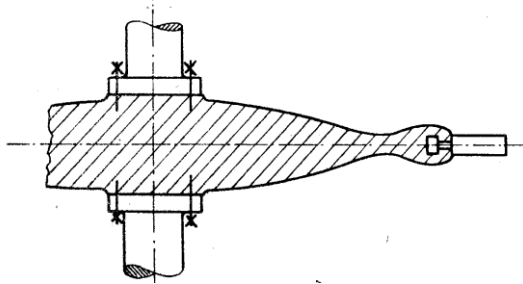
Both stresses decrease with increasing radius; radial stress to zero if the outer circumference is not loaded.

Remark. Note that the stresses in a thin disc do not depend on its thickness! No stress acts in axial direction, because the surfaces are free and nothing obstructs to the thickness changes. In a long rotating cylinder (for example a turbine with an array of blades) axial stress appears also, because radial and circumferential stresses vary with  $r$ , but the changes of length in axial direction, caused by transversal contraction, must be the same everywhere.

It is obvious from Figure 14.6 that the stresses at all places of a thin disk – with the exception of the axis – are lower. The load carrying capacity of the material is thus not fully utilised. The material will be used better if the disc thickness will decrease with increasing radius so that the equivalent stress everywhere will equal the allowable stress  $\sigma_{allow}$ . The problem „rotating disc of constant stresses“ is solved in basic textbooks of the mechanics of materials [1, 2], so that here only the resultant formula for the varying thickness will be given:

$$t(r) = t_0 \exp\left(-\frac{\rho \omega^2}{2\sigma_{allow}} r^2\right) ; \quad (14.13)$$

The distribution of thickness, shown in Fig. 14.7, resembles normal (Gauss') distribution of probability.  $t_0$  is the maximum disc thickness at the axis, which must



**Fig. 14.7.** Disc of constant stresses: one-stage turbine disc with blades [2].

be determined from the thickness at the transition to the ring with the blades. For this place, of radius  $r_{kB}$ , the centrifugal force  $F_\omega$ , caused by one blade of the known mass and position  $r_{lB}$  of its centre of gravity, is known, as well as the blade spacing  $L_B$ . The necessary thickness can be obtained from the condition that the maximum equivalent stress according to the Tresca's hypothesis must not exceed the yield strength  $\sigma_Y$ . As the axial stress in a thin disc equals zero, the equivalent stress has the same value as the radial or circumferential stress, given by expressions (14.12). The use of condition  $\sigma_{all} \leq \sigma_{Tresca}$ , or  $\sigma_{all} = \sigma_Y/s$  gives the disc thickness at the transition into the ring:

$$t_{VB} = \frac{F_\omega}{L_B \sigma_{all}} \quad (14.14)$$

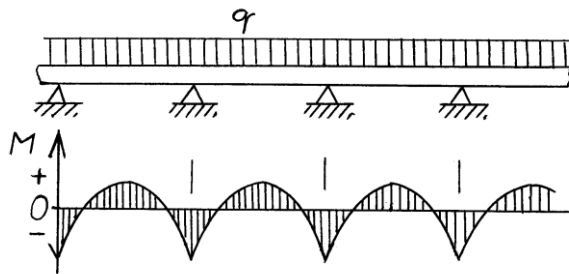
The thicknesses at other places are derived from it.

**Remark.** This problem was shown here in order to show the possibility of analytical solution. Today, similar components are solved by the finite element method, which respects better the disc connection with the shaft and the attachment of blades.

## 14.2 Optimisation of large structures

In design of large structures, for example in civil engineering, the knowledge of general distribution of internal forces is very important. Figure 14.8 shows a long bridge on several supports. It shows the distribution of transverse forces and bending moments caused by the continuously distributed load. We can see that the

bending moment is zero at small distance from every support. If the structure will be created by joining of several parts, it is suitable to put the joints just into the points with zero bending moment, because only transverse forces will be transferred here, but no bending moments. Similar approach is used for horizontal beams in steel frames of skyscrapers or in supporting the wide overhanging roofs above railway platforms, and elsewhere.



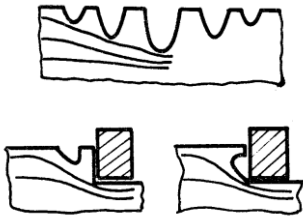
*Fig. 14.8. A long bridge as a beam on many supports, and the distribution of bending moment. This moment equals zero at small distances from every support.*

Remark. In design of large structures and buildings, all loads that could appear must be considered. The accurate methods of stress analysis would be of little use, if some loads would be forgotten. Omission of some loading states could be fatal. For example, at the beginning of twentieth century in Canada a bridge across the Saint Lawrence River in Québec collapsed during the assembly, as the designer has not realised that the forces in the unfinished bridge act in a different way than under traffic load. During the erection, some truss girders were loaded by compression instead of tension, and collapsed by buckling [21]. The collapse killed 75 people! More similar examples could be found.

### 14.3 Optimisation for complicated shapes and loads

If a complicated shape should be optimised, more sophisticated methods are used. The weakest places of any component are the regions with stress concentration, such as sudden change of shape or cross section, around a hole, or at notches. It holds generally that the stress increase at a notch is higher for deeper notches (or for larger change of the thickness or shaft diameter) and for smaller radius of curvature of the notch root or the transition (Fig. 6.3). In design we should strive for the smooth flow of forces in the component. Sometimes additional notches for

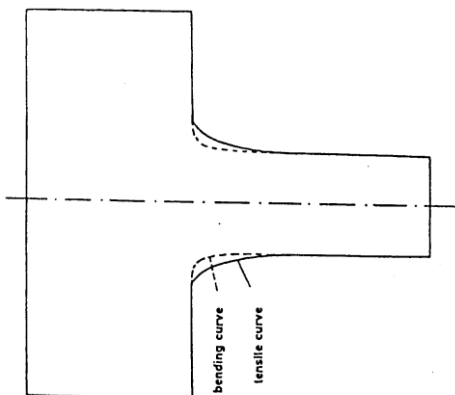
stress relieving are made at the principal notch (Fig. 14.9). Even the shape of the pertinent notch is important, and a small shape change can mean a big improvement. In design of notches with the aim of the lowest stress concentration one can learn from Nature. Only those living organisms can survive as a kind if they have sufficient strength for resisting the loads appearing most often, and – at minimum possible weight. As an example, branching of trees can be mentioned.



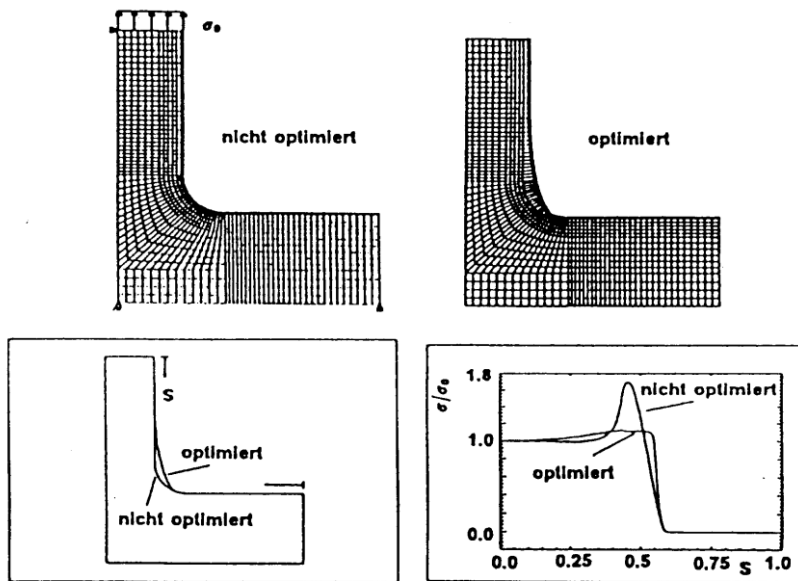
**Fig. 14.9.** Examples of stress relieving notches (force lines are indicated) [2].

If the stress concentration at the point of branch joining would be too high, all branches would break even under low forces, and the tree would die. This does not happen in the reality, and it has been found that the shape of the joints is such that nearly no concentration of stresses appears there. The tree itself promotes the growth of wood at the critical places.

Similar shape of transitions can be found at thorns of various bush, or even at deer antlers. In 1937 R. Baud has published a work based on his experiments with celluloid, where he showed that even a small change of shape can bring a substantial improvement [3]. The optimal shape without stress concentration is sometimes called Baud curve (Fig. 14.10). Figure 14.11 shows comparison of the situation at common branching and after optimisation by the finite element method.

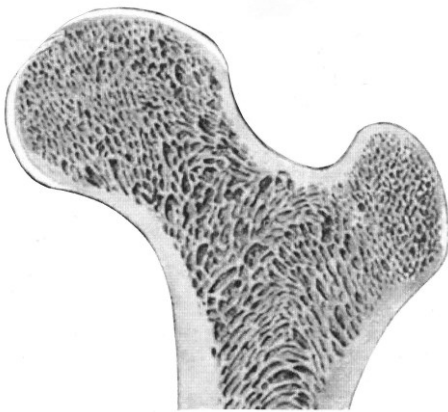


**Fig.14.10.** Baud curves for tension and bending. After [3].



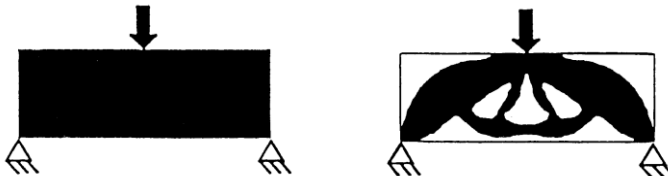
**Fig. 14.11.** Shape optimisation of branching by gradual adding of material. Down left: unoptimised and optimised; down right: comparison of stresses [8, 9].

During long evolution, Nature has developed mechanisms for shape optimisation of various natural species that must resist to various kinds of load. This was studied by Professor Mattheck from Karlsruhe, who has developed two optimisation procedures based on those used by Nature [4 – 7]. The method of adaptive growth gradually adds material at places of higher stress, similarly to trees. First, the stress is determined (by FEM) in the component that should be optimised. At places of higher stress the thicknesses of elements in the surface layer are increased, similarly to the growth of the soft cambium layer beneath the bark of a tree. This finite element calculation is repeated. After several steps, the stress distribution is achieved with significantly lower stress concentrations. For more, see [4 – 8]. The other method uses gradual material removing from the unloaded places („dying away“). Similar arrangement can be seen in spongiosis in a femur (Fig. 14.12), whose structure is such as to maximally use the material according the rule of constant stress. (Let us remind the loss of calcium in the bones during long stay of astronauts in weightless environment. Here the Nature removes in its own way the material that is not loaded.) In the stepwise optimisation via the finite element analysis, the modulus of elasticity of the elements with the lowest stress is reduced



**Fig. 14.12.** Section of the femur with spongiosis.

for the next series of FEM computations. This procedure is repeated several times, and then the elements are removed at places where the stress has substantially dropped. This optimisation algorithm was denoted as Soft Kill Option (SKO) in [9]. Figure 14.13 shows a beam on two supports, loaded in the centre by a point force, which was optimised by this method [8, 9]. In this case, the process started with a solid semi-product of rectangular shape, and the material was gradually removed from the places that were loaded only little. The danger of buckling of compressed parts was also considered. The optimisation in Nature looks similarly.



**Fig. 14.13.** The initial and final shape of a component loaded by transverse force. Optimisation by the SKO method for obtaining minimum weight [8, 9].

#### Further optimisation methods

There are many optimisation methods based on mathematics. The basic idea is to find an extreme of an objective function (stress magnitude in a component, weight, costs...), which depends on several variables and limitations. Simpler practical methods are described in Chapters 11 – 14 of the book [11] and in Chapter 19 in [16]. Both books are available without any limitations on the web; it is sufficient to



write the pertinent title into Google. Optimisation is treated in detail in books [12 – 15]; the last named is also accessible via web. Tools in Matlab (Optimization Toolbox) or Mathcad are also very suitable, with explanatory notes. Some optimisation problems can be solved by Excel. This universal tool contains (in the menu Data) so-called Solver, which has its own optimisation procedure and enables also the use of various constraints of the individual variables.

#### 14.4 Setting the necessary tolerances

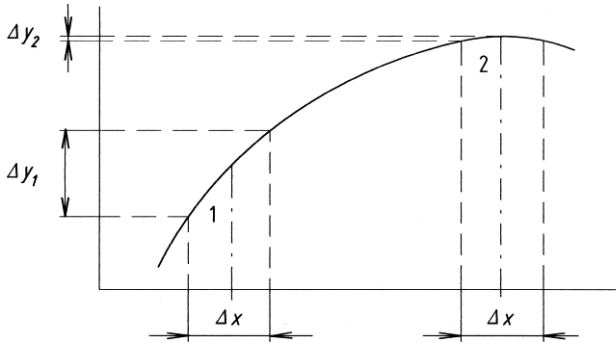
In design of a component, machine, structure or appliance, one must account for various uncertainties that can appear in the design, manufacture or erection, and during operation. A good structural design should always consist of three stages:

1. concept proposal,
2. determination of parameters,
3. determination of tolerances.

After the general concept of the object or a component (e.g. combustion engine with three cylinders and four valves in a cylinder, helical spring, etc.) has been laid down, all necessary dimensions must be determined (cylinder bore and stroke, diameters of the spring and the wire, number of turns...). However, the input quantities often vary, or can have values differing from those assumed in design. A good design must ensure that the output values will always be within the allowable limits. This can be achieved by suitable choice of nominal values of the input quantities and by prescribing their tolerances.

The nominal values of input quantities form together the **design point**. Its position should ensure low sensitivity of the output parameters to the deviations of input quantities from their nominal values [16]. This is called **robust design**. Figure 14.14 illustrates this principle on an example with one input quantity  $x$ . Operating point 1 is with high sensitivity, point 2 with low sensitivity.

One can see that the change of output quantity around the point 2 corresponding to certain change of  $x$  is much smaller than around point 1 – in both cases for the same change of  $x$ . This means that acceptable variation of the output can sometimes be achieved with lower demands on the accuracy of input variables! Reliability thus depends not only on the variance of input quantities, but also on the position of work point. Various methods exist for its finding; see e.g. 17 – 19].

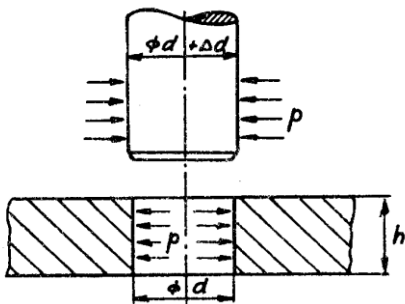


**Fig. 14.14.** Robust design. The figure shows the influence of the position of design point (1, 2) on the sensitivity of the output quantity.

As soon as the design point (i.e. the principal dimensions and parameters) was found, it is necessary to determine the sensitivity of the output on their variations. The results are then used for finding the tolerances. See, for example [16].

Importance of the determination of the possible deviations and the corresponding tolerances will be illustrated on two examples.

**Example 1.** A steel wheel should be joined strongly with a steel shaft so that it can transmit a torque. The joining will be achieved by shrink-fitting; the shaft of a somewhat larger diameter will be pushed into the smaller hole in the wheel (Fig. 14.15). Determine the necessary overlap, i.e. how much the shaft diameter should be larger than that of the hole! Determine also the maximum equivalent stress in the surface layer of the hole, and compare it with the yield strength! Determine the force needed for pressing the shaft into the wheel. Determine also the reduction of the pressure at the interface if the actual diameter of the hole were smaller by 0,01 mm than the demanded value, and how all stresses would increase if the wheel diameter is smaller by 0,01 mm.



**Fig. 14.15.** Shrink-fitted joint.

The parameters of the joint are: Outer diameter of the wheel  $D = 2b = 200$  mm, nominal diameter of the shaft, the same as that of the hole in the wheel, is  $d = 2a = 30$  mm. Wheel thickness  $h = 20$  mm. Transmitted torque  $M = 200$  Nm. Coefficient of friction between the wheel and shaft  $f = 0,1$ .  $E_1 = E_2 = 210000$  MPa,  $\mu_1 = \mu_2 = 0,3$ . Yield strength  $\sigma_Y = 400$  MPa.

Solution. The hole in the wheel becomes larger during the assembly, and the shaft diameter becomes smaller. Pressure acts between them, and thanks to friction the twisting moment  $M$  can be transferred. The necessary pressure  $p$  is [1]

$$p = \frac{2M}{\pi d^2 h f} \cdot \quad (14.15)$$

The corresponding shrinkage (the difference of the hole and shaft diameters) is

$$\Delta d = d p \left[ \frac{1}{E_1} \left( \frac{D^2 + d^2}{D^2 - d^2} + \mu_1 \right) + \frac{1}{E_2} (1 - \mu_2) \right] \cdot \quad (14.16)$$

The demanded shrinkage is of the order  $10^{-2}$  mm, i.e. negligible compared to the nominal diameter. Nominal value of  $d$  can therefore be used in Eq. (14.16).

Inserting the input values into both equations gives the necessary pressure  $p = 70,74$  MPa, and the corresponding overlap  $\Delta d = 0,02068$  mm.

The equivalent Tresca's stress in the thin layer in the surface of the wheel opening is

$$\sigma_{\text{eq}}(a) = \sigma_t(a) - \sigma_r(a) = 2(A - \sigma_r), \quad (14.17)$$

where  $\sigma_r = -p$ , and

$$A = p_a \frac{a^2}{b^2 - a^2} \cdot \quad (14.18)$$

Inserting  $p = 70,74$  MPa,  $a = 15$  mm and  $b = 100$  mm gives  $A = 1,6283$  MPa and  $\sigma_{\text{eq}} = 144,74$  MPa. Safety to attaining the yield strength is

$$k_Y = \sigma_Y / \sigma_{\text{eq}} = 400 / 144,74 = 2,76.$$

The force needed for the pressing the shaft into the wheel is

$$F = \pi d h f p = \pi \times 30 \times 20 \times 0,1 \times 70,74 = 13334 \text{ N}.$$

The press should have a sufficient force reserve to this value (see later).

Joining can also be achieved without a press, if the wheel is heated so that its diameter becomes sufficiently larger, and the shaft is inserted into the hole. The joining becomes strong during cooling. The expression for the enlargement of the opening diameter,  $\Delta d = d\alpha\Delta T$ , gives the necessary temperature increase:

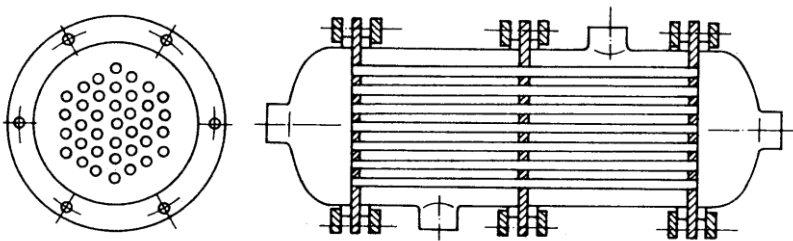
$$\Delta T = \Delta d / (d\alpha) = 0,02068 / (30 \times 12 \times 10^{-6}) = 57,44 \text{ K.}$$

Heating more than the calculated  $\Delta T$  would be used, because between the heating and joining of both parts some time would elapse, and the wheel becomes cooler.

If the actual diameter of the hole were larger (due to manufacture inaccuracy) by 0,01 mm, the overlap would be smaller, equal  $\Delta d' = 0,01068$  mm. This is 51,6  $\approx$  52% from the demanded overlap value 0,02068 mm. The pressure at the interface thus drops to 52 % (that is by 48%), and similarly also the torque that could be transferred by the joint. The corresponding tolerances of the shaft and hole diameter must be determined with respect to the minimum transferred moment demanded. They will be in  $\mu\text{m}$ . Vice versa, if the overlap were by 0,01 mm larger, the joint can transmit by 48% higher moment, but the stress in the shaft will be nearer to the yield strength. The equivalent stress will be 214,7 MPa, and the safety to the yield strength will be  $k_\gamma = 1.86$ .

Further example from [20] shows that it is important to consider all possible deviations from the ideal shape and nominal dimensions.

**Example 2.** It is necessary to check the stresses in glass tubes of a heat exchanger according to Fig. 14.16. The tubes from Simax<sup>®</sup> glass have the inner diameter  $d = 14$  mm, wall thickness  $h = 1$  mm and length  $l = 2$  m. Their ends are in tube plates allowing axial dilatations, and the centre passes through the perforated partition. Water of temperature  $T_{m,1} = 95$  °C and pressure 0,1 MPa flows through the tubes,



**Fig. 14.16.** Glass heat-exchanger [20].

and the temperature of the water outside is  $T_{m,2} = 15 \text{ }^\circ\text{C}$ . The heat transfer coefficient for the inner surface of the tube is  $\kappa_1 = 2000 \text{ Wm}^{-2}\text{K}^{-1}$ , and for the outer is  $\kappa_2 = 600 \text{ Wm}^{-2}\text{K}^{-1}$ . The work regime is stationary, with constant temperatures.

Solution. The stresses in the tubes are caused by 1) internal overpressure, and 2) difference of temperatures of the inner and outer surface. Besides them, stresses can arise due to inaccuracies in shape and dimensions of the tubes. Especially tensile stresses are dangerous for glass. Here, we shall look at their components.

### 1. Stresses due to overpressure

The internal overpressure  $p$  causes hoop stress in the tube

$$\sigma_{p,t} = p \frac{d}{2h}, \quad (14.19)$$

which is distributed uniformly across the wall thickness. With the used arrangement of the exchanger the pressure will cause no axial stresses. Inserting  $p = 0,1 \text{ MPa}$ ,  $d = 14 \text{ mm}$ , and  $h = 1 \text{ mm}$  into (14.19) gives  $\sigma_{p,t} = 0,70 \text{ MPa}$ .

### 2. Thermal stresses

As the tubes have thin walls, the situation will be similar to heat transfer across the planar wall, with approximately linear distribution of temperatures and stresses. The thermal stresses will act in circumferential and axial direction, with the same magnitude in both directions. The maximum tensile stresses will act on the outer surface, and its magnitude will be [20]

$$\sigma_{T,a} = \sigma_{T,t} = \frac{E\alpha(T_{m,1} - T_{m,2})}{2(1 - \mu)} \frac{h/\lambda}{1/\kappa_1 + h/\lambda + 1/\kappa_2}. \quad (14.20)$$

With the constants for Simax glass ( $E = 63\,000 \text{ MPa}$ ,  $\mu = 0,18$ ,  $\lambda = 1,16 \text{ Wm}^{-1}\text{K}^{-1}$ ,  $\alpha = 3,2 \times 10^{-6} \text{ K}^{-1}$ ), wall thickness  $h = 1,0 \text{ mm}$  and heat transfer coefficients  $\kappa_1 = 2000 \text{ Wm}^{-2}\text{K}^{-1}$  and  $\kappa_2 = 600 \text{ Wm}^{-2}\text{K}^{-1}$ , one obtains  $\sigma_{T,a} = \sigma_{T,t} = 2,80 \text{ MPa}$ .

The resultant maximum tensile stress will act (in this ideal case) on the external surface in the circumferential direction, and will have the magnitude

$$\sigma_{\max} = \sigma_{p,t} + \sigma_{T,t} = 2,80 + 0,70 = 3,50 \text{ MPa}.$$

In a real exchanger always additional stresses appear:

### 3. Stresses caused by the inaccuracy of shape and dimensions of the tubes

In the analysed case the following deviations of shape and dimensions appear:

- a) variations of the tube diameter ( $\pm 0,5$  mm),
- b) variations of the wall thickness ( $\pm 0,2$  mm),
- c) ovality of the cross section ( $\pm 0,5$  mm),
- d) longitudinal deflection of the tube (2 mm per 1 meter of length).

The influence of the individual deviations will be shown further.

a) *Variations of the tube diameter*

Thermal stresses do not depend on the tube diameter, but the stresses caused by the pressure difference depend. If the internal diameter  $d$  increases from 14,0 to 14,5 mm, the circumferential stress (14.19) increases to  $\sigma_{p,t} = 0,725$  MPa.

b) *Influence of the variations of the wall thickness*

The wall thickness influences both kinds of stress. The stresses due to internal overpressure decrease with increasing wall thickness, while the thermal stresses increase, as the thermal resistance of the wall and the difference of surface temperatures grow. The increase of the wall thickness by 0,2 mm to 1,2 mm changes the individual stresses according to Eqs. (14.19) and (14.20) as follows:

$$\begin{aligned}\sigma_{T,a} &= \sigma_{T,t} (h = 1,2 \text{ mm}) = 3,18 \text{ MPa,} \\ \sigma_{p,t} (h = 1,2 \text{ mm}) &= 0,58 \text{ MPa.}\end{aligned}$$

With the wall thickness drop to 0,8 mm they will be

$$\begin{aligned}\sigma_{T,a} &= \sigma_{T,t} (h = 0,8 \text{ mm}) = 2,37 \text{ MPa,} \\ \sigma_{p,t} (h = 0,8 \text{ mm}) &= 0,88 \text{ MPa.}\end{aligned}$$

In this case the increase of thickness is more dangerous; the situation under other thermal and pressure conditions can be different.

c) *Influence of the ovality of cross section*

The deviation of the cross section from perfectly circular shape will have no influence on thermal stresses, but it can significantly influence the stresses caused by the internal pressure. In oval cross section (Fig. 14.17) also bending stresses appear, because the cross section of the tube tries to attain circular shape. The maximum tensile stress caused by this bending will act in circumferential direction on the outer surface at the shorter semiaxis and also on the inner surface of the larger axis. According to [20] this stress is approximately equal

$$\sigma_{e,t} = p \frac{d}{2h} \frac{3e}{h} , \quad (14.21)$$

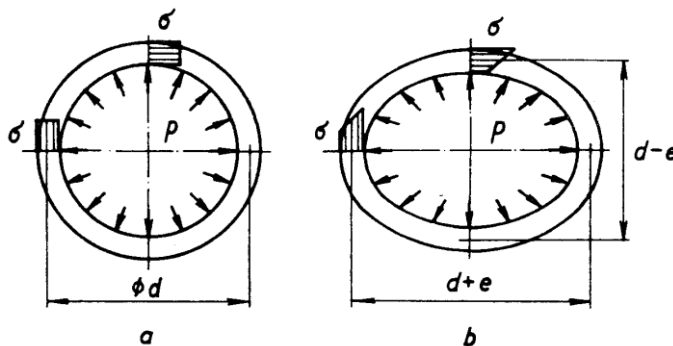
where  $e$  is the maximum deviation of the actual shape from the circular one (that is, the largest inner dimension is  $d + e$ , and the smallest is  $d - e$ ). Also bending stresses arise in axial direction:

$$\sigma_{e,a} = \mu \sigma_{e,t} . \quad (14.22)$$

Inserting the values  $d = 14$  mm,  $h = 1$  mm,  $e = 0,5$  mm and  $\mu = 0,18$  gives

$$\sigma_{e,t} = 1,305 \text{ MPa}, \quad \sigma_{e,a} = 0,19 \text{ MPa} .$$

This stress will act in addition to the membrane stress according to Eq. (14.19). The maximal stress in a tube of oval cross section can thus be several times higher than in ideally circular shape.



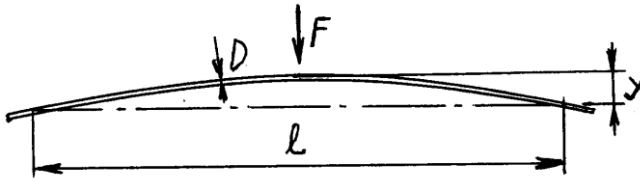
**Fig. 14.17.** Stress distribution in a tube with cross section: *a* – circular, *b* – oval. Due to varying wall thickness, the bending stresses can vary in the range:

$$\begin{aligned} \sigma_{e,t} (h = 1,2 \text{ mm}) &= 0,73 \text{ MPa}, & \sigma_{e,a} (h = 1,2 \text{ mm}) &= 0,13 \text{ MPa}, \\ \sigma_{e,t} (h = 0,8 \text{ mm}) &= 1,64 \text{ MPa}, & \sigma_{e,a} (h = 0,8 \text{ mm}) &= 0,30 \text{ MPa}. \end{aligned}$$

d) *Influence of the initial deflection of the tube*

The presence of the diaphragm in the centre of the exchanger means straightening of the tubes if they have some initial deflection from manufacture (Fig. 14.18). This causes further bending stress, this time in axial direction. These stresses can be determined like in a beam on two supports and loaded by a point transverse force. According to [1], the deflection in the centre is  $y = Fl^3/(48EJ)$ , and maximal tensile stress on the surface here is  $\sigma = M/W = FID/(8J)$ ;  $F$  is the transverse force,  $l$

is the distance of supports,  $J$  and  $W$  are the moment of inertia and section modulus in bending, and  $D$  is the beam thickness in the direction of deflection. Combination



**Fig. 14.18.** Glass tube for the exchanger – initial deflection from manufacture.

of both expressions gives the following formula for the maximum tensile (bending) stress, caused by the elimination of the initial deflection  $y$ :

$$\sigma_{y,ax} = 6E \frac{yD}{l^2} \quad (14.23)$$

The values from our example ( $l = 2000$  mm,  $y = 2 \times 2 = 4$  mm,  $D = d + 2h = 16$  mm) give  $\sigma_{y,a} = 6,14$  MPa .

This stress, from seemingly innocent deflection, is by far the highest of all acting stresses. (Note that it does not depend on the wall thickness, but only on the diameter of the tube.)

Now the total stress must be determined. We shall assume that the maximum deflection can appear simultaneously with the maximum deviation of the wall thickness and maximum ovality. (The influence of diameter change will not be considered, because the maximal possible deviation of the diameter in our case was understood as the sum of the diameter change and the ovality.) The resultant stresses in axial and circumferential direction in this case are

$$\sigma_a = \sigma_{T,a} + \sigma_{e,a} + \sigma_{y,a} \quad (14.24)$$

$$\sigma_t = \sigma_{T,t} + \sigma_{p,t} + \sigma_{e,t} \quad (14.25)$$

After insertion of the values corresponding to all investigated cases one obtains that the maximum tensile stress will act on the outer surface in axial direction, and its maximum value, attained at the wall thickness 1,2 mm, will be:

$$\sigma_a (h = 1,2 \text{ mm}) = 3,18 + 0,13 + 6,14 = 9,45 \text{ MPa.}$$

The circumferential stress will be



$$\sigma_t (h = 1,2 \text{ mm}) = 3,18 + 0,58 + 0,73 = 4,49 \text{ MPa.}$$

(With the wall thickness  $h = 1,0 \text{ mm}$  it will be  $\sigma_a = 9,13 \text{ MPa}$ ,  $\sigma_t = 4,55 \text{ MPa}$ , and for  $h = 0,8 \text{ mm}$  it will be  $\sigma_a = 8,81 \text{ MPa}$ ,  $\sigma_t = 4,89 \text{ MPa}$ .) We see that the actual maximum stress can be several times higher than in the ideal case.

In the next step, determination of tolerances could follow in order to reduce the parasitic stresses from manufacture.

### References to Chapter 14.

1. Höschl, C.: Pružnost a pevnost ve strojnictví. SNTL, Praha, 1971. 375 p.
2. Kolektiv: Pružnost a pevnost II. Skriptum ČVUT, Fakulta strojní, Praha, 1985. 214 p.
3. Baud, R.: Beiträge zur Kenntnis der Spannungsverteilung in prismatischen und keilförmigen Konstruktionselementen mit Querschnittsübergängen. Report 29, Schweiz. Verband für Materialprüfung in der Technik (Bericht 83 der Eidgen. Mat. Prüf.-Anstalt, Zürich, 1934)
4. Mattheck, C.: Design in Nature. Learning from Trees. Springer, Berlin-Heidelberg, 1998, 276 s. ISBN 978-3-642-58747-4. (také Design in der Natur. Rombach Verlag Freiburg, 1992.)
5. Mattheck, C.: Engineering components grow like trees. Materialwissensch. Werkstofftech., **21** (1990), s. 143 - 168.
6. Mattheck, C. - Burkhardt, S.: A new method of structural shape optimization based on biological growth. Int. J. Fatigue, **12** (1990), No. 3, p. 185 - 190.
7. Mattheck, C. - Bethge, K. - Erb, D. - Blömer, W.: Successful shape optimization of a pedicular screw. Medical & Biological Engineering & Computing, July 1992, p. 446 - 448.
8. Menčík, J.: Využití poznatků z biologických struktur pro optimalizaci tvaru mechanicky namáhaných konstrukcí. In: Inženýrská mechanika '99. Svratka 17-20 květen 1999. p. 551 - 556.
9. Baumgartner, A.: Ein Verfahren zur Strukturoptimierung mechanisch belasteter Bauteile auf der Basis des Axioms konstanter Spannung. Dissertation, Universität Karlsruhe, Fakultät für Maschinenbau, 1993.
10. [https://commons.wikimedia.org/wiki/Category:Femur#/media/File:Sobo\\_1909\\_215.png](https://commons.wikimedia.org/wiki/Category:Femur#/media/File:Sobo_1909_215.png)
11. Menčík, J.: Úvod do experimentální analýzy. Univerzita Pardubice, Pardubice, 2017, 142 str. Dostupné na webu: napsat: <https://dk.upce.cz/handle/10195/66960> nebo zadat název knihy do vyhledavače Google, nebo: <https://dk.upce.cz/bitstream/handle/10195/66960/Uvod%20do%20experimentalni%20analyzy.pdf?sequence=1&isAllowed=y>

12. MATLAB: <https://www.humusoft.cz/matlab/optimization/>
13. Arora, J.: Introduction to optimum design. 2<sup>nd</sup> Edition, Elsevier 2004. 728 pp., 3<sup>rd</sup> Ed. 2011. 896 pp. ISBN: 978-0-12-064155-0.
14. Rao, S. S.: Engineering Optimization: Theory and Practice, Wiley, (2009)
15. Parkinson, A.R., Balling, R., Hedengren, J.D.: [Optimization Methods for Engineering Design](#), Brigham Young University, 2013. Dostupné (27.12.2018) na <http://www.apmonitor.com/me575/index.php/Main/BookChapters>
16. Menčík, J.: Concise Reliability for Engineers. Intech, Rijeka, 2016, An open access publication: <http://www.intechopen.com/books/concise-reliability-for-engineers>, ISBN 978-3540629375. 204 p.
17. Taguchi, G.: Introduction to Quality Engineering: Designing Quality into Products and Processes. Asian Productivity Organisation, Tokyo, 1986. 191 p.
18. Taguchi, G., Chowdhury, S., Wu, Y.: Taguchi's Quality Engineering Handbook. John Wiley & Sons, Hoboken, N.J., 2005. 1696 p.
19. Ross, P. J.: Taguchi Techniques for Quality Engineering. McGraw-Hill, New York, 1996. 329 p.
20. Menčík, J.: Strength and fracture of glass and ceramics. Elsevier, Amsterdam, 1992, 357 p. (Pevnost a lom skla a keramiky. SNTL, Praha, 1990. 392 p.)
21. [https://en.wikipedia.org/wiki/Quebec\\_Bridge](https://en.wikipedia.org/wiki/Quebec_Bridge)

## 15. Dimensional analysis and theory of similarity

Design of various components, machines and structures can be improved if dimensional analysis and similarity theory are used, as they can simplify experiments (including computer modelling), reduce their extent, make the results more general, and also take over the results obtained with other objects. This chapter, based on works [1 – 5], shows various kinds of similarity and examples of dimensionless quantities, and gives advice for their creation.

### 15.1 Dimensional analysis

Every physical quantity is described by a numerical value accompanied by a unit. The numerical value says how many times the considered quantity is larger than its unit. An example of length is 5.3 m, of force is 25 N, of time is 15.6 ms. In addition to the fundamental units (meter, kilogram, second...), defined in the *Système International (SI)*, also various derived units are used, as well as prefixes ( $\mu$ , m, k, M...) denoting the order.

Every equation, describing a physical phenomenon, must be dimensionally homogeneous: its left side must have the same dimension as the right side. The check of this homogeneity should always be done before the first use of a newly derived formula. Such check also helps in formulating a correct relationship among the variables. Consider, for example, a formula for the deflection  $y$  of an elastic beam loaded by a force  $F$ . It is known from mechanics of materials that  $y$  will be directly proportional to  $F$  and indirectly proportional to the bending stiffness of the beam, defined as  $E \times J$ , where  $E$  is the Young modulus of the material and  $J$  is the moment of inertia of the cross section. The deflection will also be proportional to some power  $S$  of the beam length  $L$ . Now, imagine that we do not know the exponent  $S$ . In such case we could write the basic form of the formula:

$$y = C \times F \times L^S / (E \times J); \quad (15.1)$$

$C$  is a dimensionless constant. Replacement of the individual quantities in Eq. (15.1) by their units gives

$$m = 1 \times N \times m^S / (N/m^2 \times m^4).$$

The dimension of the right side must be the same as that of the left side, i.e. meter. The product of all terms containing  $m$  is  $m^S \times m^2 \times m^{-4} = m^{S+2-4} = m^{S-2}$ . Comparison of the exponents on the left and right side of the equation gives  $1 = S - 2$ . From this it follows  $S = 3$ , so that  $y = C \times F \times L^3 / (EJ)$ , a formula well known from mechanics. The homogeneity condition thus helped in finding the correct formula.

If one side of an equation is a sum of several terms, they all must have the same dimension. For example, vertical path  $y$  of a body falling in gravitational field is

$$y = y_0 + v_0 t + \frac{1}{2} g t^2 . \quad (15.2)$$

$t$  is time,  $y_0$  and  $v_0$  are the position and velocity of the body at  $t = 0$ , and  $g$  is the acceleration of gravity. The dimensional homogeneity demands that the individual quantities cannot exist in the physical equation independently, but only in groups of the same dimension. If Equation (15.2) is divided by one of the terms, for example  $y_0$ , it changes to non-dimensional form

$$y/y_0 = 1 + v_0 t/y_0 + \frac{1}{2} g t^2/y_0 \quad (15.3)$$

with normalised quantities  $y/y_0$ ,  $v_0 t/y_0$  and  $g t^2/y_0$ .

Nearly every physical equation can be transformed to non-dimensional form. The use of normalised quantities has many advantages. Physical equations, expressed by means of non-dimensional variables, are more general. The relative displacement or path,  $y/y_0$ , does not depend simply on  $v_0$ ,  $t$  and  $y_0$ , but only on their certain combinations, such as those in Eq. (15.3). Dimensionless quantities thus enable one to combine the results of experiments made with specimens of various initial velocity and position, the only condition being their proper combination. Therefore, more data and a wider range of parameters can be used for the formulation of a certain law. The results expressed in non-dimensional form are also more universal, valid for the whole class of similar objects, with similar geometry or physical properties. Moreover – and this is very important – the use of non-dimensional quantities can spare experimental work, because

***the relationship among  $N$  quantities, whose dimensions can be expressed by means of  $D$  basic dimensions, may usually be replaced by a relationship of only***

$$P = N - D \quad (15.4)$$

***nondimensional parameters II.***

According to this *Buckingham theorem* [1 – 4], the determination of less regression

constants needs less experiments. The reduction of experimental work is significant especially if the investigated relationship contains many quantities and if the number of variables,  $N$ , is closer to the number of basic dimensions,  $D$ . This can be illustrated on the previous example of a falling body. Equation (15.2) represents relationship of 5 quantities:  $y$ ,  $y_0$ ,  $v_0$ ,  $g$  and  $t$ ; that is  $N = 5$ . These quantities can be expressed by means of two basic dimensions: meter and second; thus  $D = 2$ . According to Eq. (15.4), the number of non-dimensional parameters should be  $P = N - D = 5 - 2 = 3$ . And really, Equation (15.3) is the relationship of 3 dimensionless parameters:  $y/y_0$ ,  $v_0t/y_0$  and  $gt^2/y_0$ . The determination of the necessary number of experiments will be discussed later in this book. Nevertheless, an idea can be obtained from a simple example. If the influence of six factors should be investigated, with each on two levels (low and high), the number of necessary experiments would be  $2^6 = 64$ . If the number of dimensionless factors would be only 4, the number of necessary experiments drops to  $2^4 = 16$ , i.e. to 25%!

All this holds also for computer modelling! Its extent can often be reduced if a general analysis is done first and principal relationships revealed.

### **Similarity**

The use of non-dimensional quantities is also of prime importance in the study of real objects by means of models. Building of a large structure is accompanied with many uncertainties, and the potential losses due to wrong design would be very high. Therefore, usually a smaller model is built first and tested. However, if the model should adequately reflect the behaviour of the actual structure, similarity between them must exist. There are various kinds of similarity, for example:

Geometric similarity, which means identity of shape, equality of corresponding angles, and proportionality between the corresponding dimensions (so-called scale factor). The following relation holds:

$$\text{Model dimension} = \text{Scale factor} \times \text{Dimension of the real object}$$

Static similarity means that the relative deformations of a model under constant stress are in the same proportion as the corresponding deformations of the object.

Kinematic similarity is based on the ratio of the time proportionality between corresponding events in the model and the object.

Dynamic similarity exists if the forces acting at corresponding times and locations in the model and object are in a fixed ratio.

The **theory of similarity** works with so-called **similarity numbers**. Those, who have attended a college course of physics, know, e.g., the Reynolds number (Re), which helps in assessing whether flow of a liquid is laminar or turbulent. The similarity numbers are dimensionless; in fact, every non-dimensional quantity can serve as a similarity number.

**Dimensionless variables** can be created in various ways. The simplest case is the ratio of some quantity to its characteristic value, for example  $x/x_0$  or  $\Delta x/x_0$  for distance or displacement. Well known in mechanics are: strain, defined as relative elongation ( $\varepsilon = \Delta L/L$ ), Poisson number  $\mu$  (the ratio of relative shortening in transverse direction to the relative elongation in the direction of stress action), or coefficient of friction  $f$ , defined as the ratio of the force, needed to slide a body along another body, and the normal force pressing both bodies together. Another example is relative position of a point in a body, for example

$$\xi = (x - x_{\min})/(x_{\max} - x_{\min}) ; \quad (15.5)$$

$x$ ,  $x_{\max}$  and  $x_{\min}$  represent the coordinates. Similarly it is possible to express time. Non-dimensional temperature,  $\theta = (T - T_{\infty})/(T_0 - T_{\infty})$ , is used for the description of processes of heat transfer ( $T_0$  is the initial temperature and  $T_{\infty}$  the final). The instructions for creation of dimensionless parameters can be found in [1 – 5].

Non-dimensional must also be the arguments in mathematical functions sin, cos, log or exp. Otherwise any change of units, e.g. meter instead of mm) would change the numerical value of the result. Dimensionless are also the arguments in probability distributions. Normal distribution uses the argument  $\{1/2[(x - \mu)/\sigma]^2\}$ , where  $\mu$  and  $\sigma$  are the mean value and standard deviation. The expression in the composed brackets is nothing else than standardised non-dimensional variable, which expresses the distance of  $x$  from  $\mu$  as a multiple of standard variable  $\sigma$ .

### 15.3 Further recommendations

1) Sometimes the form of the non-dimensional parameters does not correspond to our intentions or experimental possibilities. Generally, it is possible to create new parameters (or similarity numbers) by making a product or ratio of the original ones, or to change them by making their reciprocal or some power. As they are

dimensionless, the new parameters obtained by such transformations will again be dimensionless. It is possible to create several dimensionless parameters and select from them the most suitable, which have certain physical sense.

2) If several quantities of the same dimension appear in one problem, it is also possible to create non-dimensional parameters directly as their ratios. This can reduce the number of arguments, which must be determined by solution of the system of equations such as those given under point 4 above. This will be illustrated on the example of the deflection  $y$  of a beam with rectangular cross section ( $w \times h$ ) and length  $L$  loaded by a point force  $P$ . The modulus of elasticity is  $E$ . The variables and their dimensions are:  $y(\text{m})$ ,  $w(\text{m})$ ,  $h(\text{m})$ ,  $L(\text{m})$ ,  $P(\text{N})$ ,  $E(\text{Nm}^{-2})$ ; that is 6 variables with 2 dimensions. The number of non-dimensional parameters needed for the description of the problem is  $P = N - D = 6 - 2 = 4$ . We can immediately create three parameters  $\Pi_1 = y/h$ ,  $\Pi_2 = b/h$  and  $\Pi_3 = L/h$ . Two quantities remain ( $P$  and  $E$ ), which must be contained in the fourth parameter. With respect to their dimensions and the condition of non-dimensionality also one geometric quantity must be included in  $\Pi_4$ , for example  $h$  or its power. We obtain this parameter as  $\Pi_4 = P/(Eh^2)$ . The studied relationship can thus be written in the following non-dimensional form:

$$y/h = f[P/(Eh^2), L/h, b/h]. \quad (15.6)$$

One should remember that for the study of relative deflection  $y/h$  are important not the individual quantities  $L$  or  $P$ , etc., but their ratios.

3) In some problems always dimensionless quantities appear. Examples are coefficient of friction, Poisson's number  $\mu$  or angle  $\varphi$  (rad). These quantities automatically become arguments in the non-dimensional relationships.

4) The creation of dimensionless parameters can be facilitated by using the existing knowledge on the investigated or similar problems. For example, we know that elastic deflection of a beam is directly proportional to the load and indirectly to the modulus of elasticity. Sometimes, analytical solution is known for very small or very large values of certain variable. This can help in searching for proper form of the arguments. Sometimes it is known that some quantities must appear in certain combination. This combination can be considered as a new variable, which can enable reduction of the total number of variables. Consider, for example, force

acting in the contact area of two bodies. If friction should be investigated, the force  $F$  (N) and contact area  $A$  ( $\text{m}^2$ ) can be replaced by contact pressure  $p = F/A$  ( $\text{N}/\text{m}^2$ ).

5) When an experiment is prepared, all quantities must be included, which may play a role. Otherwise wrong and misleading results can be obtained. It is less dangerous to include a quantity, whose importance is uncertain (and, perhaps, later it may be omitted), than to omit a quantity, which would appear later as important. The use of dimensional analysis sometimes reveals shortcomings. For example, if some dimension appears only at one quantity, this quantity falls out and will not be included in any non-dimensional parameter. However, if this quantity is obviously necessary for the description of the investigated phenomenon, it is necessary to add another quantity having the same dimension. This can be illustrated on a study of wear rate of a cutting tool. The quantities playing a role are: wear rate  $w$  (m/s), velocity of mutual sliding  $v$  (m/s) and the pressure in the contact area  $p$  ( $\text{N}/\text{m}^2$ ). The non-dimensional parameter could be searched in the form

$$\Pi = w^{x_1} v^{x_2} p^{x_3}. \quad (15.7)$$

This expression can be written by means of the dimensions of the individual quantities, m, s, N:

$$[\text{m}]^0 [\text{s}]^0 [\text{N}]^0 = [\text{m} \times \text{s}^{-1}]^{x_1} \times [\text{m} \times \text{s}^{-1}]^{x_2} \times [\text{N} \times \text{m}^{-2}]^{x_3} \quad (15.8)$$

However, from the condition of equality of exponents at the same base,  $\text{N}^0 = \text{N}^{x_3}$  it will follow that  $x_3 = 0$ . But it is well known from experiments that the wear rate does depend on the contact pressure, so that  $x_3$  cannot equal 0. It is thus necessary to include some further quantity, which would also have the dimension  $\text{Nm}^{-2}$ . This could be, for example, hardness  $H$  ( $\text{Nm}^{-2}$ ), which characterises the resistance of the material. Now, the general form of the non-dimensional parameter is

$$\Pi = w^{x_1} v^{x_2} p^{x_3} H^{x_4} \quad (15.9)$$

From this expression, we can easily formulate the appropriate relationship of dimensionless parameters as  $w/v = f(p/H)$ , and perform a series of experiments in order to find the appropriate form of the function  $f$ .

#### 15.4 Limitations of similarity principle

Dimensioning of a component is based on the material properties determined on standardised or specially prepared specimens. Generally, the tested specimen must



be representative. This means that its properties must be the same as those of the component that should be created. This is related to the dimensions. The specimen can be homogeneous or nonhomogeneous, with respect to its dimensions. For example, concrete contains cement, sand, gravel and pores. The sand grains have various sizes, and even larger differences exist with gravel. If the concrete quality of an existing structure should be determined, usually a specimen is taken off by cutting or using a trepanation drill. The tested specimen must be sufficiently large, so that all parts of the material are represented. Its diameter or thickness must be significantly larger than the largest expected pieces of gravel, for example. Otherwise we do not obtain the modulus of elasticity of the concrete, but a value near to the modulus of gravel. Similar situation is in metallic materials with polycrystalline structure. The individual grains are anisotropic, so that a sufficient number of crystals must be in the cross section in order to obtain the average property, not influenced by the grain orientation. Another example: it is well known that the strength of glass fibers is much higher than the strength of massive glass, partly because the small diameter of the fiber limits the maximum size of flaws responsible for the low strength.

If a component with a crack can break, an important characteristic of its resistance to crack growth is fracture toughness of the material  $K_{IC}$ . This is such value of the stress intensity factor  $K_I$ , at which the crack propagation becomes fast and unstable. High stresses in front of the crack in metallic materials cause plastic flow in a small region around the crack tip. And here, a role can be played by the difference between the plane stress state on the side surfaces of the specimen and the plane strain state in the region remote from surfaces. The radius of the region with plastic flow under plane stress is much larger than at places under plane strain (Fig. 7.7). If the standard value  $K_{IC}$  of fracture toughness should be obtained, the test specimen must have certain minimum thickness, which is prescribed by the pertinent standard. Thinner specimens would yield higher values, and their use for the components with larger thickness of the wall could be dangerous, as the crack would start growing earlier than we expected. If the values from material data sheets are used, the user should know the conditions of their usability.

The principle of similarity, enabling the transfer of measured values on the designed object, holds only under some conditions, and outside them it loses its validity [10]. An example is the transition from elastic to elastic-plastic deformations in components from ductile materials. If the stresses are lower than

the yield strength, the deformations are elastic, linear relationship exists between stresses and strains, and the superposition principle may be used, which allows obtaining the resultant deformations and stresses of several loads as the sum of the values calculated for the individual loads. However, the relationships in the elastic-plastic region are nonlinear and the situation must be solved for various loads individually.

Another case is the strength dependence of brittle bodies on the size of loaded area or volume. Brittle fracture usually starts in the weakest point, with some defect. Smaller size of a loaded area means lower probability of occurrence of a larger defect. Very small objects are therefore stronger. Similarly, also the fatigue limit of metal components depends on the component size. A coefficient accounting for the size is therefore used in the fatigue calculations.

Sometimes simultaneously quantities appear that depend on different powers of another quantity. For example, the energy consumed in fracture, is proportional to the area of fracture ( $m^2$ ), while strain energy accumulated in the body is proportional to its volume ( $m^3$ ). Sometimes it is necessary to check whether both components are similarly important, and, if possible, to neglect one of them.

The processes in fast plastic deforming depend sometimes on the strain-rate. If the effects of impact load should be studied on a model, whose dimensions ( $L_m$ ) are smaller than of the actual object ( $L_p$ ), one should not forget that different velocity of impact,  $v_0$ , must be used in order to obtain the same strain rate of forming,

$$v_{0m}/v_{0p} = L_m/L_p ; \quad (15.10)$$

the subscripts m and p denote model and prototype.

Generally, one must have in mind that sometimes the investigated quantity changes with the changes of a certain parameter relatively slowly, but at its certain level it can change very quickly. The relationship, describing some behaviour or process, is often valid only within certain range of parameters. If the pertinent process is described by means of non-dimensional quantities, the conditions for a transition from one mode to another are characterised by a **critical value** of some of these quantities. A well-known example is the change from laminar to turbulent flow at the critical value of Reynolds number. One must therefore always consider all possible influences, and reduce their number only after a thorough analysis.

**Example.**

Expression of the pertinent formulae in non-dimensional form facilitates one to understand the basic relationships and trends, and can contribute to the more economical design. This can be illustrated on example of a column from reinforced concrete loaded by tensile force (Fig. 15.1). This force is transferred by the reinforcement (component a) and concrete (component b), so that it holds

$$F = F_a + F_b \tag{15.11}$$

Both components will be deformed as a whole, so that the change of the initial length  $l$  is  $\Delta l_a = \Delta l_b$ . Expressing these elongations by means of Hooke's law gives

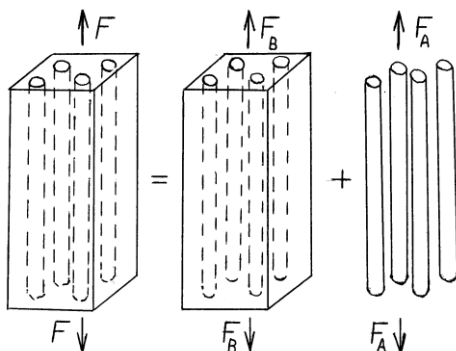
$$\frac{F_a l}{E_a S_a} = \frac{F_b l}{E_b S_b} . \tag{15.12}$$

With respect to Eq. (14.11), some rearrangements give the following formulae for relative forces in the components  $a$  and  $b$ :

$$\frac{F_a}{F} = 1 / \left( 1 + \frac{E_b S_b}{E_a S_a} \right); \quad \frac{F_b}{F} = 1 / \left( 1 + \frac{E_a S_a}{E_b S_b} \right); \tag{15.13}$$

The equation at right was obtained by interchanging the subscripts. Equations (14.11) – (14.13) are valid for any two-component part, including fiber composites.

We see that the relative magnitudes of forces in the individual components do not depend on the particular values of moduli of elasticity or area of the cross section, but only on the ratios of elastic moduli and the cross sections. This is advantageous in design when the final dimensions are not known yet and when the material can be selected from several candidates. The task can be optimised. For example, the unit (kg) prices of the individual materials are known, and such configuration of the object is sought, which will guarantee the lowest price. The actual size of the cross section will then be determined with respect to the actual load  $F$ .



*Fig. 15.1. Reinforced concrete – components and forces*

## 15.5 Examples of non-dimensional quantities

### Material properties

$E_1/E_2, H_1/H_2$	ratio of elastic moduli or hardnesses; subscripts denote the components,
$E(x)/E_0, H(x)/H_0$	ratios as above, subscript 0 denotes the characteristic value,
$H/Y, E/Y, E/H$	ratio of hardness and yield strength or elastic modulus,
$\sigma/\sigma_Y, \sigma/\sigma_u$	ratio of stress to yield strength $\sigma_Y$ or ultimate strength ( $\sigma_u$ ),

### Geometry

$x/d$	$x$ – distance, $d$ – characteristic dimension (contact radius, specimen length, width, height or diameter, coating thickness, size of plastic zone...),
$\Delta/L$	relative displacement or elongation, $L$ – basic length,
$h/R, h/t_c$	ratio of indenter penetration $h$ to the tip radius $R$ or coating thickness $t_c$ ,

### Forces and stresses

$F/F_0$	ratio of load $F$ and characteristic force,
$\sigma/\sigma_m$	ratio of the stress $\sigma$ to the nominal or mean stress $\sigma_m$ .

### Time

$t/t_0$	$t_0$ – characteristic time (of load increase, relaxation time).
---------	--

## References to Chapter 15.

1. Menčík, J.: Introduction to experimental analysis. University of Pardubice, Pardubice, 2017. Available free at: <http://hdl.handle.net/10195/66960>.
2. Kožešník, J.: Teorie podobnosti a modelování. Academia, Praha, 1983. 216 p.
3. Zlokarnik, M.: Scale-up in Chemical Engineering. 2nd Edition, Wiley, 2006, 296 p.
4. Szirtes, T.: Applied Dimensional Analysis and Modeling, McGraw-Hill, New York, 1997, 2nd Ed. 2007. 856 p.
5. Cheng, Y.T., Cheng, C.M.: Scaling, dimensional analysis, and indentation measurements, *Mat. Sci. Eng. R44* (2004) pp. 91 – 149.

## Index (the numbers in brackets denote the chapters)

Baud curve (no stress concentration)	169 (14)
bending, elastic, plastic	44 (4)
bimaterial, Dundurs' parameters	124, 125 (11)
Buckingham rule	183 (15)
Burgers model	106 (10)
coatings, measurement of mechanical properties	132 (11)
component of constant stresses	161 (14)
component without stress concentration	169, 170 (14)
composites (fibrous, particulate)	136 (12)
composites orthotropic	149 (12)
composites with long, short fibers	136, 137, 143 (12)
composites, failure	147 (12)
composites, mechanics	136 (12)
composites, stiffness, strength	137, 139, 140, 141 (12)
crack in the coating, propagation	125, 126, 130 (11)
crack opening, modes	83 (8)
crack, propagation	69 (6), 132 (11)
cracks, network of	132, 133 (11)
creep	100 (10)
criterion for failure and plastic flow	31, 32, 33 (3), 51 (4)
deformation work	2, 21 (1), 66 (6)
deformations elastic,	17 (1)
deformations large, deflection	157 (13)
design point	172, 173 (14)
dimensional analysis	182 (15)
disc of constant stresses	167 (14)
dispersion of properties	146 (12)
distribution of random quantity, Weibull	146 (12)
Dundurs' parameters	124, 125 (11)
elastomers	153 (13)
energy release rate	85 (8)
failure, hypotheses	31 (3)
fatigue crack, nucleation, velocity	76 (7)
fatigue curve (low cycle, high cycle)	74, 77 (7)

fatigue fracture	93 (9)
fiber length, critical	145 (12)
fiber properties, variance	146 (12)
fibers, long, short	137, 143 (12)
fictitious cut, method	9 (1)
filament winding	142 (12)
finite element method (FEM), software	23, 26 (2)
fraction of fibres in a composite	137 (12)
fracture analysis	93 (9)
fracture mechanics	81 (8), 124 (11)
fracture toughness	83 (8), 134 (11)
fracture, brittle	31 (3)
glass strengthening (tempering)	58 (5)
homogeneity of dimensions	182 (15)
Hooke's law	18 (1), 149, 150 (12)
hypotheses of failure and plastic deforming	31, 32, 33 (3)
hysteresis	111 (10)
Kelvin-Voigt model	103 (10)
knitted material (fabric)	158 (13)
Lagrange principle	23 (2)
lamina, laminate	150, 151 (11)
Laplace equation (for membrane)	118, 119 (11)
limit load	41 (4)
limit state	50 (4)
load transfer length	145 (12)
material elastic (Hookean)	98 (10)
material elastic-plastic	37 (4)
material hyperelastic	147 (12)
material model, Burgers	106 (10)
material model: Mooney-Rivlin	155 (13)
material model: neo-hookean	155, 156 (13)
material viscous (Newtonian)	99 (10)
materials orthotropic	149, 150 (12)
materials viscoelastic, response	101, 103 (9)
Maxwell model	100 (10)
mechanics of materials	7

membrane, Laplace equation	118, 119 (11), 159 (13)
method of adaptive growth	170 (14)
method Soft Kill Option	171 (14)
methods analytical and numerical	26 (2)
modulus of elasticity (in tension, shear)	18 (1)
modulus: complex, instantaneous, loss	110 (10)
Mohr's circle	10, 12, 14, 19 (1)
moment, limit value	45 (4)
non-dimensional quantity	183 (15)
notch toughness, Charpy hammer	66 (6)
notch	65 (6), 169 (14)
optimisation of a continuous beam	167, 168 (14)
optimisation of cross section	164, 165 (14)
optimisation	161 (14)
parameter dimensionless (non-dimensional)	183 (15)
parameter dimensionless, non-dimensional	183 (15)
plane stress	10 (1)
plastic hinge	46 (4)
plastic zone in front of the crack	82, 87 (8)
plasticity	35 (4)
Poisson's number	18 (1)
prepreg	150 (12)
principal stresses, directions	12, 16 (1)
relaxation (retardation) time	102, 104 (10)
relaxation of stresses, forces	101 (10)
residual forces, stresses, deformations	43 (4)
resistance to crack propagation	90 (8)
Ritz method	24 (2)
robust design	172 (14)
safety factor	34 (3)
section modulus	45 (4)
section modulus, plastic	46 (4)
shear strain $\gamma$	17 (1)
shear stresses, complementary	11 (1)
shrink-fitted joint	173 (14)
similarity	182, 184 (15)

specimens: sandwich, UCSB	134 (11)
Standard Linear Solid (SLS)	105 (10)
stiffness, stiffness matrix	24, 25 (2)
strain energy density	21 (1), 156 (13)
strain energy	20 (1)
strain	17, 19 (1)
strengthening, strain hardening	58, 61, 62 (5)
stress (normal, shear)	9 (1)
stress equivalent	31, 32, 33 (2)
stress intensity factor	82, 84 (8)
stress intensity factor, interface crack	125, 126, 127 (11)
stress intensity	51 (4)
stress, concentration	64, 65 (6)
stress, contact	70 (6)
stress, in coating	116, 118, 119 (11)
stress, in front of a crack	82 (8), 124 (11)
stress, membrane	116 (11)
stress, principal	12, 16 (1)
stress, residual	47 (4)
stress, thermal	54 (5)
stretch ratio	153 (13)
stretch, invariant	154 (13)
textile fibers	157 (13)
theory of similarity	185 (15)
thermal expansion	55 (5), 113 (11)
thick wall vessel, cylindrical	48, 50 (4)
tolerance	172 (14)
triaxial stress	16 (1)
variable non-dimensional	183 (15)
viscoelasticity	98 (10)
work diagram of a body	41 (4)
work diagram of material	35, 36 (4)
yield strength, ultimate strength	19 (1)



Book title: Applied mechanics of materials  
Author: prof. Ing. Jaroslav Menčík, CSc.  
Publisher: University of Pardubice  
Print: June 2019  
No. of pages: 196  
No. of copies: 20  
Edition: first  
Printed by: Polygrafické středisko Univerzity Pardubice

ISBN 978-80-7560-228-2 (print)

ISBN 978-80-7560-229-9 (pdf)

The book is accessible on <https://hdl.handle.net/10195/72948> or after writing its title into Google.

ISBN 978-80-7560-228-2



9 788075 160228 2